Web crippling behaviour of cold-formed stainless steel lipped channel sections with edge-stiffened web holes under two-flange loading conditions

A thesis

submitted in fulfilment

of the requirements for the degree

of

Master of Engineering with endorsement in Civil Engineering

at

The University of Waikato

by

Maria Fe Glorieta B. Opulencia

THE UNIVERSITY OF
WAIKATO
Te Whare Wānanga o Waikato

2024

Abstract

In New Zealand, edge-stiffened holes have been recently introduced to cold-formed steel channels (CFS) to facilitate the installation of plumbing and electrical systems. Previous studies on cold-formed carbon steel (CFCS) channels have demonstrated that using edge-stiffened web holes provides nearly the same strength as an equivalent channel section with a plain web when facing web crippling. However, there is a lack of experimental or numerical investigations into the application of edge-stiffened web holes in cold-formed stainless steel (CFSS) channels in the existing literature.

This thesis builds upon previous studies conducted on CFCS channel sections. It presents a comprehensive numerical examination of the web crippling behaviour of CFSS channel sections with edge-stiffened circular web holes under interior-two-flange (ITF) and end-two-flange (ETF) loading conditions. Three stainless steel grades were considered: EN 1.4509 (Ferritic), EN 1.4462 (Duplex), and EN 1.4301 (Austenitic). A parametric study involving 3,744 non-linear finite element (FE) models was developed for both fastened and un-fastened flange cases. The study covered the impact of different hole sizes, edge-stiffener lengths, channel inner radius, and the length of the bearing plates.

The results of the parametric study were used to establish new equations for web crippling strength and strength reduction factors through non-linear regression analysis. These proposed design equations outperformed predictions from American Society of Civil Engineers Specification (ASCE 8-02), American Iron and Steel Institute Specification, Australian/New Zealand Standard (AISI&AS/NZS), and Eurocode 3. Finally, a reliability analysis was conducted, revealing that the proposed design equations accurately predict the web crippling strength of CFSS channel sections with plain webs, unstiffened web holes, and edge-stiffened web holes under two-flange loading conditions.

Acknowledgements

First and foremost, I would like to express my deepest gratitude to God Almighty for His boundless grace, steadfast love, and infinite wisdom throughout my life. Without Him, none of this would have come to fruition. His enduring guidance, generous provisions, and divine support have been the cornerstone of my life. All praises and glory be unto Him, now and forever.

I am deeply thankful to my main research adviser, Arthur Fang, as well as my secondary advisors, Prof. James Lim, and Dr. Krishanu Roy. Your insightful guidance, unwavering support, and depth of knowledge in this field have been truly invaluable to me. I deeply appreciate the dedication, time, and meticulous attention you've given in reviewing my thesis, providing feedback, and suggesting improvements, all of which greatly enhanced its quality. Thank you immensely!

To the entire CFS research team, I extend my sincere gratitude! It's been a joy getting to connect with each of you this past year. Whether it was through guidance, assistance with my questions, moments in the tearoom, providing lab and office access, or sharing personal experiences and insights, each of you has made a significant contribution. I value every conversation and act of kindness. A special shoutout to Ahmad, Bikram, Parsa, and Shubam for your technical know-how. Our collaborations have enriched me with valuable knowledge and skills that are particularly beneficial for my research endeavours. Your consistent support and commitment have meant a lot to me.

I would like to give special thanks to Ate Shiela and Kuya Raffy Madlang-awa for being my spiritual mum and dad. During my most challenging moments as a student, you provided unwavering support, and warmest love and welcomed me into your home. Your family is a tremendous blessing to me and my family. I am truly thankful to God for your lives.

To my beloved family, thank you so much for your immense support, constant prayers, and boundless love you've showered me and my children as I embarked on this new journey. Your presence and

encouragement have been my pillars of strength during this challenging times. A special acknowledgement goes to my dear mommy, Gloria, for her unwavering love, patience, and support throughout my life. I extend my exceptional gratitude to ate Jing and kuya Rhodel Lagayan, for welcoming my children into their home and caring for them as their own. The challenges I faced were daunting, but with your collective love and support, I found the strength to persevere. I am profoundly thankful for each one of you and I couldn't have completed this academic journey without all of you. God has truly blessed me with such a wonderful family.

Lastly, I want to express my greatest appreciation to my wonderful, sweet, and loving children, Ethan & Enzo Ramirez. Moving away to pursue higher studies was a difficult decision for our family, and I sincerely apologize. However, your understanding and support during this time mean the world to me. I deeply miss both of you and fervently hope that we can reunite soon. You are my treasured blessings, and I am proud to be your mom.

Table of Contents

List of figures

List of tables

Glossary

a	diameter of channel web hole
a/h	the ratio of hole diameter to web flat depth
bf	length of channel width
bl	length of channel lip
CFS	cold-formed steel
CFCS	cold-formed carbon steel
CFSS	cold-formed stainless steel
C_P	correction factor
COV	coefficient of variation
d	channel depth
DSM	Direct Strength Method
E	Young's modulus of elasticity
ETF	end-two-flange
FE	finite element
FEA	finite element analysis
f_y	yield strength
F_m	mean value of fabrication factor
f_u	ultimate tensile strength
h	web flat depth
h/t	the ratio of web flat depth to thickness
ITF	interior-two-flange
L	length of channels
M_m	mean value of material factor
N	number of data
N	length of bearing length
N/h	the ratio of bearing length to web flat depth
N/t	the ratio of bearing length to web thickness
P_{ASCE}	nominal web crippling strengths of CFSS channels obtained from American Standard
$P_{AISI\&AS/NZS}$	nominal web crippling strengths of CFCS channels obtained from American and Australian/New Zealand Standard

$P_{AS/NZS}$	nominal web crippling strengths of CFSS channels obtained from Australian/New Zealand Standard
P_{EC}	nominal web crippling strengths of CFCS channels obtained from Eurocode
P_{EXP}	web crippling strengths obtained from the experimental tests
P_{FANG}	web crippling strengths of CFSS sections obtained from Fang et. al [11,12] proposed design equations
P_{FEA}	web crippling strengths obtained from the FE model numerical result
$P_{FEA,SH}$	web crippling strengths of CFSS channel sections with edge-stiffened web holes obtained from the FE model numerical result
$P_{FEA,UH}$	web crippling strengths of CFSS channel sections with unstiffened web holes obtained from the FE model numerical result
P_m	mean value of tested-to-predicted load ratio
P_n	web crippling strength of CFSS channel sections
P_{PROP}	proposed web crippling strength for CFSS channel sections without web holes
r	channel inside bend radius
r/t	the ratio of inside bend radius to web thickness
q	channel edge-stiffener length
q/h	the ratio of stiffener length to web flat depth
r	channel radius
ri	radius of channel edge-stiffener hole
R_{FANG}	reduction factor of web crippling strength of CFSS channel sections with unstiffened web holes obtained from Fang et. al [11,12] proposed design equations.
R_p	reduction factor of web crippling strength
R_S	reduction factor of web crippling strength for channels with edge-stiffened web hole
R_{UZZ}	web crippling strength of CFCS channel sections with unstiffened web holes obtained from Fang et. al [11,12] proposed design equations.
$R_{S,PROP}$	proposed reduction factor of web crippling strength for CFSS channel section with edge-stiffened web hole
R_U	reduction factor of web crippling strength for channels with unstiffened web hole

$R_{U,PROP}$	proposed reduction factor of web crippling strength for CFSS channel section with unstiffened web hole
R_{UZZ}	web crippling strength for CFCS channel sections with edge-stiffened web holes obtained from Uzzaman et.al [27,29] proposed reduction factor
t	thickness of channel section
V_F	coefficient of variation of fabrication factor
V_M	coefficient of variation of material factor
V_P	coefficient of variation of tested-to-predicted load ratio
V_Q	coefficient of variation of load effect
x	horizontal clear distance of the web hole to the near edge of the bearing plate
x/h	the ratio of hole distance to web flat depth
σ	engineering stress
σ_{true}	Abaqus true stress
ε	engineering strain
ε_{true}	Abaqus true strain
θ	angle between web and bearing surface
β	reliability index
φ	resistance factor

Chapter 1: Introduction

Stainless steel, renowned for its distinctive properties, aesthetic appeal, and inherent resistance to heat and corrosion, has emerged as a preferred material for structural applications (refer to Figure 1.1). Structural channels made of stainless steel are often designed with web holes to facilitate the installation of various services. However, these modifications can introduce localized weaknesses, especially around these openings, potentially leading to web failure under transverse concentrated loads.

An innovatively designed edge-stiffened web hole (see Figure 1.2) has been widely adopted, with previous studies [7, 27-31] suggesting that sections featuring these reinforced openings can maintain load-bearing capacities comparable to those of unperforated sections. Despite this, there is a noticeable research gap regarding the web crippling strength of cold-formed stainless steel (CFSS) channels with edge-stiffened web holes.

This study aims to investigate the web crippling strength of CFSS channel sections under two-flange loading conditions, specifically interior-two-flange (ITF) and end-two-flange (ETF) conditions, as illustrated in Figures 1.3 and 1.4, respectively. Material properties for the considered stainless steel types, namely EN 1.4509 (Ferritic), EN 1.4462 (Duplex), and EN 1.4301 (Austenitic), were extracted from the literature [3, 11, 12].

Several studies have delved into web crippling in cold-formed stainless steel (CFSS) channel sections, particularly those with plain webs and unstiffened web holes. Korvink et al. [17, 18] conducted both experimental and numerical investigations on the structural behavior of ferritic and austenitic CFSS channel sections with single flange webs under exterior-one-flange loading conditions. Bock et al. [6] focused on the one-flange web crippling behavior of CFSS hollow and hat channel sections, emphasizing ferritic CFSS channel sections in their numerical study.

Figure 1.1: Structural stainless steel at Gent Sint Pieters railway station in Belgium. Photo: Patrick Lints [41,11]

Figure 1.2: CFS channels with edge-stiffened web holes used in buildings [7]

Regarding sections with web holes, Yousefi et al. [34-38] performed one-flange web crippling experimental tests on ferritic CFSS unlipped channel sections, proposing strength reduction factor equations specifically for the reduction of web failure strength due to web holes; however, their study exclusively considered ferritic CFSS. For lipped channel sections, Yousefi et al. [39] presented a

numerical study encompassing ferritic, duplex, and austenitic CFSS channel sections with plain webs and unstiffened web holes under interior-one-flange loading conditions. Fang et al. [10-12] investigated the One- and Two-flange web crippling behavior of CFSS sections with unstiffened web holes, proposing relevant equations. However, there is still a lack of studies understanding the web crippling behaviour of CFSS channel sections with edge-stiffened web holes.

In the realm of cold-formed carbon steel (CFCS) sections under web crippling, literature offers some insights. Gunalan and Mahendran [14] explored the two-flange web crippling strength of CFCS lipped and unlipped plain channel sections using the Direct Strength Method (DSM). Nguyen et al. [23-26] further refined the DSM for CFCS plain sections subjected to One- and Two-flange loading cases. Uzzaman et al. [27-33] and Lian et al. [19-22] reported numerous studies, combining experimental and numerical investigations, and proposed web crippling strength reduction factor equations for CFCS channel sections with web holes under both one- and two-flange loading conditions. Chen et al. [7] investigated the web crippling capacity of CFCS channel sections with plain webs, unstiffened web holes, and stiffened web holes.

Design guidelines for web crippling performance are provided by ASCE 8-02 [3] and AS/NZS 4673:2001 [4] for CFSS sections. AISI S100-16 [2], AS/NZS 4600:2018 [5], and EN 1993-1-3 [9] offer guidelines for the web crippling performance of CFCS sections. With the exception of AS/NZS 4600:2018 [5], which considers CFCS channel sections with unstiffened web holes, these guidelines predominantly focus on channel sections with plain webs. The research methodology developed for CFCS can be applied to investigate CFSS since the only difference in the numerical simulation of these channels lies in the material properties.

This thesis presents a detailed numerical investigation to study the web crippling strength and behaviour of CFSS channel sections with unstiffened and edge-stiffened web holes, loaded under two-flange loading conditions. The three most popular stainless-steel types i.e. EN 1.4509 (Ferritic), EN

1.4462 (Duplex) and EN 1.4301 (Austenitic) were used in this study. A total of 3744 FE models were considered for the parametric study to determine the ratio of inside bend radius to web thickness (*r/t*), the ratio of web flat depth to thickness (*h/t*), the ratio of hole diameter to web flat depth (*a/d*), the ratio of bearing length to web flat depth (*N/h*), the ratio of hole distance to web flat depth (*x/h*), the ratio of stiffener length to web flat depth (*q/h*), and the condition of the flange (fastened or unfastened) on web crippling capacity of CFSS channels. Based on the results of FEA, design recommendations in the form of web crippling strength reduction factors are proposed for CFSS channel sections with web holes under two-flange loading conditions. A reliability analysis was then performed, which showed that the proposed equations can closely predict the web crippling strength of CFSS channel sections with and without web holes under two-flange loading condition.

Chapter 2: Summary of experiments by Yousefi et. al [36] and Chen et. al. [7]

As stated in Chapter 1, no experimental tests specifically addressing web crippling strength under both ETF and ITF conditions for edge-stiffened web holes in CFSS channel sections were identified. Notably, Yousefi et al. [36] and Chen et al. [7] conducted experiments to examine the web crippling behaviour of CFSS channel sections with unstiffened web holes under ITF loading condition while Chen et al. investigated CFCS channel sections with edge-stiffened web holes under ITF and ETF loading conditions.

The experimental tests conducted by Yousefi et al. [36] focused on CFSS ferritic unlipped channel sections with plain webs and unstiffened web holes. The web holes were located at either centred or offset to the bearing plates and the ratio of the hole diameter to the depth of the flat portion of the webs was kept constant at 0.4. The tests considered both channels with fastened and unfastened flanges subjected to ITF loading conditions. The summary of the experimental tests and their web crippling strength results are presented in Table 2.

In the experimental study conducted by Chen et al. [7], CFCS channels with plain webs, unstiffened web holes, and edge-stiffened web holes were considered. These channels had both fastened and unfastened flanges and were subjected to both ITF and ETF loading conditions (see Figure 2.1 and Figure 2.2). All web holes had a nominal diameter of 90 mm and were located at the mid-depth and mid-length of the web. Details of the experimental tests, including web crippling strength results, are provided in Table 2.

Both experimental results were then used to validate the non-linear FE modelling techniques developed in the current research.

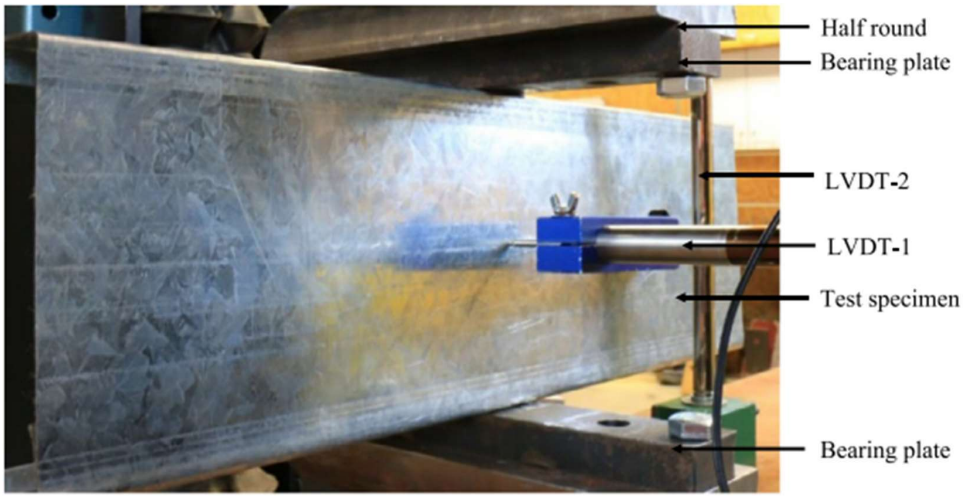

a. Interior-two-flange (ITF) loading conditions

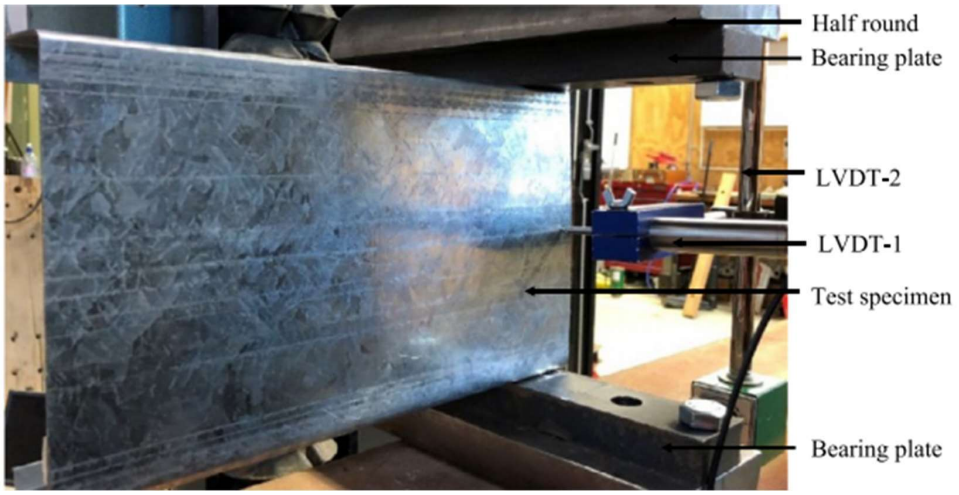

b. End-two-flange (ETF) loading conditions

Figure 2.1: Photographs of web crippling test under two-flange loading case by Chen et. al. [7]

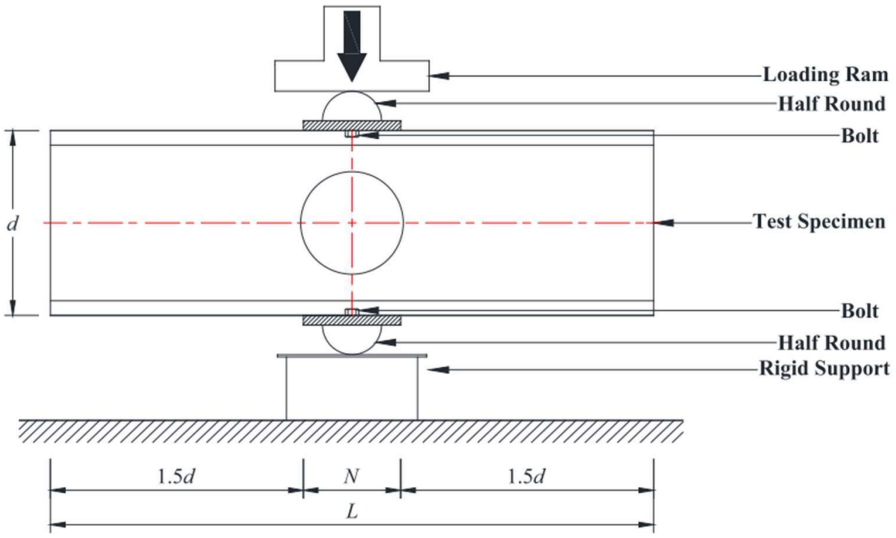

a. Interior-two-flange (ITF) loading conditions

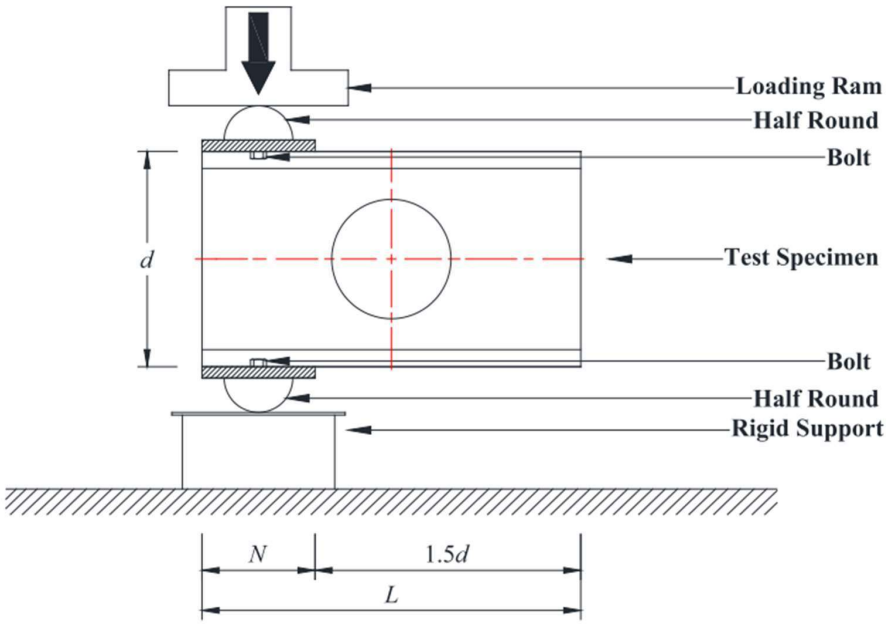

b. End-two-flange (ETF) loading conditions

Figure 2.1: Schematic front view of testing setup by Chen et. al. [7]

Chapter 3: Finite element analysis

3.1 General

ABAQUS [1] was used to develop nonlinear FE models to simulate the web crippling behaviour of CFSS channels with plain web, unstiffened web holes and edge-stiffened web holes under ITF and ETF loading conditions. It is to be noted that the modelling techniques used were similar for both load conditions.

3.2 Material modelling

Ferritic, duplex and austenitic stainless steel materials were selected in this study to follow the requirements of ASCE 8-02 [3]. Specifically, the material properties of EN 1.4509 (Ferritic), EN 1.4462 (Duplex) and EN 1.4301 (Austenitic) stainless steel were considered and summarized in Table 3.1.

Table 3.1: Material property summary

Property	Material		
	Ferritic stainless steel EN 1.4509	Duplex stainless steel EN 1.4462	Austenitic stainless steel EN 1.4301
f_y (MPa)	205	450	205
f_u (MPa)	597	860	825
E (GPa)	200	200	193
m	2.5	3.27	2.31
n	14	8	7

It should be noted that the enhanced material properties of the corners of the channels were not included in the FE model though it will bring higher strength material properties due to the cold-forming procedure. The reason for this is the effect of corner enhancements would offset the effect of residual stresses around the corners which was confirmed by Yousefi et al. [34] and Lian et. al. [21, 22].

Equations (1) and (2) were incorporated to convert the engineering stress-strain material curve to the true stress-strain material curve as outlined in the ABAQUS manual [1],

$$\sigma_{true} = \sigma(1 + \varepsilon) \quad (1)$$

$$\varepsilon_{true} = \ln(1 + \varepsilon) - \frac{\sigma_{true}}{E} \quad (2)$$

Where E is the Young's modulus, $\sigma_{true}, \varepsilon_{true}$, are the true stress and strain, and σ, ε are the engineering stress and strain.

3.3 Element and mesh size

S4R shell elements were utilized to model the CFSS channel sections, while solid C3R8 elements were chosen for the bearing plate. A mesh sensitivity analysis was performed, and mesh sizes of 5mm × 5mm and 10mm × 10mm were applied for the CFSS channel sections and bearing plates, respectively (see Figure 3.1). Finer mesh sizes were used around the web holes and rounded corners (see Figure 2b) to ensure accurate results from FEA.

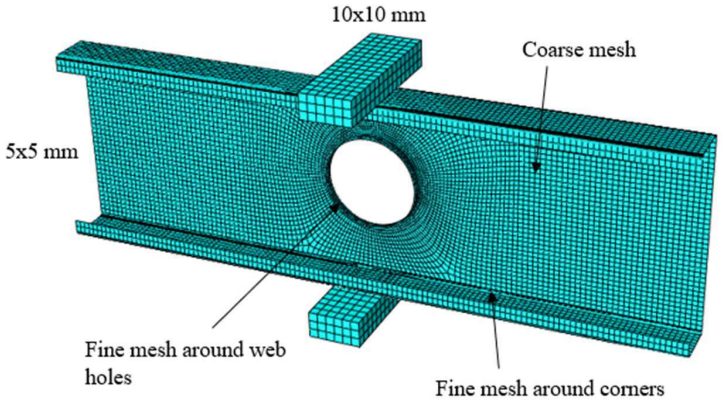

a. Interior-two-flange (ITF) loading condition

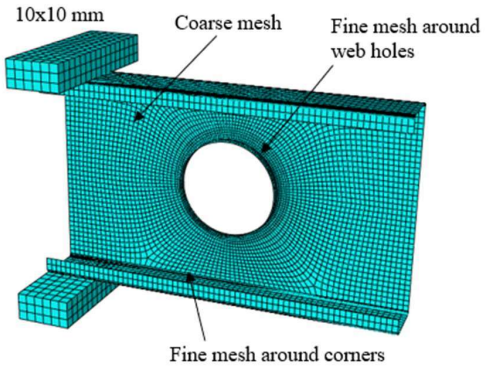

b. End-two-flange (ETF) loading condition

Figure 3.1: Meshing types used in FE models

3.4 Loading and boundary conditions

Surface-to-surface contact was used to model the interface between the bearing plates and the channel flanges. The bearing plates were defined as the master surface while the channel as the slave surface. These two contact surfaces were restricted from penetrating each other. A displacement of 10mm was applied to simulate the vertical load imposed on the channel (see Figure 3.2). To simulate the boundary condition, the top bearing plate was constrained in all degrees of freedom except in the y-direction, which corresponds to the direction of the applied displacement. Subsequently, the bottom bearing plate was restrained in all degrees of freedom.

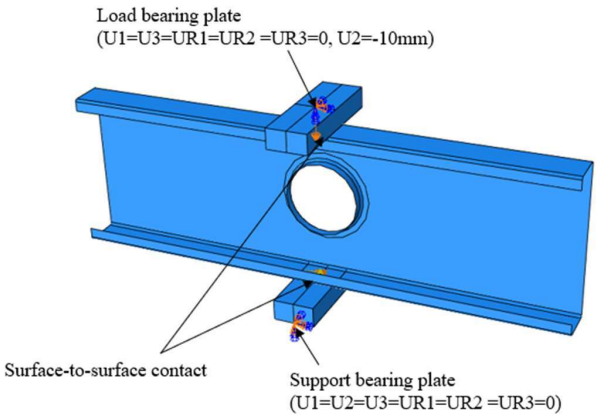

a. Interior-two-flange (ITF) loading condition

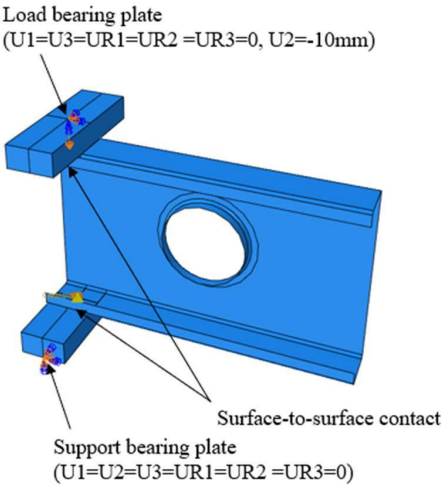

a. End-two-flange (ETF) loading condition

Figure 3.2: Boundary conditions used in FE models

3.5 Initial geometric imperfection and residual stresses

Effects of initial geometric imperfections and residual stresses were not included in FE models for this study. As confirmed by several research studies [5,10,11,14,19-26,28,30-33,35,37-39], geometric imperfection and residual stresses effect can be neglected in web crippling studies.

3.6 Validation of FE model

To validate the developed FE models, data from 48 experiments conducted by Chen et al. [7] and Yousefi et al. [36] were utilized. Tables 3.2a and 3.2b present a comparison of the web crippling strengths obtained from the experimental tests (P_{EXP}) [7, 36] and the FE model numerical results (P_{FEA}) in the current study for both ITF and ETF loading conditions, respectively. Figure 3.3 shows the dimension of the channel section used in the study. For the ITF loading condition, the mean value of the P_{EXP}/P_{FEA} ratio is 1.02 with a coefficient of variation (*COV*) of 0.03 for sections with un-fastened flanges and 0.98 with *COV* of 0.04 for sections with fastened flanges. While for the ETF loading

condition, the mean value of the P_{EXP}/P_{FEA} ratio is 0.95 with a *COV* of 0.04 for sections with un-fastened flanges, and 0.97 with *a COV* of 0.04 for sections with fastened flanges.

Figures 3.4 and 3.5 present the comparison of deformed shapes at failure between FE model analysis results and the experiments performed by Chen et. al [7] and Yousefi et. al [36] for ITF and ETF loading conditions, respectively. The comparison of load versus vertical displacement curves between the FE model analysis results and the literature [7, 36] is plotted in Figure 3.6. These validation results indicate that the developed FE models can accurately predict the web crippling strength of CFSS and CFCS channel sections under ITF and ETF loading conditions.

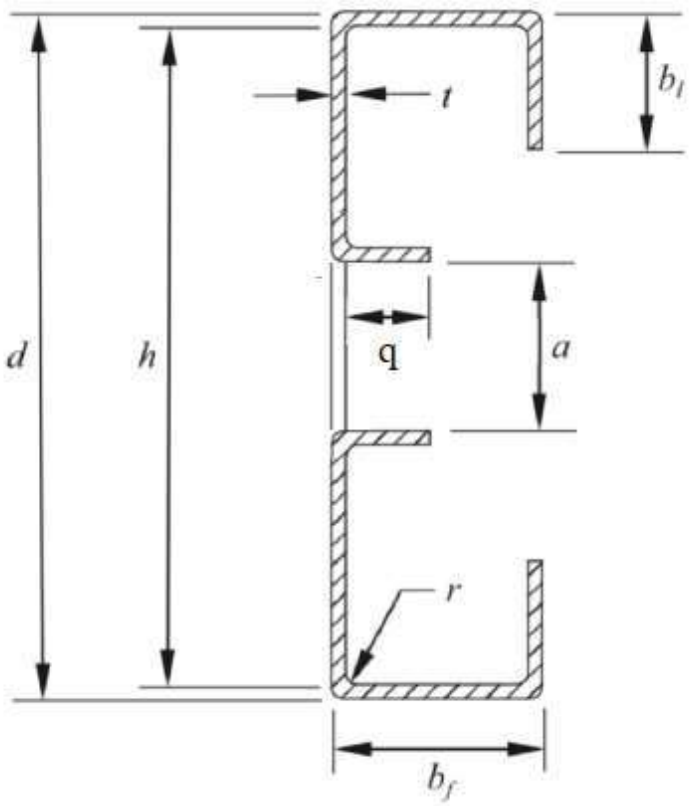

Figure 3.3: Section Dimension of the channels

Table 3.2: Comparison of experimental results and FEA results of sections from the literature [7, 36]

a. ITF Loading Condition

Specimen ID	Material	Web d (mm)	Flange bf (mm)	Lip bl (mm)	Bend Radius r (mm)	Thickness t (mm)	Bearing Length N (mm)	Hole Dia a (mm)	Stiffener length q (mm)	Fillet radius ri (mm)	Exp. Load P_{EXP} (kN)	FEA result P_{FEA} (kN)	P_{EXP} / P_{FEA}
Sections with un-fastened flanges													
1	Ferritic	203.86	74.99	0	1.2	1.09	50	0	0	0	3.4	3.44	0.99
2	Ferritic	203.62	75.01	0	1.2	1.08	50	78.92	0	0	3.03	3.05	0.99
3	Ferritic	203.44	75.02	0	1.2	1.08	75	0	0	0	3.49	3.56	0.98
4	Ferritic	203.53	75.06	0	1.2	1.06	75	78.9	0	0	3.06	3.00	1.02
5	Ferritic	203.64	74.99	0	1.2	1.12	100	0	0	0	4.16	4.08	1.02
6	Ferritic	203.73	75.02	0	1.2	1.09	100	78.93	0	0	3.47	3.33	1.04
7	CFCS	190.5	45.2	14.8	3	1.5	50	0	0	0	8.27	8.05	1.03
8	CFCS	190.3	45	15	3	1.5	75	0	0	0	8.78	8.74	1.00
9	CFCS	190.5	44.8	15.1	3	1.5	100	0	0	0	9.21	8.39	1.10
10	CFCS	190	45	14.9	3	1.5	50	90	0	0	6.45	6.38	1.01
11	CFCS	190.2	45.1	15.5	3	1.5	75	90	0	0	6.64	6.53	1.02
12	CFCS	190.5	45.5	15.5	3	1.5	100	90	0	0	6.89	6.70	1.03
13	CFCS	190.5	45.5	15	3	1.5	50	90	13	3	7.88	8.12	0.97
14	CFCS	190.1	45	14.8	3	1.5	75	90	13	3	8.29	8.20	1.01
15	CFCS	190.5	45.3	15.3	3	1.5	100	90	13	3	8.61	8.36	1.03
Average													**1.02**
COV													**0.03**

Specimen ID	Material	Web d (mm)	Flange bf (mm)	Lip bl (mm)	Bend Radius r (mm)	Thickness t (mm)	Bearing Length N (mm)	Hole Dia a (mm)	Stiffener length q (mm)	Fillet radius ri (mm)	Exp. Load P_{EXP} (kN)	FEA result P_{FEA} (kN)	P_{EXP} / P_{FEA}
Sections with fastened flanges													
16	Ferritic	203.68	75.05	0	1.2	1.13	50	0	0	0	6.32	6.34	1.00
17	Ferritic	203.62	75.13	0	1.2	1.1	50	78.95	0	0	5.11	5.10	1.00
18	Ferritic	203.63	75.49	0	1.2	1.14	75	0	0	0	6.53	6.90	0.95
19	Ferritic	203.78	75.04	0	1.2	1.13	75	78.92	0	0	5.42	5.77	0.94
20	Ferritic	203.61	75.21	0	1.2	1.14	100	0	0	0	6.61	7.04	0.94
21	Ferritic	203.47	75.04	0	1.2	1.12	100	78.9	0	0	5.52	5.81	0.95
22	CFCS	190.5	44.9	15	3	1.5	50	0	0	0	11.3	11.10	1.02
23	CFCS	189.5	45.3	14.8	3	1.5	75	0	0	0	11.82	12.64	0.94
24	CFCS	190.3	45.5	15.3	3	1.5	100	0	0	0	12.2	12.23	1.00
25	CFCS	189.7	45.3	15	3	1.5	50	90	0	0	8.62	8.59	1.00
26	CFCS	190.5	44.8	14.8	3	1.5	75	90	0	0	8.75	9.31	0.94
27	CFCS	190	45	15.3	3	1.5	100	90	0	0	8.92	9.35	0.95
28	CFCS	190	45	15	3	1.5	50	90	13	3	10.71	10.13	1.06
29	CFCS	190.5	44.6	15.3	3	1.5	75	90	13	3	11.23	10.99	1.02
30	CFCS	189.5	45.5	14.9	3	1.5	100	90	13	3	11.55	11.46	1.01
Average													**0.98**
COV													**0.04**

b. ETF Loading Condition

Specimen ID	Material	Web d (mm)	Flange bf (mm)	Lip bl (mm)	Bend Radius r (mm)	Thickness t (mm)	Bearing Length N (mm)	Hole Dia a (mm)	Stiffener length q (mm)	Fillet radius ri (mm)	Exp. Load P_{EXP} (kN)	FEA result P_{FEA} (kN)	P_{EXP} / P_{FEA}
Sections with un-fastened flanges													
31	Carbon Steel	190	45.1	15.2	3	1.5	50	0	0	0	2.56	2.70	0.95
32	Carbon Steel	189.8	45.5	14.8	3	1.5	75	0	0	0	2.77	2.96	0.94
33	Carbon Steel	190.5	44.9	15	3	1.5	100	0	0	0	3.08	3.33	0.92
34	Carbon Steel	189.5	44.9	15.2	3	1.5	50	90	0	0	1.98	2.20	0.90
35	Carbon Steel	190.3	45.5	15	3	1.5	75	90	0	0	2.2	2.45	0.90
36	Carbon Steel	189.7	44.8	14.8	3	1.5	100	90	0	0	2.45	2.55	0.96
37	Carbon Steel	189.8	44.8	14.9	3	1.5	50	90	13	3	2.72	2.74	0.99
38	Carbon Steel	190.2	45.2	15.2	3	1.5	75	90	13	3	3.08	3.13	0.98
39	Carbon Steel	190.5	45.5	15	3	1.5	100	90	13	3	3.41	3.51	0.97
Average													**0.95**
COV													**0.04**
Sections with fastened flanges													
40	Carbon Steel	189.8	45	15	3	1.5	50	0	0	0	4.34	4.66	0.93
41	Carbon Steel	190.2	44.8	14.7	3	1.5	75	0	0	0	4.72	4.71	1.00
42	Carbon Steel	190.6	44.9	15	3	1.5	100	0	0	0	5.48	5.86	0.93
43	Carbon Steel	189.5	45.5	15	3	1.5	50	90	0	0	3.44	3.69	0.93
44	Carbon Steel	190.5	44.8	14.9	3	1.5	75	90	0	0	3.75	3.99	0.94
45	Carbon Steel	190	45	15.1	3	1.5	100	90	0	0	4.31	4.57	0.94
46	Carbon Steel	190.3	45	14.8	3	1.5	50	90	13	3	4.61	4.74	0.97
47	Carbon Steel	190	44.9	15.2	3	1.5	75	90	13	3	5.03	4.96	1.01
48	Carbon Steel	189.7	45.3	15	3	1.5	100	90	13	3	5.87	5.73	1.02
Average													**0.97**
COV													**0.04**

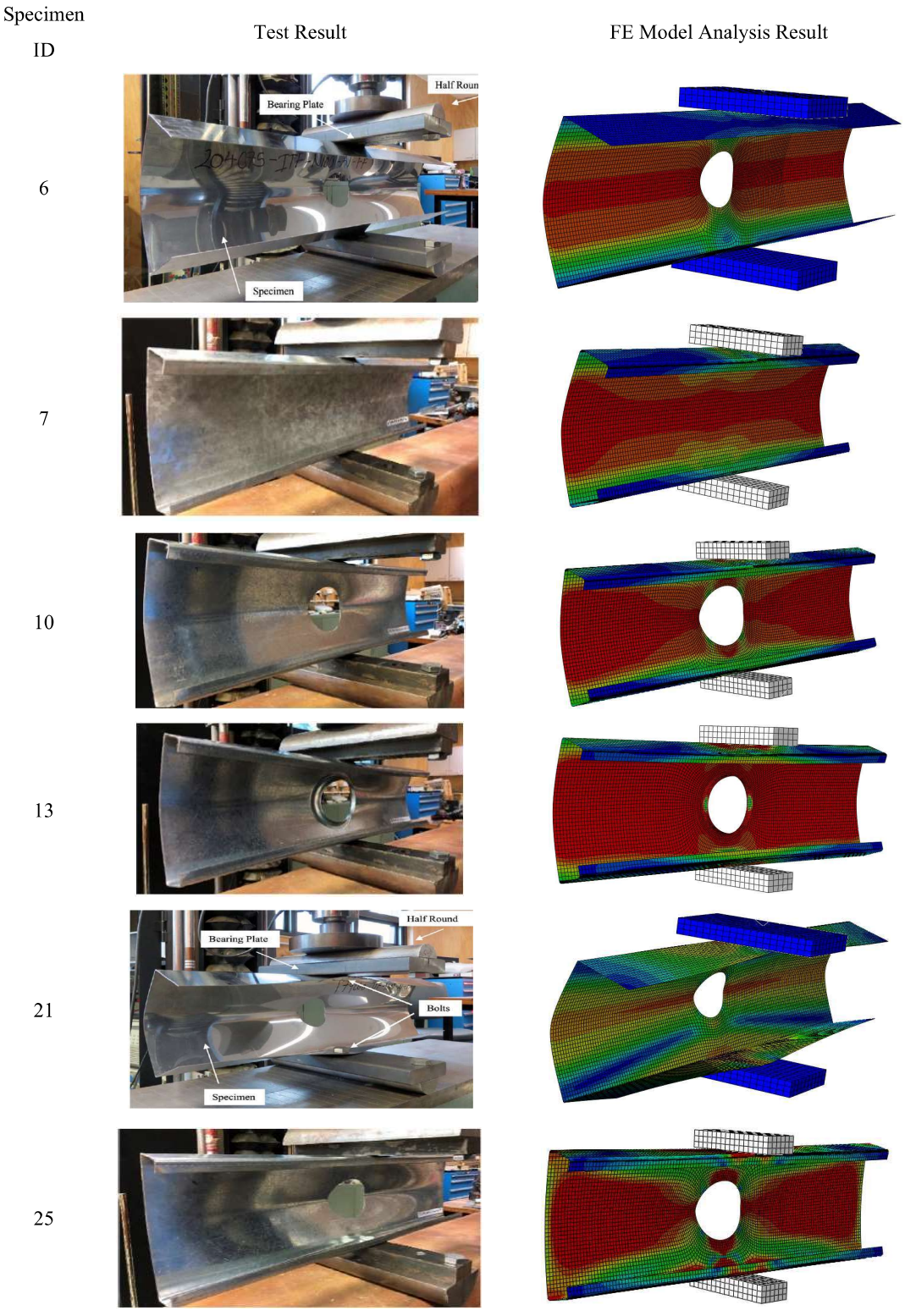

Figure 3.4: Comparison of deformed shapes at failure for ITF loading condition between FE model analysis results and the literature [7, 36]

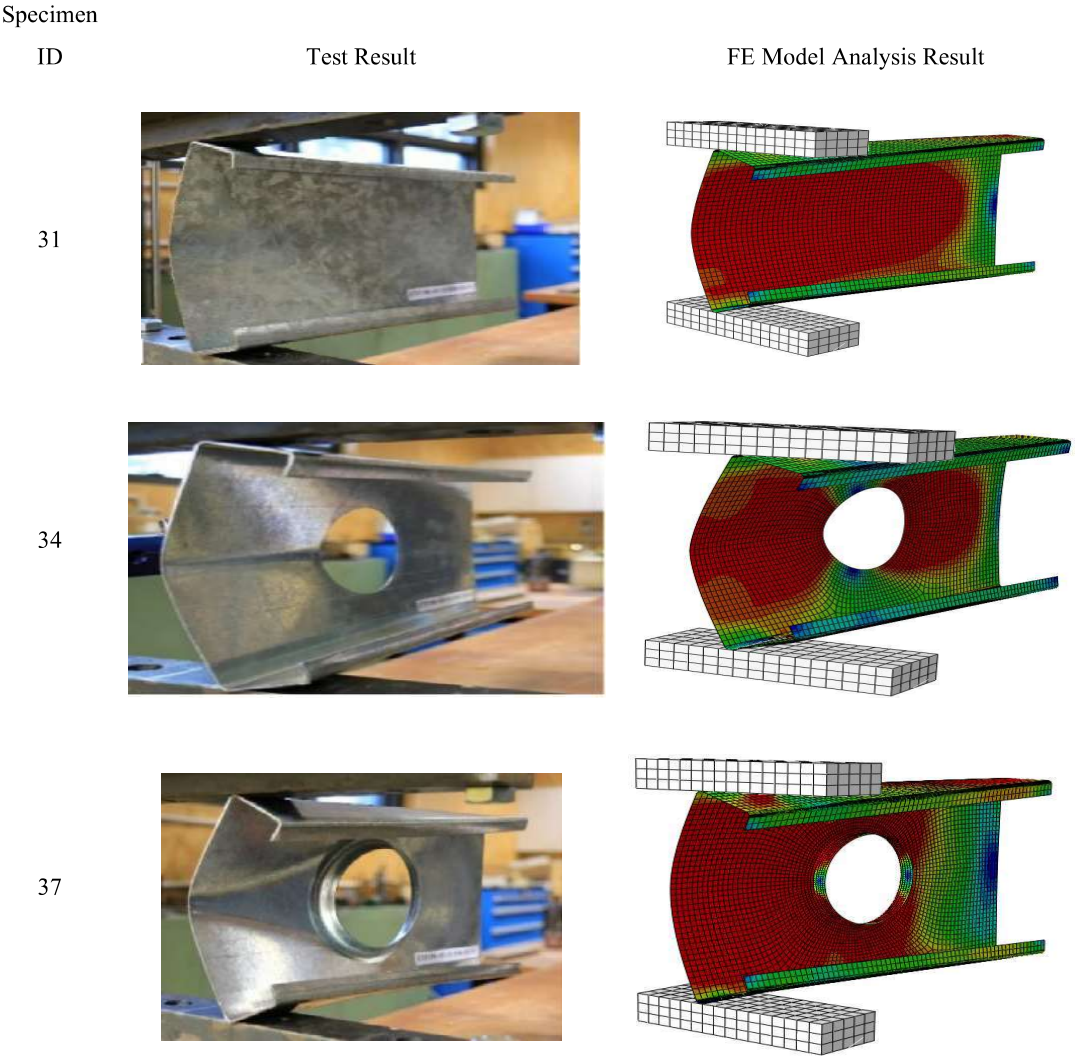

Figure 3.5: Comparison of deformed shapes at failure for ETF loading condition between FE model analysis results and the literature [7, 36]

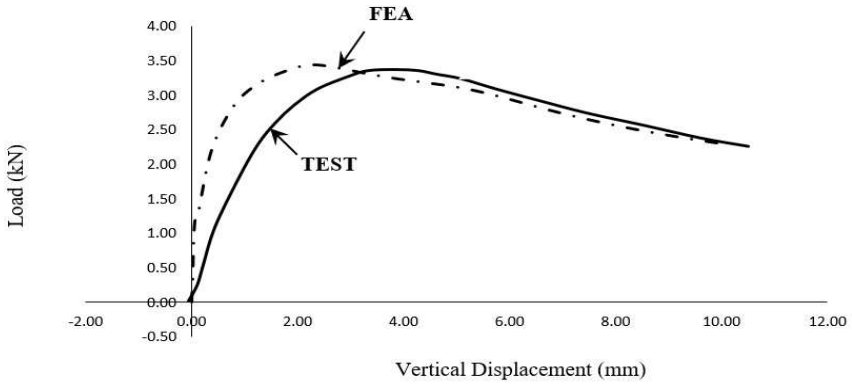

Specimen ID #1

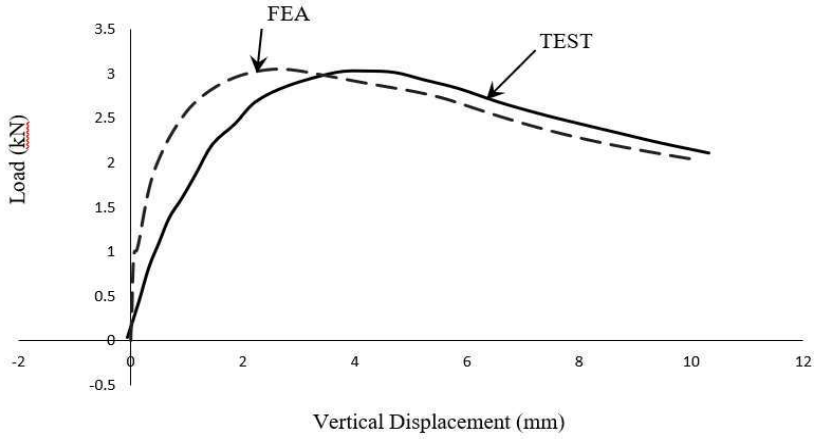

Specimen ID #2

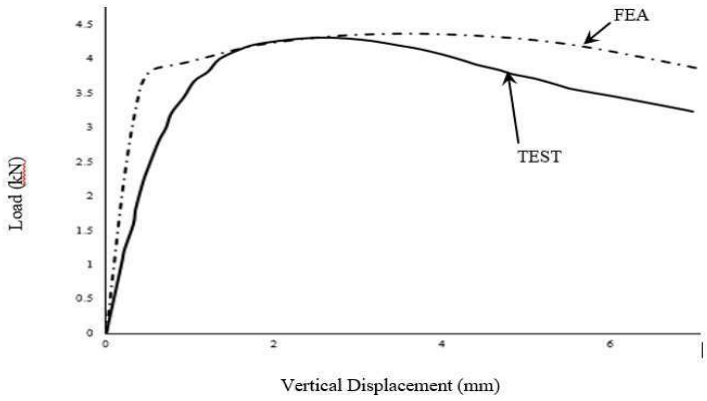

Specimen ID #40

Figure 3.6: Load versus vertical displacement curves between FE model analysis results and the literature [7, 36]

Chapter 4: Parametric study

4.1 General

Using the same Finite Element (FE) modelling techniques outlined in Chapter 3, an extensive parametric investigation was carried out to examine how edge-stiffened web holes affect the web crippling strength of CFSS channel sections under both ITF and ETF loading conditions. A total of 3744 FE models, varying in dimensions and thicknesses, were analysed for three grades of stainless steel: EN 1.4509 (Ferritic), EN 1.4462 (Duplex) and EN 1.4301 (Austenitic).

For this study, two channel sections referenced in literature [12] were employed to explore the influences of several factors with a parametric range taken from the industry. These factors include the ratio of inside bend radius to web thickness (r/t), the ratio of web flat depth to thickness (h/t), the ratio of hole diameter to web flat depth (a/h), ratio of bearing length to web flat depth (N/h), the ratio of hole distance to web flat depth (x/h), ratio of stiffener length to web flat depth (q/h), and the condition of the flange (fastened or unfastened) on the reduction factor of web crippling strength (R_p).

Table 4.1 outlines the various parameters considered, while Table 4.2 provides specific details and dimensions of the CFSS channel sections investigated in this study. The web crippling strength results for CFSS channel sections, encompassing plain webs, unstiffened web holes, and edge-stiffened web holes, as obtained from the FE analysis, are summarized in Tables 4.3a-4.3d and Tables 4.4a-4.4d for ITF and ETF loading conditions, respectively. Figure 4.1 illustrates the labelling of specimens in the parameter study.

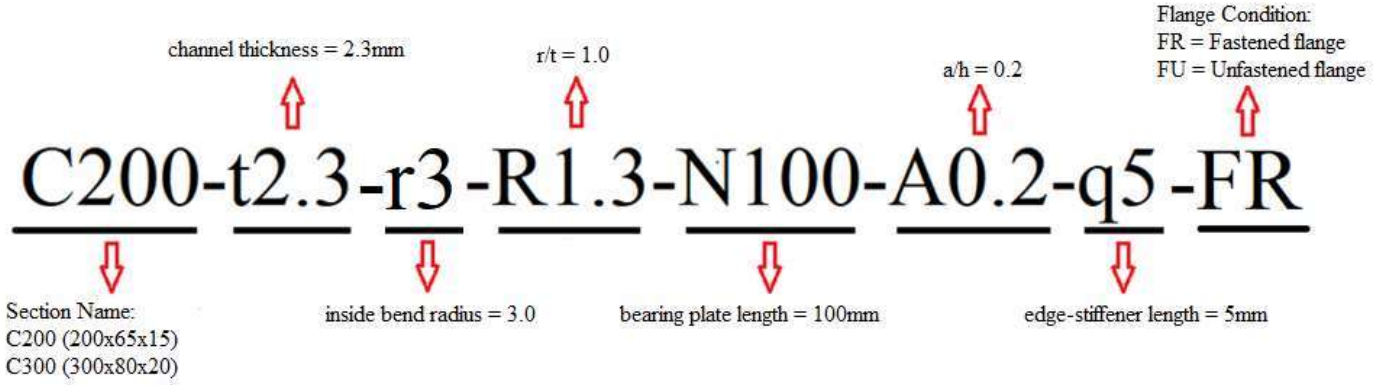

Figure 4.1: Specimen labelling for parametric study

Table 4.1: Different variables used in the parametric study.

Stainless Steel Material	Load Condition	Section	Flange condition	Inside bend radius *r* (mm)	The ratio of inside bend radius to thickness *R* (*r*/*t*)	The ratio of hole diameter to web flat depth *A* (*a*/*h*)	Bearing length *N* (mm)	Edge-stiffener length *q* (mm)
Austenitic, Duplex, Ferritic	ETF, ITF	200 x 65 x 15 300 x 80 x 20	Unfastened flange, Fastened flange	3, 4	1.3, 1.5, 2	0, 0.2, 0.4, 0.6	50, 100	0, 3, 5, 7

Table 4.2: Details of CFSS channel sections investigated in the parametric study.

Specimen Name	Section Name	Web d (mm)	Flange b_f (mm)	Lip b_l (mm)	Thickness t (mm)	Inside bend radius, r (mm)	Length, L [ITF] (mm)	Length, L [ETF] (mm)	Bearing plate, N (mm)
C200-t1.5-R2-N50	200x65x15	200	65	15	1.5	3.0	650	350	50
C200-t2-R1.5-N50	200x65x15	200	65	15	2.0	3.0	650	350	50
C200-t2.3-R1.3-N50	200x65x15	200	65	15	2.3	3.0	650	350	50
C200-t2-R2-N50	200x65x15	200	65	15	2.0	4.0	650	350	50
C200-t2.7-R1.5-N50	200x65x15	200	65	15	2.7	4.0	650	350	50
C200-t3.1-R1.3-N50	200x65x15	200	65	15	3.1	4.0	650	350	50
C200-t1.5-R2-N100	200x65x15	200	65	15	1.5	3.0	700	400	100
C200-t2-R1.5-N100	200x65x15	200	65	15	2.0	3.0	700	400	100
C200-t2.3-R1.3-N100	200x65x15	200	65	15	2.3	3.0	700	400	100
C200-t2-R2-N100	200x65x15	200	65	15	2.0	4.0	700	400	100
C200-t2.7-R1.5-N100	200x65x15	200	65	15	2.7	4.0	700	400	100
C200-t3.1-R1.3-N100	200x65x15	200	65	15	3.1	4.0	700	400	100
C300-t1.5-R2-N50	300x80x20	300	80	20	1.5	3.0	950	500	50
C300-t2-R1.5-N50	300x80x20	300	80	20	2.0	3.0	950	500	50
C300-t2.3-R1.3-N50	300x80x20	300	80	20	2.3	3.0	950	500	50
C300-t2-R2-N50	300x80x20	300	80	20	2.0	4.0	950	500	50
C300-t2.7-R1.5-N50	300x80x20	300	80	20	2.7	4.0	950	500	50
C300-t3.1-R1.3-N50	300x80x20	300	80	20	3.1	4.0	950	500	50
C300-t1.5-R2-N100	300x80x20	300	80	20	1.5	3.0	1000	550	100
C300-t2-R1.5-N100	300x80x20	300	80	20	2.0	3.0	1000	550	100
C300-t2.3-R1.3-N100	300x80x20	300	80	20	2.3	3.0	1000	550	100
C300-t2-R2-N100	300x80x20	300	80	20	2.0	4.0	1000	550	100
C300-t2.7-R1.5-N100	300x80x20	300	80	20	2.7	4.0	1000	550	100
C300-t3.1-R1.3-N100	300x80x20	300	80	20	3.1	4.0	1000	550	100

Table 4.3a: Web crippling predicted from FEA for CFSS channel sections with 200 x 65 x 15 unfastened flanges under ITF loading condition.

Specimen	Web crippling strength per web predicted from FEA, P_{FEA} (kN)													
	Austenitic					Duplex					Ferritic			
	Plain Web	Unstiffened web hole	Edge-stiffened web hole			Plain Web	Unstiffened web hole	Edge-stiffened web hole			Plain Web	Un-stiffened web hole	Edge-stiffened web hole		
			q = 3mm	*q* = 5mm	*q* = 7mm			*q* = 3mm	*q* = 5mm	*q* = 7mm			q = 3 mm	q = 5 mm	q = 7mm
C200-t1.5-R2-N50-A0.2-FU	6.1	5.8	5.9	6.1	11.4	8.0	7.7	7.9	8.2	16.5	6.2	5.9	6.1	6.2	11.7
C200-t1.5-R2-N50-A0.4-FU	6.1	5.2	5.3	5.7	10.8	8.0	7.1	7.2	7.8	16.1	6.2	5.3	5.4	5.8	11.0
C200-t1.5-R2-N50-A0.6-FU	6.1	4.3	4.4	4.8	9.2	8.0	6.1	6.3	6.8	13.7	6.2	4.4	4.5	4.9	9.4
C200-t1.5-R2-N100-A0.2-FU	6.5	6.2	6.3	6.4	12.0	8.6	8.3	8.5	8.7	17.5	6.6	6.3	6.4	6.6	12.2
C200-t1.5-R2-N100-A0.4-FU	6.5	5.5	5.7	6.1	11.6	8.6	7.6	7.8	8.3	17.1	6.6	5.7	5.8	6.2	11.8
C200-t1.5-R2-N100-A0.6-FU	6.5	4.7	4.9	5.2	10.0	8.6	6.7	6.9	7.3	14.9	6.6	4.8	5.0	5.3	10.2
C200-t2-R1.5-N50-A0.2-FU	12.2	11.5	11.7	12.1	22.4	17.0	16.1	16.4	17.0	33.6	12.5	11.7	12.0	12.3	22.6
C200-t2-R1.5-N50-A0.4-FU	12.2	10.1	10.3	10.9	20.2	17.0	14.4	14.7	15.4	30.8	12.5	10.3	10.5	11.1	20.5
C200-t2-R1.5-N50-A0.6-FU	12.2	8.2	8.5	9.0	17.0	17.0	11.9	12.3	13.0	25.5	12.5	8.4	8.7	9.2	17.3
C200-t2-R1.5-N100-A0.2-FU	13.0	12.2	12.4	12.8	23.5	18.1	17.0	17.3	18.0	35.1	13.3	12.4	12.7	13.1	23.8
C200-t2-R1.5-N100-A0.4-FU	13.0	10.8	11.1	11.6	21.8	18.1	15.4	15.7	16.5	32.7	13.3	11.0	11.3	11.8	22.2
C200-t2-R1.5-N100-A0.6-FU	13.0	9.1	9.4	9.9	18.8	18.1	13.1	13.5	14.2	27.9	13.3	9.2	9.5	10.1	19.1
C200-t2-R2-N50-A0.2-FU	11.5	10.7	10.9	11.3	11.4	16.4	15.6	15.9	16.4	16.5	11.7	10.9	11.0	11.6	11.7
C200-t2-R2-N50-A0.4-FU	11.5	9.5	9.7	10.1	10.8	16.4	14.0	14.3	15.0	16.1	11.7	9.6	9.8	10.3	11.0
C200-t2-R2-N50-A0.6-FU	11.5	7.8	8.0	8.4	9.2	16.4	11.6	12.0	12.7	13.7	11.7	7.9	8.2	8.6	9.4
C200-t2-R2-N100-A0.2-FU	12.1	11.4	11.6	11.9	12.0	17.5	16.5	16.8	17.4	17.5	12.3	11.6	11.8	12.2	12.2
C200-t2-R2-N100-A0.4-FU	12.1	10.1	10.3	10.8	11.6	17.5	15.0	15.3	16.0	17.1	12.3	10.3	10.5	11.0	11.8
C200-t2-R2-N100-A0.6-FU	12.1	8.5	8.8	9.2	10.0	17.5	12.7	13.1	13.8	14.9	12.3	8.7	8.9	9.4	10.2
C200-t2.3-R1.3-N50-A0.2-FU	16.9	15.8	16.0	16.5	29.6	24.2	22.6	22.9	23.8	45.8	17.2	16.1	16.3	16.8	29.9
C200-t2.3-R1.3-N50-A0.4-FU	16.9	13.8	14.1	14.7	26.7	24.2	20.0	20.3	21.2	41.3	17.2	14.0	14.3	15.0	27.1
C200-t2.3-R1.3-N50-A0.6-FU	16.9	11.2	11.6	12.2	22.6	24.2	16.3	16.8	17.6	34.1	17.2	11.5	11.8	12.4	23.0
C200-t2.3-R1.3-N100-A0.2-FU	18.0	16.8	17.0	17.6	31.6	25.3	23.9	24.2	25.0	48.1	18.3	17.1	17.3	18.0	32.1
C200-t2.3-R1.3-N100-A0.4-FU	18.0	14.8	15.1	15.8	29.0	25.3	21.4	21.8	22.6	44.1	18.3	15.1	15.4	16.1	29.5
C200-t2.3-R1.3-N100-A0.6-FU	18.0	12.4	12.8	13.4	25.0	25.3	17.9	18.4	19.3	37.5	18.3	12.6	13.0	13.7	25.4
C200-t2.7-R1.5-N50-A0.2-FU	22.4	20.8	21.1	22.2	22.4	34.0	31.5	31.8	33.0	33.6	22.7	21.1	21.5	22.5	22.6
C200-t2.7-R1.5-N50-A0.4-FU	22.4	18.2	18.5	19.1	20.2	34.0	27.6	28.1	29.1	30.8	22.7	18.5	18.8	19.4	20.5
C200-t2.7-R1.5-N50-A0.6-FU	22.4	15.0	15.3	16.0	17.0	34.0	22.4	23.0	24.0	25.5	22.7	15.2	15.6	16.2	17.3
C200-t2.7-R1.5-N100-A0.2-FU	23.8	22.2	22.5	23.2	23.5	35.3	33.2	33.5	34.6	35.1	24.2	22.6	22.8	23.6	23.8
C200-t2.7-R1.5-N100-A0.4-FU	23.8	19.6	20.0	20.7	21.8	35.3	29.6	30.0	31.0	32.7	24.2	20.0	20.3	21.0	22.2
C200-t2.7-R1.5-N100-A0.6-FU	23.8	16.5	16.9	17.6	18.8	35.3	24.7	25.3	26.4	27.9	24.2	16.8	17.2	17.9	19.1
C200-t3.1-R1.3-N50-A0.2-FU	29.6	28.0	28.4	29.4	29.6	46.8	43.2	43.6	44.9	45.8	29.9	28.5	28.8	29.8	29.9
C200-t3.1-R1.3-N50-A0.4-FU	29.6	24.4	24.7	25.4	26.7	46.8	37.5	38.1	39.3	41.3	29.9	24.7	25.0	25.8	27.1
C200-t3.1-R1.3-N50-A0.6-FU	29.6	20.1	20.6	21.3	22.6	46.8	30.4	31.1	32.4	34.1	29.9	20.5	20.9	21.6	23.0
C200-t3.1-R1.3-N100-A0.2-FU	32.1	30.0	30.2	31.1	31.6	48.7	45.5	45.9	47.3	48.1	32.6	30.5	30.7	31.6	32.1
C200-t3.1-R1.3-N100-A0.4-FU	32.1	26.4	26.8	27.6	29.0	48.7	40.2	40.8	42.0	44.1	32.6	26.9	27.2	28.0	29.5
C200-t3.1-R1.3-N100-A0.6-FU	32.1	22.3	22.8	23.7	25.0	48.7	33.5	34.3	35.6	37.5	32.6	22.7	23.2	24.1	25.4

Table 4.3b: Web crippling strength predicted from FEA for CFSS channel sections with 200 x 65 x 15 fastened flanges under ITF loading condition.

Specimen	Web crippling strength per web predicted from FEA, P_{FEA} (kN)														
	Austenitic					Duplex					Ferritic				
	Plain Web	Unstiffened web hole	Edge-stiffened web hole			Plain Web	Unstiffened web hole	Edge-stiffened web hole			Plain Web	Unstiffened web hole	Edge-stiffened web hole		
			q = 3mm	*q* = 5mm	*q* = 7mm			*q* = 3mm	*q* = 5mm	*q* = 7mm			q = 3 mm	q = 5 mm	q = 7mm
C200-t1.5-R2-N50-A0.2-FR	8.3	8.2	8.2	8.2	13.1	13.6	13.1	13.3	13.6	23.7	8.3	8.3	8.3	8.3	13.2
C200-t1.5-R2-N50-A0.4-FR	8.3	7.8	8.1	8.2	13.0	13.6	11.6	11.9	12.6	23.5	8.3	8.0	8.3	8.2	13.1
C200-t1.5-R2-N50-A0.6-FR	8.3	6.6	6.8	7.2	12.8	13.6	9.3	9.6	10.4	20.0	8.3	6.7	6.9	7.3	12.9
C200-t1.5-R2-N100-A0.2-FR	9.9	9.6	9.8	9.9	16.7	14.1	13.7	13.9	14.2	25.8	10.0	9.8	9.9	10.1	16.9
C200-t1.5-R2-N100-A0.4-FR	9.9	8.5	8.7	9.2	16.1	14.1	12.2	12.5	13.2	24.8	10.0	8.7	8.9	9.3	16.3
C200-t1.5-R2-N100-A0.6-FR	9.9	7.2	7.4	7.9	14.1	14.1	10.2	10.5	11.2	22.0	10.0	7.3	7.5	8.0	14.3
C200-t2-R1.5-N50-A0.2-FR	14.5	14.6	14.5	14.5	23.7	26.2	25.2	25.5	26.1	43.3	14.7	14.7	14.7	14.7	24.0
C200-t2-R1.5-N50-A0.4-FR	14.5	14.6	14.5	14.5	23.5	26.2	22.0	22.6	23.5	43.2	14.7	14.7	14.6	14.6	23.7
C200-t2-R1.5-N50-A0.6-FR	14.5	12.3	12.5	13.0	22.5	26.2	18.0	18.5	19.6	36.8	14.7	12.5	12.7	13.2	22.7
C200-t2-R1.5-N100-A0.2-FR	18.7	18.1	18.4	18.7	30.6	27.5	26.6	26.9	27.5	50.7	19.0	18.4	18.7	19.0	30.9
C200-t2-R1.5-N100-A0.4-FR	18.7	16.0	16.3	17.0	29.4	27.5	23.5	24.0	25.0	47.2	19.0	16.3	16.6	17.3	29.8
C200-t2-R1.5-N100-A0.6-FR	18.7	13.5	13.8	14.5	25.9	27.5	19.8	20.3	21.4	41.6	19.0	13.8	14.1	14.7	26.2
C200-t2-R2-N50-A0.2-FR	13.2	13.1	13.1	13.1	13.1	23.8	23.5	23.6	23.7	23.7	13.4	13.3	13.2	13.2	13.2
C200-t2-R2-N50-A0.4-FR	13.2	13.0	13.0	12.9	13.0	23.8	20.7	21.2	22.1	23.5	13.4	13.2	13.1	13.1	13.1
C200-t2-R2-N50-A0.6-FR	13.2	11.3	11.6	12.2	12.8	23.8	17.0	17.5	18.3	20.0	13.4	11.4	11.8	12.4	12.9
C200-t2-R2-N100-A0.2-FR	16.4	16.6	16.7	16.7	16.7	25.8	24.9	25.2	25.6	25.8	16.5	16.8	16.9	16.9	16.9
C200-t2-R2-N100-A0.4-FR	16.4	14.7	15.0	15.5	16.1	25.8	22.1	22.6	23.4	24.8	16.5	14.9	15.3	15.8	16.3
C200-t2-R2-N100-A0.6-FR	16.4	12.5	12.7	13.3	14.1	25.8	18.6	19.0	19.9	22.0	16.5	12.7	13.0	13.5	14.3
C200-t2.3-R1.3-N50-A0.2-FR	19.2	19.2	19.1	19.1	31.1	35.4	34.6	35.0	35.3	57.1	19.4	19.4	19.3	19.3	31.5
C200-t2.3-R1.3-N50-A0.4-FR	19.2	19.1	19.0	19.0	30.9	35.4	30.1	30.8	31.9	56.8	19.4	19.3	19.2	19.2	31.2
C200-t2.3-R1.3-N50-A0.6-FR	19.2	16.4	16.6	17.2	29.2	35.4	24.6	25.3	26.6	48.6	19.4	16.7	16.9	17.5	29.5
C200-t2.3-R1.3-N100-A0.2-FR	25.1	24.5	24.7	25.2	40.3	38.1	36.6	37.1	37.9	68.6	25.4	24.8	25.1	25.5	40.6
C200-t2.3-R1.3-N100-A0.4-FR	25.1	21.5	22.0	22.7	38.5	38.1	32.3	33.0	34.2	63.1	25.4	21.9	22.3	23.0	39.0
C200-t2.3-R1.3-N100-A0.6-FR	25.1	18.2	18.6	19.4	34.2	38.1	27.2	27.8	29.1	54.6	25.4	18.5	18.9	19.7	34.7
C200-t2.7-R1.5-N50-A0.2-FR	23.7	23.6	23.6	23.6	23.7	43.7	43.5	43.3	43.3	43.3	24.0	23.9	23.9	23.9	24.0
C200-t2.7-R1.5-N50-A0.4-FR	23.7	23.5	23.3	23.4	23.5	43.7	39.9	40.9	42.2	43.2	24.0	23.8	23.6	23.6	23.7
C200-t2.7-R1.5-N50-A0.6-FR	23.7	20.7	21.3	21.8	22.5	43.7	33.0	33.6	34.8	36.8	24.0	21.0	21.6	22.0	22.7
C200-t2.7-R1.5-N100-A0.2-FR	29.9	30.8	30.7	30.6	30.6	50.9	48.9	49.4	50.4	50.7	30.1	31.1	31.0	30.9	30.9
C200-t2.7-R1.5-N100-A0.4-FR	29.9	27.5	27.9	28.5	29.4	50.9	43.0	43.9	45.2	47.2	30.1	27.9	28.2	28.8	29.8
C200-t2.7-R1.5-N100-A0.6-FR	29.9	23.5	23.7	24.4	25.9	50.9	36.4	37.0	38.4	41.6	30.1	23.8	24.1	24.8	26.2
C200-t3.1-R1.3-N50-A0.2-FR	31.1	31.0	31.0	31.0	31.1	57.4	57.2	57.1	57.0	57.1	31.4	31.3	31.4	31.4	31.5
C200-t3.1-R1.3-N50-A0.4-FR	31.1	30.7	30.5	30.6	30.9	57.4	53.6	54.8	55.9	56.8	31.4	31.0	30.9	31.0	31.2
C200-t3.1-R1.3-N50-A0.6-FR	31.1	26.7	27.2	27.9	29.2	57.4	44.2	44.9	46.3	48.6	31.4	27.0	27.5	28.2	29.5
C200-t3.1-R1.3-N100-A0.2-FR	39.3	40.4	40.3	40.2	40.3	69.1	66.1	66.6	68.0	68.6	39.7	40.7	40.6	40.5	40.6
C200-t3.1-R1.3-N100-A0.4-FR	39.3	36.2	36.5	37.2	38.5	69.1	58.0	59.2	60.7	63.1	39.7	36.6	36.9	37.6	39.0
C200-t3.1-R1.3-N100-A0.6-FR	39.3	31.0	31.2	32.2	34.2	69.1	49.2	49.9	51.7	54.6	39.7	31.4	31.6	32.7	34.7

Table 4.3c: Web crippling strength predicted from FEA for CFSS channel sections with 300 x 80 x 20 unfastened flanges under ITF loading condition.

Specimen	Web crippling strength per web predicted from FEA, P_{FEA} (kN)													
	Austenitic					Duplex					Ferritic				
	Plain Web	Unstiffened web hole	Edge-stiffened web hole			Plain Web	Unstiffened web hole	Edge-stiffened web hole			Plain Web	Unstiffened web hole	Edge-stiffened web hole		
			q = 3mm	*q* = 5mm	*q* = 7mm			*q* = 3mm	*q* = 5mm	*q* = 7mm			q = 3 mm	q = 5 mm	q = 7mm
C300-t1.5-R2-N50-A0.2-FU	4.9	4.7	4.8	5.0	11.4	5.9	5.7	5.8	6.0	16.5	5.1	4.9	5.0	5.1	11.7
C300-t1.5-R2-N50-A0.4-FU	4.9	4.3	4.4	4.6	9.7	5.9	5.3	5.4	5.7	12.7	5.1	4.5	4.5	4.8	9.9
C300-t1.5-R2-N50-A0.6-FU	4.9	3.8	3.9	4.1	8.0	5.9	4.8	4.9	5.2	11.1	5.1	3.9	3.9	4.2	8.2
C300-t1.5-R2-N100-A0.2-FU	5.2	5.0	5.0	5.2	10.8	6.2	6.0	6.1	6.3	13.8	5.3	5.1	5.2	5.3	11.1
C300-t1.5-R2-N100-A0.4-FU	5.2	4.6	4.6	4.8	10.2	6.2	5.6	5.7	6.0	13.3	5.3	4.7	4.8	5.0	10.4
C300-t1.5-R2-N100-A0.6-FU	5.2	4.0	4.1	4.3	8.5	6.2	5.0	5.2	5.4	11.7	5.3	4.1	4.2	4.4	8.7
C300-t2-R2-N50-A0.2-FU	10.2	9.8	9.9	10.2	11.4	13.0	12.4	12.6	12.9	16.5	10.5	10.1	10.2	10.4	11.7
C300-t2-R2-N50-A0.4-FU	10.2	8.8	8.9	9.2	9.7	13.0	11.4	11.5	12.0	12.7	10.5	9.0	9.1	9.4	9.9
C300-t2-R2-N50-A0.6-FU	10.2	7.1	7.3	7.6	8.0	13.0	10.0	10.1	10.5	11.1	10.5	7.3	7.4	7.8	8.2
C300-t2-R2-N100-A0.2-FU	10.8	10.4	10.5	10.7	10.8	13.6	13.1	13.2	13.6	13.8	11.1	10.6	10.7	11.0	11.1
C300-t2-R2-N100-A0.4-FU	10.8	9.3	9.4	9.7	10.2	13.6	12.0	12.1	12.5	13.3	11.1	9.5	9.6	9.9	10.4
C300-t2-R2-N100-A0.6-FU	10.8	7.6	7.8	8.1	8.5	13.6	10.5	10.7	11.1	11.7	11.1	7.7	7.9	8.2	8.7
C300-t2-R1.5-N50-A0.2-FU	10.6	10.1	10.2	10.5	21.3	13.3	12.8	12.9	13.3	28.8	10.9	10.4	10.5	10.7	21.7
C300-t2-R1.5-N50-A0.4-FU	10.6	9.0	9.2	9.5	18.9	13.3	11.6	11.8	12.2	26.4	10.9	9.3	9.4	9.7	19.2
C300-t2-R1.5-N50-A0.6-FU	10.6	7.4	7.6	7.8	15.4	13.3	10.2	10.4	10.9	22.4	10.9	7.6	7.8	7.9	15.7
C300-t2-R1.5-N100-A0.2-FU	11.1	10.6	10.7	10.9	22.2	13.9	13.4	13.5	13.9	29.9	11.3	10.8	10.9	11.2	22.6
C300-t2-R1.5-N100-A0.4-FU	11.1	9.5	9.6	9.9	19.8	13.9	12.2	12.4	12.8	27.5	11.3	9.7	9.8	10.1	20.2
C300-t2-R1.5-N100-A0.6-FU	11.1	7.9	8.0	8.4	16.3	13.9	10.8	10.9	11.3	23.5	11.3	8.0	8.2	8.5	16.6
C300-t2.3-R1.3-N50-A0.2-FU	15.2	14.4	14.5	14.8	29.0	19.4	18.5	18.7	19.2	40.7	15.5	14.7	14.8	15.2	29.4
C300-t2.3-R1.3-N50-A0.4-FU	15.2	12.7	12.8	13.2	25.4	19.4	16.8	16.9	17.4	36.6	15.5	12.9	13.1	13.5	25.9
C300-t2.3-R1.3-N50-A0.6-FU	15.2	10.2	10.5	10.5	20.7	19.4	14.4	14.6	15.3	30.4	15.5	10.4	10.7	10.6	21.1
C300-t2.3-R1.3-N100-A0.2-FU	15.8	15.0	15.1	15.5	30.2	20.3	19.4	19.5	20.0	42.1	16.2	15.3	15.5	15.8	30.8
C300-t2.3-R1.3-N100-A0.4-FU	15.8	13.2	13.4	13.8	26.6	20.3	17.6	17.8	18.2	38.0	16.2	13.5	13.7	14.1	27.1
C300-t2.3-R1.3-N100-A0.6-FU	15.8	10.8	11.1	0.0	22.0	20.3	15.2	15.4	15.9	32.0	16.2	11.1	11.3	11.7	22.4
C300-t2.7-R1.5-N50-A0.2-FU	21.6	20.1	20.3	20.8	21.3	28.8	27.4	27.6	28.2	28.8	22.0	20.5	20.7	21.2	21.7
C300-t2.7-R1.5-N50-A0.4-FU	21.6	17.5	17.7	18.2	18.9	28.8	24.6	24.8	25.4	26.4	22.0	17.8	18.1	18.5	19.2
C300-t2.7-R1.5-N50-A0.6-FU	21.6	14.0	14.2	14.8	15.4	28.8	20.5	20.9	21.6	22.4	22.0	14.3	14.5	15.1	15.7
C300-t2.7-R1.5-N100-A0.2-FU	22.5	21.1	21.3	21.7	22.2	29.9	28.5	28.7	29.3	29.9	22.9	21.5	21.7	22.2	22.6
C300-t2.7-R1.5-N100-A0.4-FU	22.5	18.4	18.7	19.0	19.8	29.9	25.7	25.9	26.3	27.5	22.9	18.7	19.0	19.4	20.2
C300-t2.7-R1.5-N100-A0.6-FU	22.5	14.8	15.1	15.6	16.3	29.9	21.6	22.0	22.6	23.5	22.9	15.1	15.4	15.9	16.6
C300-t3.1-R1.3-N50-A0.2-FU	29.3	27.6	27.8	28.4	29.0	41.1	38.9	39.1	39.8	40.7	29.6	28.1	28.3	28.9	29.4
C300-t3.1-R1.3-N50-A0.4-FU	29.3	23.8	24.1	24.6	25.4	41.1	34.4	34.7	35.4	36.6	29.6	24.2	24.5	25.0	25.9
C300-t3.1-R1.3-N50-A0.6-FU	29.3	19.1	19.3	20.0	20.7	41.1	27.9	28.4	29.3	30.4	29.6	19.4	19.7	20.4	21.1
C300-t3.1-R1.3-N100-A0.2-FU	30.8	28.8	28.9	29.6	30.2	42.7	40.3	40.5	41.3	42.1	31.4	29.3	29.5	30.1	30.8
C300-t3.1-R1.3-N100-A0.4-FU	30.8	24.9	25.2	25.7	26.6	42.7	35.9	36.2	36.7	38.0	31.4	25.4	25.7	26.1	27.1
C300-t3.1-R1.3-N100-A0.6-FU	30.8	20.2	20.5	21.2	22.0	42.7	29.5	30.0	30.9	32.0	31.4	20.5	20.9	21.6	22.4

Table 4.3d: Web crippling strength predicted from FEA for CFSS channel sections with 300 x 80 x 20 fastened flanges under ITF loading condition.

Specimen	Web crippling strength per web predicted from FEA, P_{FEA} (kN)														
	Austenitic					Duplex					Ferritic				
	Plain Web	Unstiffened web hole	Edge-stiffened web hole			Plain Web	Unstiffened web hole	Edge-stiffened web hole			Plain Web	Unstiffened web hole	Edge-stiffened web hole		
			q = 3mm	*q* = 5mm	*q* = 7mm			*q* = 3mm	*q* = 5mm	*q* = 7mm			q = 3 mm	q = 5 mm	q = 7mm
C300-t1.5-R2-N50-A0.2-FR	8.0	7.8	7.9	7.9	13.1	11.1	10.7	10.8	11.2	23.7	8.1	7.9	8.0	8.0	13.2
C300-t1.5-R2-N50-A0.4-FR	8.0	7.1	7.2	7.5	12.7	11.1	9.7	9.9	10.3	20.3	8.1	7.2	7.3	7.6	12.9
C300-t1.5-R2-N50-A0.6-FR	8.0	5.8	6.0	6.3	11.9	11.1	8.2	8.4	8.8	16.8	8.1	5.9	6.1	6.4	12.1
C300-t1.5-R2-N100-A0.2-FR	8.8	8.5	8.5	8.7	17.0	11.6	11.1	11.2	11.6	23.3	9.0	8.6	8.7	8.9	17.3
C300-t1.5-R2-N100-A0.4-FR	8.8	7.5	7.7	7.9	15.8	11.6	10.1	10.3	10.7	21.8	9.0	7.7	7.8	8.1	16.1
C300-t1.5-R2-N100-A0.6-FR	8.8	6.1	6.3	6.6	13.9	11.6	8.5	8.8	9.2	19.2	9.0	6.2	6.4	6.8	14.2
C300-t2-R2-N50-A0.2-FR	12.9	12.8	12.8	12.7	13.1	21.4	20.7	20.8	21.3	23.7	13.1	0.7	13.0	12.9	13.2
C300-t2-R2-N50-A0.4-FR	12.9	12.7	12.7	12.7	12.7	21.4	18.5	18.7	19.3	20.3	13.1	12.9	12.8	12.9	12.9
C300-t2-R2-N50-A0.6-FR	12.9	10.6	10.8	11.2	11.9	21.4	15.0	15.3	16.0	16.8	13.1	10.8	11.0	11.5	12.1
C300-t2-R2-N100-A0.2-FR	17.1	16.4	16.5	16.8	17.0	23.3	22.3	22.5	23.0	23.3	17.5	16.7	16.9	17.2	17.3
C300-t2-R2-N100-A0.4-FR	17.1	14.4	14.6	15.1	15.8	23.3	19.9	20.1	20.7	21.8	17.5	14.7	14.9	15.4	16.1
C300-t2-R2-N100-A0.6-FR	17.1	11.8	12.2	12.7	13.9	23.3	16.3	16.7	17.4	19.2	17.5	12.1	12.4	13.0	14.2
C300-t2-R1.5-N50-A0.2-FR	14.3	14.2	14.2	14.3	23.3	22.4	21.4	21.6	22.1	41.8	14.5	14.4	14.4	14.4	23.6
C300-t2-R1.5-N50-A0.4-FR	14.3	13.5	13.7	14.1	23.3	22.4	19.1	19.3	19.9	39.2	14.5	13.7	14.0	14.3	23.6
C300-t2-R1.5-N50-A0.6-FR	14.3	11.1	11.4	11.9	22.2	22.4	15.4	15.8	16.5	32.4	14.5	11.4	11.7	12.2	22.6
C300-t2-R1.5-N100-A0.2-FR	17.1	16.4	16.5	16.8	33.6	23.3	22.3	22.5	23.0	47.4	17.5	16.7	16.9	17.2	34.2
C300-t2-R1.5-N100-A0.4-FR	17.1	14.4	14.6	15.1	30.3	23.3	19.9	20.1	20.7	42.9	17.5	14.7	14.9	15.4	30.8
C300-t2-R1.5-N100-A0.6-FR	17.1	11.8	12.2	12.7	25.7	23.3	16.3	16.7	17.4	36.7	17.5	12.1	12.4	13.0	26.2
C300-t2.3-R1.3-N50-A0.2-FR	19.0	18.9	18.9	18.9	30.7	31.3	29.9	30.1	30.7	55.5	19.1	19.1	19.1	19.1	31.1
C300-t2.3-R1.3-N50-A0.4-FR	19.0	18.4	18.6	18.9	30.8	31.3	26.3	26.7	27.4	53.0	19.1	18.8	18.9	19.1	31.1
C300-t2.3-R1.3-N50-A0.6-FR	19.0	15.3	15.6	16.2	29.3	31.3	21.2	21.7	22.6	43.9	19.1	15.6	15.9	16.5	29.8
C300-t2.3-R1.3-N100-A0.2-FR	23.7	22.6	22.7	23.1	45.4	32.6	31.1	31.3	31.9	65.4	24.1	23.0	23.2	23.6	46.2
C300-t2.3-R1.3-N100-A0.4-FR	23.7	19.7	20.0	20.6	40.6	32.6	27.4	27.8	28.5	58.5	24.1	20.1	20.4	21.0	41.3
C300-t2.3-R1.3-N100-A0.6-FR	23.7	16.2	16.7	17.4	34.6	32.6	22.4	23.0	24.0	49.7	24.1	16.6	17.0	17.7	35.3
C300-t2.7-R1.5-N50-A0.2-FR	23.4	23.3	23.3	23.3	23.3	41.9	41.3	41.4	41.6	41.8	23.7	23.6	23.6	23.6	23.6
C300-t2.7-R1.5-N50-A0.4-FR	23.4	23.3	23.2	23.3	23.3	41.9	36.3	36.8	37.7	39.2	23.7	23.6	23.5	23.6	23.6
C300-t2.7-R1.5-N50-A0.6-FR	23.4	20.5	20.9	21.6	22.2	41.9	29.4	30.0	31.0	32.4	23.7	20.9	21.3	22.0	22.6
C300-t2.7-R1.5-N100-A0.2-FR	34.0	32.4	32.6	33.2	33.6	47.9	45.4	45.7	46.5	47.4	34.6	33.0	33.3	33.9	34.2
C300-t2.7-R1.5-N100-A0.4-FR	34.0	28.1	28.6	29.3	30.3	47.9	39.7	40.3	41.3	42.9	34.6	28.6	29.1	29.8	30.8
C300-t2.7-R1.5-N100-A0.6-FR	34.0	23.2	23.8	24.7	25.7	47.9	32.6	33.4	34.7	36.7	34.6	23.6	24.2	25.1	26.2
C300-t3.1-R1.3-N50-A0.2-FR	30.9	30.8	30.7	30.7	30.7	55.9	55.6	55.6	55.5	55.5	31.2	31.2	31.1	31.1	31.1
C300-t3.1-R1.3-N50-A0.4-FR	30.9	30.7	30.6	30.7	30.8	55.9	49.5	50.1	51.4	53.0	31.2	31.1	31.0	31.1	31.1
C300-t3.1-R1.3-N50-A0.6-FR	30.9	27.4	27.9	28.7	29.3	55.9	40.3	41.0	42.3	43.9	31.2	27.9	28.5	29.2	29.8
C300-t3.1-R1.3-N100-A0.2-FR	45.7	43.8	44.1	44.9	45.4	66.6	62.7	63.2	64.2	65.4	46.2	44.6	44.9	45.7	46.2
C300-t3.1-R1.3-N100-A0.4-FR	45.7	37.9	38.5	39.4	40.6	66.6	54.6	55.3	56.7	58.5	46.2	38.6	39.2	40.1	41.3
C300-t3.1-R1.3-N100-A0.6-FR	45.7	31.3	32.1	33.2	34.6	66.6	44.7	45.8	47.6	49.7	46.2	31.9	32.7	33.8	35.3

Table 4.4a: Web crippling strength predicted from FEA for CFSS channel sections with 200 x 65 x 15 unfastened flanges under ETF loading condition

Specimen	Web crippling strength per web predicted from FEA, P_{FEA} (kN)														
	Austenitic					Duplex					Ferritic				
	Plain Web	Unstiffened web hole	Edge-stiffened web hole			Plain Web	Unstiffened web hole	Edge-stiffened web hole			Plain Web	Unstiffened web hole	Edge-stiffened web hole		
			q = 3mm	*q* = 5mm	*q* = 7mm			*q* = 3mm	*q* = 5mm	*q* = 7mm			q = 3 mm	q = 5 mm	q = 7mm
C200-t1.5-R2-N50-A0.2-FU	2.2	2.1	2.2	2.2	4.3	2.8	2.6	2.8	2.9	6.0	2.2	2.1	2.2	2.3	4.4
C200-t1.5-R2-N50-A0.4-FU	2.2	1.9	2.0	2.3	4.4	2.8	2.4	2.5	3.0	6.3	2.2	1.9	2.0	2.3	4.5
C200-t1.5-R2-N50-A0.6-FU	2.2	1.6	1.8	2.1	4.2	2.8	2.0	2.2	2.9	6.1	2.2	1.6	1.8	2.2	4.3
C200-t1.5-R2-N100-A0.2-FU	2.8	2.7	2.8	2.9	5.5	3.6	3.4	3.6	3.7	7.7	2.9	2.7	2.9	3.0	5.6
C200-t1.5-R2-N100-A0.4-FU	2.8	2.4	2.6	2.9	5.7	3.6	3.1	3.3	3.8	8.1	2.9	2.5	2.7	3.0	5.8
C200-t1.5-R2-N100-A0.6-FU	2.8	2.2	2.3	2.8	5.5	3.6	2.7	3.0	3.7	7.9	2.9	2.2	2.4	2.9	5.6
C200-t2-R2-N50-A0.2-FU	4.2	4.0	4.2	4.3	4.3	5.8	5.4	5.6	5.9	6.0	4.3	4.1	4.3	4.4	4.4
C200-t2-R2-N50-A0.4-FU	4.2	3.6	3.8	4.2	4.4	5.8	4.9	5.1	5.7	6.3	4.3	3.7	3.9	4.3	4.5
C200-t2-R2-N50-A0.6-FU	4.2	3.1	3.3	3.8	4.2	5.8	4.2	4.4	5.2	6.1	4.3	3.2	3.4	3.8	4.3
C200-t2-R2-N100-A0.2-FU	5.4	5.2	5.3	5.5	5.5	7.5	7.1	7.3	7.6	7.7	5.5	5.3	5.4	5.6	5.6
C200-t2-R2-N100-A0.4-FU	5.4	4.7	4.9	5.4	5.7	7.5	6.4	6.6	7.3	8.1	5.5	4.8	5.0	5.5	5.8
C200-t2-R2-N100-A0.6-FU	5.4	4.2	4.4	4.9	5.5	7.5	5.6	5.9	6.8	7.9	5.5	4.3	4.5	5.0	5.6
C200-t2-R1.5-N50-A0.2-FU	4.6	4.3	4.5	4.6	8.9	6.0	5.7	5.9	6.2	12.6	4.7	4.4	4.6	4.7	9.0
C200-t2-R1.5-N50-A0.4-FU	4.6	3.9	4.1	4.5	8.8	6.0	5.1	5.3	6.0	12.6	4.7	4.0	4.2	4.6	8.9
C200-t2-R1.5-N50-A0.6-FU	4.6	3.4	3.6	4.1	8.2	6.0	4.4	4.7	5.5	11.6	4.7	3.5	3.7	4.2	8.3
C200-t2-R1.5-N100-A0.2-FU	5.9	5.6	5.8	6.0	11.4	7.9	7.4	7.7	8.0	16.3	6.0	5.8	6.0	6.1	11.6
C200-t2-R1.5-N100-A0.4-FU	5.9	5.1	5.4	5.9	11.4	7.9	6.7	7.0	7.8	16.5	6.0	5.3	5.5	6.0	11.6
C200-t2-R1.5-N100-A0.6-FU	5.9	4.5	4.8	5.4	10.8	7.9	5.9	6.3	7.2	15.5	6.0	4.6	4.9	5.5	11.0
C200-t2.3-R1.3-N50-A0.2-FU	6.4	6.1	6.3	6.5	12.2	8.7	8.2	8.5	8.8	17.7	6.6	6.3	6.5	6.6	12.4
C200-t2.3-R1.3-N50-A0.4-FU	6.4	5.6	5.8	6.3	12.0	8.7	7.3	7.6	8.4	17.4	6.6	5.7	5.9	6.4	12.2
C200-t2.3-R1.3-N50-A0.6-FU	6.4	4.8	5.1	5.7	11.1	8.7	6.3	6.7	7.6	16.0	6.6	4.9	5.2	5.8	11.3
C200-t2.3-R1.3-N100-A0.2-FU	8.4	8.0	8.3	8.5	15.9	11.4	10.7	11.0	11.4	23.1	8.6	8.2	8.4	8.6	16.1
C200-t2.3-R1.3-N100-A0.4-FU	8.4	7.3	7.6	8.2	15.7	11.4	9.7	10.1	11.0	22.9	8.6	7.5	7.8	8.4	15.9
C200-t2.3-R1.3-N100-A0.6-FU	8.4	6.4	6.8	7.5	14.6	11.4	8.6	9.0	10.1	21.3	8.6	6.6	6.9	7.7	14.9
C200-t2.7-R1.5-N50-A0.2-FU	8.8	8.4	8.6	8.8	8.9	12.5	11.7	12.0	12.5	12.6	8.9	8.5	8.7	9.0	9.0
C200-t2.7-R1.5-N50-A0.4-FU	8.8	7.6	7.8	8.3	8.8	12.5	10.5	10.9	11.7	12.6	8.9	7.7	8.0	8.5	8.9
C200-t2.7-R1.5-N50-A0.6-FU	8.8	6.6	6.9	7.5	8.2	12.5	9.1	9.5	10.4	11.6	8.9	6.7	7.0	7.6	8.3
C200-t2.7-R1.5-N100-A0.2-FU	11.3	10.8	11.1	11.3	11.4	16.1	15.2	15.6	16.1	16.3	11.5	11.0	11.3	11.5	11.6
C200-t2.7-R1.5-N100-A0.4-FU	11.3	9.9	10.2	10.8	11.4	16.1	13.9	14.3	15.3	16.5	11.5	10.0	10.4	11.0	11.6
C200-t2.7-R1.5-N100-A0.6-FU	11.3	8.7	9.1	9.8	10.8	16.1	12.3	12.7	13.8	15.5	11.5	8.8	9.2	10.0	11.0
C200-t3.1-R1.3-N50-A0.2-FU	12.1	11.7	11.9	12.1	12.2	17.6	16.5	16.9	17.4	17.7	12.3	11.9	12.1	12.3	12.4
C200-t3.1-R1.3-N50-A0.4-FU	12.1	10.6	10.9	11.4	12.0	17.6	14.9	15.4	16.4	17.4	12.3	10.8	11.1	11.6	12.2
C200-t3.1-R1.3-N50-A0.6-FU	12.1	9.2	9.6	10.2	11.1	17.6	13.0	13.5	14.6	16.0	12.3	9.4	9.7	10.4	11.3
C200-t3.1-R1.3-N100-A0.2-FU	15.7	15.1	15.4	15.7	15.9	22.7	21.7	22.1	22.8	23.1	16.0	15.3	15.7	16.0	16.1
C200-t3.1-R1.3-N100-A0.4-FU	15.7	13.7	14.2	14.9	15.7	22.7	19.8	20.3	21.4	22.9	16.0	14.0	14.4	15.1	15.9
C200-t3.1-R1.3-N100-A0.6-FU	15.7	12.0	12.5	13.4	14.6	22.7	17.5	18.0	19.3	21.3	16.0	12.3	12.8	13.7	14.9

Table 4.4b: Web crippling strength predicted from FEA for CFSS channel sections with 200 x 65 x 15 fastened flanges under ETF loading condition.

Specimen	Web crippling strength per web predicted from FEA, P_{FEA} (kN)													
	Austenitic					Duplex					Ferritic				
	Plain Web	Unstiffened web hole	Edge-stiffened web hole			Plain Web	Unstiffened web hole	Edge-stiffened web hole			Plain Web	Unstiffened web hole	Edge-stiffened web hole		
			q = 3mm	*q* = 5mm	*q* = 7mm			*q* = 3mm	*q* = 5mm	*q* = 7mm			q = 3 mm	q = 5 mm	q = 7mm
C200-t1.5-R2-N50-A0.2-FR	3.9	3.8	3.9	3.9	6.8	5.4	5.3	5.5	5.6	10.3	4.0	3.9	4.0	4.0	6.9
C200-t1.5-R2-N50-A0.4-FR	3.9	3.6	3.7	3.9	6.6	5.4	5.0	5.3	5.7	10.5	4.0	3.6	3.8	3.9	6.7
C200-t1.5-R2-N50-A0.6-FR	3.9	3.3	3.4	3.6	6.4	5.4	4.6	4.9	5.3	9.9	4.0	3.4	3.5	3.7	6.5
C200-t1.5-R2-N100-A0.2-FR	5.3	5.2	5.3	5.3	9.2	7.4	7.3	7.5	7.6	14.1	5.4	5.3	5.4	5.4	9.4
C200-t1.5-R2-N100-A0.4-FR	5.3	5.0	5.2	5.3	9.2	7.4	6.9	7.3	7.8	14.3	5.4	5.1	5.3	5.4	9.4
C200-t1.5-R2-N100-A0.6-FR	5.3	4.7	4.9	5.2	9.2	7.4	6.5	7.0	7.6	14.3	5.4	4.8	5.0	5.3	9.4
C200-t2-R2-N50-A0.2-FR	6.8	6.6	6.7	6.7	6.8	10.2	9.9	10.1	10.3	10.3	6.9	6.8	6.8	6.8	6.9
C200-t2-R2-N50-A0.4-FR	6.8	6.3	6.4	6.6	6.6	10.2	9.3	9.6	10.0	10.5	6.9	6.4	6.5	6.7	6.7
C200-t2-R2-N50-A0.6-FR	6.8	5.9	6.0	6.2	6.4	10.2	8.6	8.9	9.4	9.9	6.9	6.0	6.1	6.3	6.5
C200-t2-R2-N100-A0.2-FR	9.2	9.1	9.2	9.2	9.2	13.9	13.6	13.9	14.1	14.1	9.3	9.2	9.3	9.4	9.4
C200-t2-R2-N100-A0.4-FR	9.2	8.7	8.9	9.1	9.2	13.9	13.1	13.4	14.0	14.3	9.3	8.9	9.1	9.3	9.4
C200-t2-R2-N100-A0.6-FR	9.2	8.3	8.5	8.9	9.2	13.9	12.3	12.8	13.5	14.3	9.3	8.4	8.7	9.1	9.4
C200-t2-R1.5-N50-A0.2-FR	7.5	7.4	7.4	7.5	12.9	11.0	10.7	11.0	11.1	20.3	7.6	7.5	7.6	7.6	13.0
C200-t2-R1.5-N50-A0.4-FR	7.5	7.1	7.2	7.3	12.7	11.0	10.2	10.5	10.9	20.0	7.6	7.2	7.3	7.4	12.9
C200-t2-R1.5-N50-A0.6-FR	7.5	6.6	6.8	7.0	12.4	11.0	9.4	9.8	10.3	19.5	7.6	6.7	6.9	7.1	12.5
C200-t2-R1.5-N100-A0.2-FR	10.5	10.3	10.4	10.5	18.3	15.4	15.0	15.3	15.5	28.7	10.6	10.5	10.6	10.7	18.5
C200-t2-R1.5-N100-A0.4-FR	10.5	10.0	10.2	10.4	18.2	15.4	14.4	14.8	15.5	28.8	10.6	10.2	10.4	10.6	18.5
C200-t2-R1.5-N100-A0.6-FR	10.5	9.5	9.8	10.2	18.0	15.4	13.6	14.2	15.0	28.6	10.6	9.7	10.0	10.4	18.3
C200-t2.3-R1.3-N50-A0.2-FR	10.2	10.1	10.1	10.2	17.2	15.3	15.0	15.2	15.3	27.8	10.4	10.3	10.3	10.3	17.4
C200-t2.3-R1.3-N50-A0.4-FR	10.2	9.8	9.9	10.0	17.0	15.3	14.2	14.6	14.9	27.4	10.4	9.9	10.1	10.1	17.2
C200-t2.3-R1.3-N50-A0.6-FR	10.2	9.2	9.4	9.6	16.5	15.3	13.3	13.7	14.3	26.6	10.4	9.3	9.6	9.8	16.7
C200-t2.3-R1.3-N100-A0.2-FR	14.5	14.3	14.5	14.5	24.7	21.6	21.2	21.6	21.7	39.7	14.7	14.6	14.7	14.7	25.1
C200-t2.3-R1.3-N100-A0.4-FR	14.5	13.9	14.2	14.4	24.6	21.6	20.4	20.9	21.6	39.7	14.7	14.2	14.4	14.7	24.9
C200-t2.3-R1.3-N100-A0.6-FR	14.5	13.2	13.7	14.1	24.3	21.6	19.3	20.0	21.0	39.4	14.7	13.5	13.9	14.4	24.6
C200-t2.7-R1.5-N50-A0.2-FR	12.9	12.8	12.8	12.8	12.9	20.4	20.0	20.2	20.3	20.3	13.0	13.0	13.0	13.0	13.0
C200-t2.7-R1.5-N50-A0.4-FR	12.9	12.4	12.6	12.6	12.7	20.4	19.1	19.4	19.8	20.0	13.0	12.6	12.7	12.8	12.9
C200-t2.7-R1.5-N50-A0.6-FR	12.9	11.6	11.9	12.1	12.4	20.4	17.8	18.3	18.8	19.5	13.0	11.8	12.1	12.3	12.5
C200-t2.7-R1.5-N100-A0.2-FR	18.2	18.0	18.2	18.2	18.3	28.6	28.2	28.5	28.7	28.7	18.5	18.3	18.4	18.5	18.5
C200-t2.7-R1.5-N100-A0.4-FR	18.2	17.5	17.8	18.0	18.2	28.6	27.2	27.7	28.4	28.8	18.5	17.7	18.0	18.3	18.5
C200-t2.7-R1.5-N100-A0.6-FR	18.2	16.6	17.1	17.5	18.0	28.6	25.8	26.5	27.4	28.6	18.5	16.8	17.3	17.7	18.3
C200-t3.1-R1.3-N50-A0.2-FR	17.1	17.1	17.1	17.2	17.2	27.8	27.4	27.6	27.7	27.8	17.3	17.3	17.4	17.4	17.4
C200-t3.1-R1.3-N50-A0.4-FR	17.1	16.6	16.9	16.9	17.0	27.8	26.3	26.8	27.1	27.4	17.3	16.9	17.1	17.1	17.2
C200-t3.1-R1.3-N50-A0.6-FR	17.1	15.8	16.1	16.3	16.5	27.8	24.8	25.4	25.9	26.6	17.3	16.0	16.3	16.5	16.7
C200-t3.1-R1.3-N100-A0.2-FR	24.6	24.4	24.7	24.7	24.7	39.6	39.1	39.5	39.6	39.7	24.9	24.7	25.0	25.0	25.1
C200-t3.1-R1.3-N100-A0.4-FR	24.6	23.7	24.1	24.4	24.6	39.6	37.9	38.5	39.2	39.7	24.9	24.0	24.4	24.7	24.9
C200-t3.1-R1.3-N100-A0.6-FR	24.6	22.4	23.1	23.6	24.3	39.6	36.0	37.0	38.0	39.4	24.9	22.7	23.4	23.8	24.6

Table 4.4c: Web crippling strength predicted from FEA for CFSS channel sections with 300 x 80 x 20 unfastened flanges under ETF loading condition.

Specimen	Web crippling strength per web predicted from FEA, P_{FEA} (kN)														
	Austenitic					Duplex					Ferritic				
	Plain Web	Unstiffened web hole	Edge-stiffened web hole			Plain Web	Unstiffened web hole	Edge-stiffened web hole			Plain Web	Unstiffened web hole	Edge-stiffened web hole		
			q = 3mm	*q* = 5mm	*q* = 7mm			*q* = 3mm	*q* = 5mm	*q* = 7mm			q = 3 mm	q = 5 mm	q = 7mm
C300-t1.5-R2-N50-A0.2-FU	1.6	1.5	1.6	1.6	4.3	1.9	1.8	1.9	2.0	6.0	1.6	1.5	1.6	1.7	4.4
C300-t1.5-R2-N50-A0.4-FU	1.6	1.3	1.4	1.6	3.7	1.9	1.6	1.7	1.9	4.4	1.6	1.4	1.5	1.7	3.7
C300-t1.5-R2-N50-A0.6-FU	1.6	1.2	1.3	1.5	3.6	1.9	1.4	1.5	1.8	4.3	1.6	1.2	1.3	1.6	3.6
C300-t1.5-R2-N100-A0.2-FU	1.9	1.8	1.9	2.0	7.7	2.3	2.2	2.3	2.4	9.2	2.0	1.9	1.9	2.0	7.8
C300-t1.5-R2-N100-A0.4-FU	1.9	1.6	1.7	1.9	7.5	2.3	2.0	2.1	2.3	9.0	2.0	1.7	1.8	2.0	7.6
C300-t1.5-R2-N100-A0.6-FU	1.9	1.4	1.5	1.8	7.2	2.3	1.7	1.8	2.2	8.6	2.0	1.5	1.6	1.9	7.3
C300-t2-R2-N50-A0.2-FU	3.5	3.6	3.7	3.7	4.3	4.1	4.3	4.3	4.3	6.0	3.5	3.7	3.7	3.7	4.4
C300-t2-R2-N50-A0.4-FU	3.5	3.6	3.7	3.7	3.7	4.1	4.2	4.3	4.3	4.4	3.5	3.7	3.7	3.6	3.7
C300-t2-R2-N50-A0.6-FU	3.5	3.6	3.6	3.6	3.6	4.1	4.2	4.3	4.3	4.3	3.5	3.6	3.6	3.6	3.6
C300-t2-R2-N100-A0.2-FU	7.4	7.4	7.7	7.7	7.7	8.6	8.9	9.2	9.2	9.2	7.4	7.5	7.8	7.8	7.8
C300-t2-R2-N100-A0.4-FU	7.4	7.3	7.5	7.5	7.5	8.6	8.7	9.0	9.0	9.0	7.4	7.2	7.6	7.6	7.6
C300-t2-R2-N100-A0.6-FU	7.4	6.9	7.1	7.2	7.2	8.6	8.5	8.7	8.6	8.6	7.4	6.8	7.2	7.3	7.3
C300-t2-R1.5-N50-A0.2-FU	3.5	3.3	3.4	3.5	7.5	4.2	4.0	4.1	4.3	9.6	3.6	3.4	3.5	3.6	7.7
C300-t2-R1.5-N50-A0.4-FU	3.5	2.9	3.1	3.4	7.3	4.2	3.6	3.7	4.1	9.4	3.6	3.0	3.1	3.4	7.4
C300-t2-R1.5-N50-A0.6-FU	3.5	2.5	2.7	3.0	6.5	4.2	3.1	3.2	3.7	8.6	3.6	2.6	2.7	3.1	6.6
C300-t2-R1.5-N100-A0.2-FU	4.2	4.0	4.1	4.2	11.9	5.1	4.9	5.0	5.2	14.0	4.3	4.1	4.2	4.4	11.9
C300-t2-R1.5-N100-A0.4-FU	4.2	3.6	3.7	4.0	11.4	5.1	4.4	4.5	4.9	14.5	4.3	3.7	3.8	4.2	11.4
C300-t2-R1.5-N100-A0.6-FU	4.2	3.1	3.3	3.7	11.2	5.1	3.8	4.0	4.4	14.5	4.3	3.2	3.4	3.8	11.4
C300-t2.3-R1.3-N50-A0.2-FU	5.0	4.8	4.9	5.1	10.6	6.2	5.9	6.0	6.3	13.7	5.2	4.9	5.0	5.2	10.8
C300-t2.3-R1.3-N50-A0.4-FU	5.0	4.3	4.4	4.7	10.0	6.2	5.2	5.4	5.8	13.2	5.2	4.4	4.5	4.9	10.2
C300-t2.3-R1.3-N50-A0.6-FU	5.0	3.7	3.8	4.2	8.9	6.2	4.5	4.7	5.2	11.8	5.2	3.8	3.9	4.3	9.1
C300-t2.3-R1.3-N100-A0.2-FU	6.1	5.8	5.9	6.1	14.9	7.5	7.2	7.3	7.6	18.3	6.2	5.9	6.1	6.3	15.2
C300-t2.3-R1.3-N100-A0.4-FU	6.1	5.2	5.4	5.8	14.4	7.5	6.4	6.6	7.0	18.2	6.2	5.4	5.5	5.9	14.9
C300-t2.3-R1.3-N100-A0.6-FU	6.1	4.6	4.7	5.2	14.0	7.5	5.6	5.8	6.4	18.2	6.2	4.7	4.9	5.3	14.4
C300-t2.7-R1.5-N50-A0.2-FU	7.4	7.0	7.1	7.4	7.5	9.3	8.8	9.0	9.3	9.6	7.5	7.2	7.3	7.6	7.7
C300-t2.7-R1.5-N50-A0.4-FU	7.4	6.2	6.4	6.8	7.3	9.3	7.8	8.0	8.5	9.4	7.5	6.4	6.5	6.9	7.4
C300-t2.7-R1.5-N50-A0.6-FU	7.4	5.4	5.6	5.9	6.5	9.3	6.7	6.9	7.5	8.6	7.5	5.5	5.8	6.0	6.6
C300-t2.7-R1.5-N100-A0.2-FU	11.5	11.9	11.9	11.9	11.9	14.0	14.1	14.0	14.0	14.0	11.5	12.2	11.9	11.9	11.9
C300-t2.7-R1.5-N100-A0.4-FU	11.5	11.4	11.4	11.4	11.4	14.0	14.3	14.5	14.5	14.5	11.5	11.8	11.4	11.4	11.4
C300-t2.7-R1.5-N100-A0.6-FU	11.5	11.2	11.0	11.1	11.2	14.0	13.9	14.3	14.0	14.5	11.5	10.9	11.3	11.3	11.4
C300-t3.1-R1.3-N50-A0.2-FU	10.4	9.9	10.1	10.4	10.6	13.5	12.7	12.9	13.3	13.7	10.6	10.1	10.3	10.6	10.8
C300-t3.1-R1.3-N50-A0.4-FU	10.4	8.8	9.0	9.4	10.0	13.5	11.4	11.5	12.1	13.2	10.6	9.0	9.2	9.7	10.2
C300-t3.1-R1.3-N50-A0.6-FU	10.4	7.6	7.7	8.2	8.9	13.5	9.7	9.9	10.6	11.8	10.6	7.7	7.9	8.4	9.1
C300-t3.1-R1.3-N100-A0.2-FU	14.6	14.7	14.9	14.9	14.9	17.6	17.8	18.3	18.3	18.3	14.9	14.7	15.2	15.2	15.2
C300-t3.1-R1.3-N100-A0.4-FU	14.6	14.4	14.4	14.4	14.4	17.6	17.5	18.1	18.2	18.2	14.9	14.4	14.8	14.9	14.9
C300-t3.1-R1.3-N100-A0.6-FU	14.6	13.9	13.9	14.0	14.0	17.6	17.2	18.2	18.2	18.2	14.9	14.4	14.3	14.3	14.4

Table 4.4d: Web crippling strength predicted from FEA for CFSS channel sections with 300 x 80 x 20 fastened flanges under ETF loading condition.

Specimen	Web crippling strength per web predicted from FEA, P_{FEA} (kN)														
	Austenitic					Duplex					Ferritic				
	Plain Web	Unstiffened web hole	Edge-stiffened web hole			Plain Web	Unstiffened web hole	Edge-stiffened web hole			Plain Web	Unstiffened web hole	Edge-stiffened web hole		
			q = 3mm	*q* = 5mm	*q* = 7mm			*q* = 3mm	*q* = 5mm	*q* = 7mm			q = 3 mm	q = 5 mm	q = 7mm
C300-t1.5-R2-N50-A0.2-FR	3.2	3.1	3.2	3.3	6.8	4.0	3.8	4.0	4.1	10.3	3.3	3.2	3.3	3.3	6.9
C300-t1.5-R2-N50-A0.4-FR	3.2	2.9	3.1	3.3	6.1	4.0	3.6	3.8	4.2	8.4	3.3	3.0	3.1	3.4	6.2
C300-t1.5-R2-N50-A0.6-FR	3.2	2.6	2.7	3.0	5.4	4.0	3.3	3.5	4.1	7.9	3.3	2.7	2.8	3.0	5.5
C300-t1.5-R2-N100-A0.2-FR	4.0	3.9	4.0	4.1	7.4	5.1	4.9	5.1	5.2	10.1	4.1	4.0	4.1	4.2	7.6
C300-t1.5-R2-N100-A0.4-FR	4.0	3.7	3.9	4.1	7.5	5.1	4.6	4.9	5.3	10.5	4.1	3.8	4.0	4.2	7.6
C300-t1.5-R2-N100-A0.6-FR	4.0	3.5	3.6	3.8	7.0	5.1	4.3	4.6	5.2	10.1	4.1	3.6	3.7	3.9	7.1
C300-t2-R2-N50-A0.2-FR	5.9	5.7	5.8	6.0	6.8	7.9	7.6	7.7	8.0	10.3	6.1	5.8	6.0	6.1	6.9
C300-t2-R2-N50-A0.4-FR	5.9	5.3	5.4	5.8	6.1	7.9	7.1	7.3	7.9	8.4	6.1	5.4	5.6	5.9	6.2
C300-t2-R2-N50-A0.6-FR	5.9	4.7	4.9	5.1	5.4	7.9	6.4	6.7	7.3	7.9	6.1	4.8	5.0	5.2	5.5
C300-t2-R2-N100-A0.2-FR	7.3	7.1	7.2	7.4	7.4	9.9	9.6	9.8	10.0	10.1	7.4	7.2	7.4	7.5	7.6
C300-t2-R2-N100-A0.4-FR	7.3	6.7	6.8	7.2	7.5	9.9	9.0	9.3	9.8	10.5	7.4	6.8	7.0	7.3	7.6
C300-t2-R2-N100-A0.6-FR	7.3	6.4	6.6	6.7	7.0	9.9	8.4	8.7	9.3	10.1	7.4	6.5	6.7	6.8	7.1
C300-t2-R1.5-N50-A0.2-FR	6.4	6.2	6.4	6.5	11.9	8.5	8.2	8.4	8.6	16.9	6.5	6.4	6.5	6.6	12.1
C300-t2-R1.5-N50-A0.4-FR	6.4	5.9	6.0	6.2	11.4	8.5	7.8	8.0	8.6	16.6	6.5	6.0	6.1	6.3	11.6
C300-t2-R1.5-N50-A0.6-FR	6.4	5.3	5.5	5.7	10.6	8.5	7.1	7.3	7.8	15.2	6.5	5.5	5.6	5.8	10.8
C300-t2-R1.5-N100-A0.2-FR	8.1	8.0	8.1	8.2	14.7	10.9	10.7	10.9	11.1	21.3	8.3	8.2	8.3	8.4	15.0
C300-t2-R1.5-N100-A0.4-FR	8.1	7.7	7.8	8.0	14.5	10.9	10.1	10.4	11.0	21.2	8.3	7.8	8.0	8.2	14.8
C300-t2-R1.5-N100-A0.6-FR	8.1	7.2	7.4	7.7	13.9	10.9	9.4	9.8	10.4	20.0	8.3	7.4	7.5	7.8	14.1
C300-t2.3-R1.3-N50-A0.2-FR	8.8	8.7	8.8	8.9	15.9	12.0	11.7	12.0	12.2	23.3	9.0	8.9	9.0	9.0	16.2
C300-t2.3-R1.3-N50-A0.4-FR	8.8	8.2	8.3	8.5	15.3	12.0	11.1	11.3	11.9	22.6	9.0	8.3	8.5	8.7	15.7
C300-t2.3-R1.3-N50-A0.6-FR	8.8	7.5	7.7	7.9	14.4	12.0	10.1	10.3	10.8	21.1	9.0	7.7	7.8	8.1	14.7
C300-t2.3-R1.3-N100-A0.2-FR	11.4	11.2	11.3	11.4	20.1	15.6	15.3	15.5	15.8	29.7	11.6	11.5	11.6	11.6	20.5
C300-t2.3-R1.3-N100-A0.4-FR	11.4	10.8	11.0	11.2	19.8	15.6	14.5	14.9	15.5	29.4	11.6	11.0	11.2	11.4	20.1
C300-t2.3-R1.3-N100-A0.6-FR	11.4	10.2	10.4	10.7	18.9	15.6	13.6	14.0	14.6	28.1	11.6	10.4	10.6	11.0	19.2
C300-t2.7-R1.5-N50-A0.2-FR	11.8	11.5	11.7	11.8	11.9	16.7	16.1	16.4	16.7	16.9	12.0	11.7	11.9	12.0	12.1
C300-t2.7-R1.5-N50-A0.4-FR	11.8	10.7	10.9	11.1	11.4	16.7	15.1	15.4	15.9	16.6	12.0	10.9	11.1	11.3	11.6
C300-t2.7-R1.5-N50-A0.6-FR	11.8	9.7	9.8	10.2	10.6	16.7	13.8	14.0	14.5	15.2	12.0	10.0	10.1	10.4	10.8
C300-t2.7-R1.5-N100-A0.2-FR	14.6	14.4	14.5	14.7	14.7	21.1	20.6	20.8	21.1	21.3	14.9	14.7	14.8	15.0	15.0
C300-t2.7-R1.5-N100-A0.4-FR	14.6	13.7	13.9	14.2	14.5	21.1	19.5	19.8	20.5	21.2	14.9	14.0	14.1	14.5	14.8
C300-t2.7-R1.5-N100-A0.6-FR	14.6	12.8	13.0	13.4	13.9	21.1	18.2	18.5	19.2	20.0	14.9	13.1	13.2	13.6	14.1
C300-t3.1-R1.3-N50-A0.2-FR	16.0	15.7	15.7	15.9	15.9	23.2	22.5	22.8	23.1	23.3	16.3	16.0	16.1	16.2	16.2
C300-t3.1-R1.3-N50-A0.4-FR	16.0	14.7	14.8	15.1	15.3	23.2	21.2	21.5	22.0	22.6	16.3	15.0	15.1	15.4	15.7
C300-t3.1-R1.3-N50-A0.6-FR	16.0	13.6	13.7	14.0	14.4	23.2	19.4	19.7	20.3	21.1	16.3	13.9	14.0	14.3	14.7
C300-t3.1-R1.3-N100-A0.2-FR	20.0	19.7	19.9	20.1	20.1	29.6	29.0	29.2	29.6	29.7	20.4	20.1	20.3	20.4	20.5
C300-t3.1-R1.3-N100-A0.4-FR	20.0	18.9	19.0	19.4	19.8	29.6	27.7	28.0	28.6	29.4	20.4	19.2	19.4	19.7	20.1
C300-t3.1-R1.3-N100-A0.6-FR	20.0	17.7	17.9	18.3	18.9	29.6	25.9	26.3	27.0	28.1	20.4	18.1	18.2	18.6	19.2

4.2 Parametric study on web crippling strength (P_n) of CFSS channel sections with plain webs

According to the studies cited in references [10, 11, 35, 40], the web crippling strength of a channel is primarily influenced by the following factors: the ratio of inside bend radius to web thickness (*r/t*), the ratio of bearing length to web thickness (*N/t*), the ratio of web flat depth to thickness (*h/t*), and the condition of the flange (fastened or unfastened). A comprehensive study was undertaken to thoroughly explore the effects of these mentioned variables.

4.2.1 Effects of r/t ratio on the web crippling strength (P_n)

The effects of the *r/t* ratio on the web crippling strength of CFSS channel sections with plain webs were studied. Specimens with similar characteristics, except for web thickness (*t*) and inner radius (*r*), were grouped to isolate the effect of the *r/t* ratio. The results for ITF loading conditions were depicted in Figures 4.2a-4.2c and Figures 4.3a-4.3c for sections with unfastened and fastened flanges, respectively. Similarly, results for ETF loading conditions were shown in Figures 4.4a-4.4c and Figures 4.5a-4.5c for sections with unfastened and fastened flanges, respectively.

As observed in these figures, the *r/t* ratio indeed has a noticeable impact on the web crippling strength of CFSS channel sections. When the *r/t* ratio changes from 1.3 to 2.0, the web crippling strength for CFSS austenitic, duplex, and ferritic channel sections with unfastened flanges under ITF loading condition decreased by an average of 65%, 67%, and 64%, respectively. For channels with fastened flanges, the decrease was 59%, 63%, and 59%, respectively.

A similar trend was observed for the web crippling strength under ETF loading condition. The average decrease amounted to 64%, 66%, and 65% for channels with unfastened flanges and 63%, 66%, and 63% for channels with fastened flanges, respectively, for austenitic, duplex, and ferritic stainless-steel channel sections.

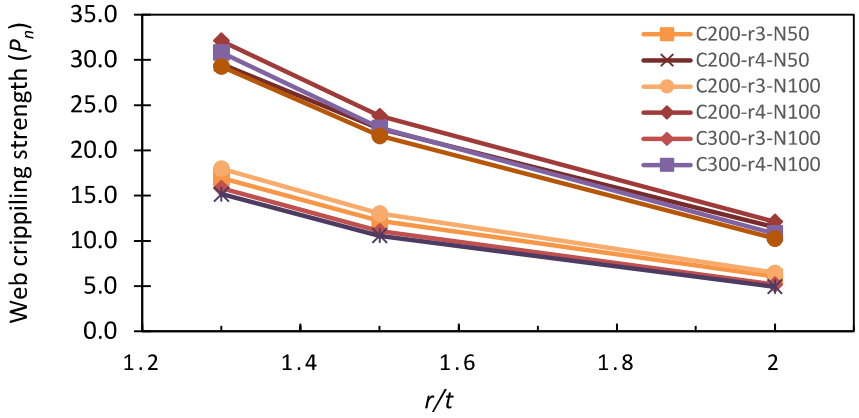

a. CFSS austenitic channel section

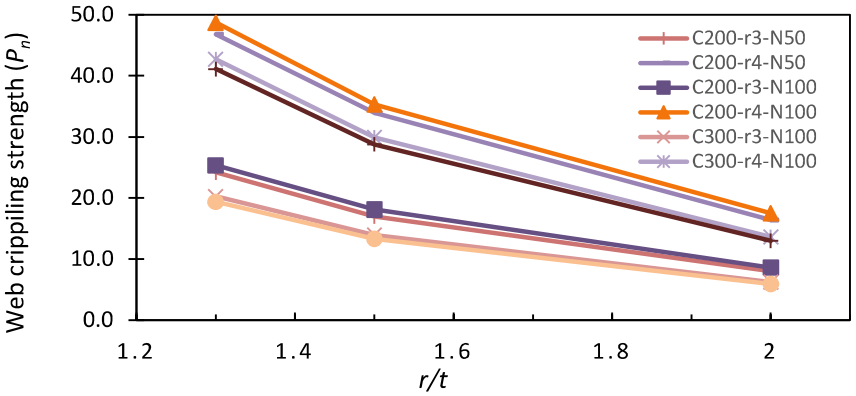

b. CFSS duplex channel section

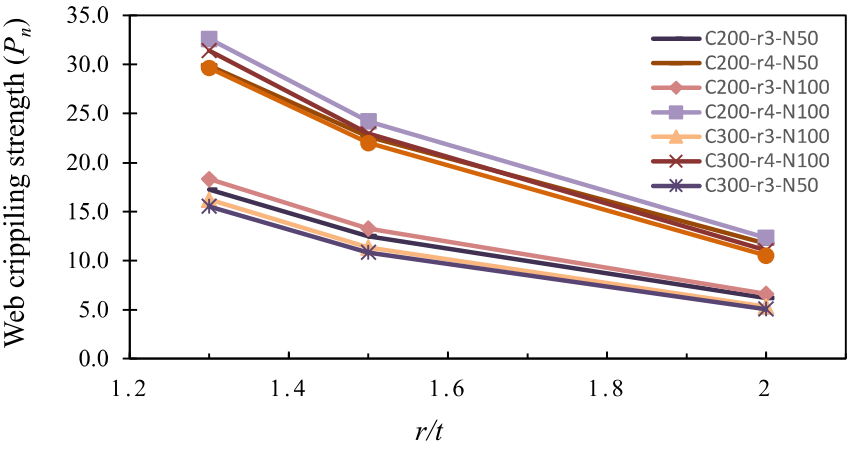

c. CFSS ferritic channel section

Figure 4.2: Web crippling strength against r/t for plain web sections with unfastened flange under ITF loading condition.

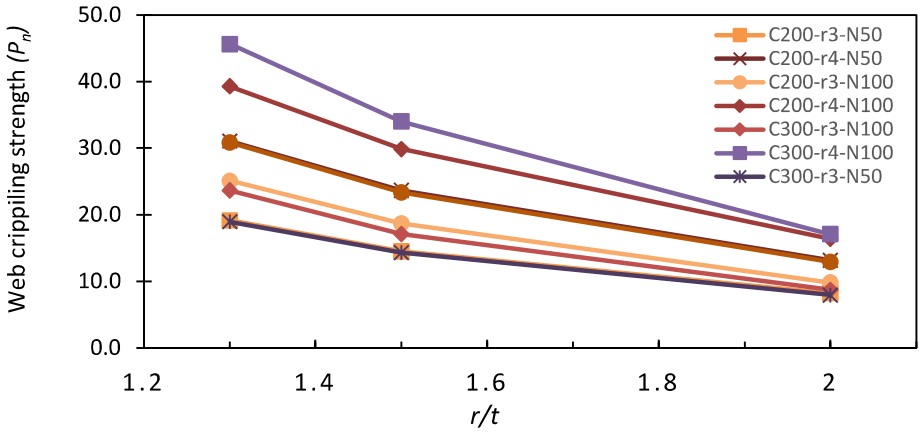

a. CFSS austenitic channel section

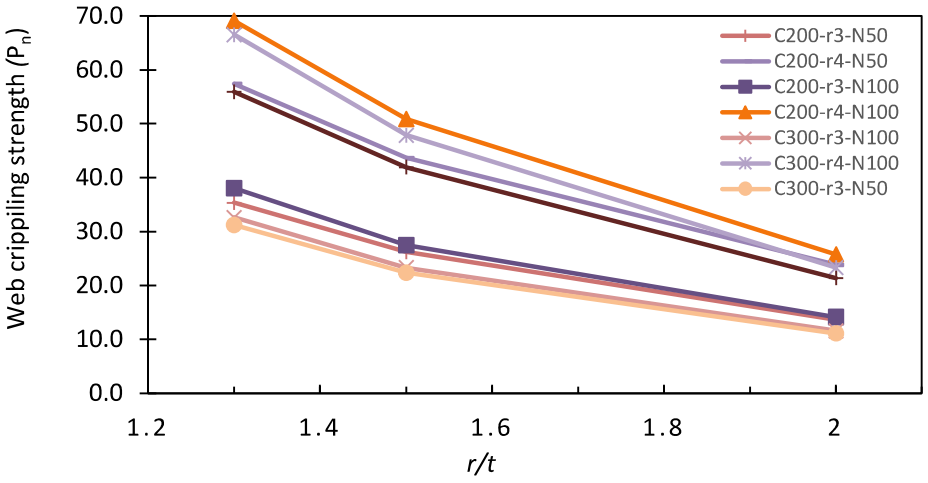

b. CFSS duplex channel section

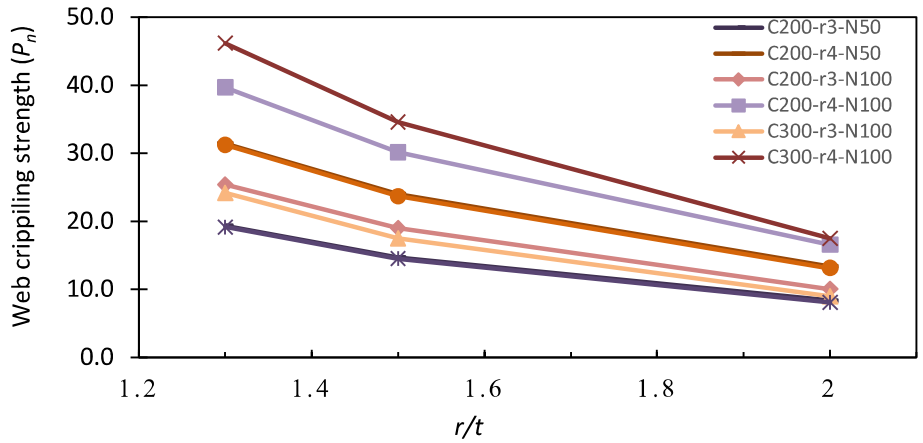

c. CFSS ferritic channel section

Figure 4.3: Web crippling strength against *r/t* for plain web sections with fastened flange under ITF loading conditions.

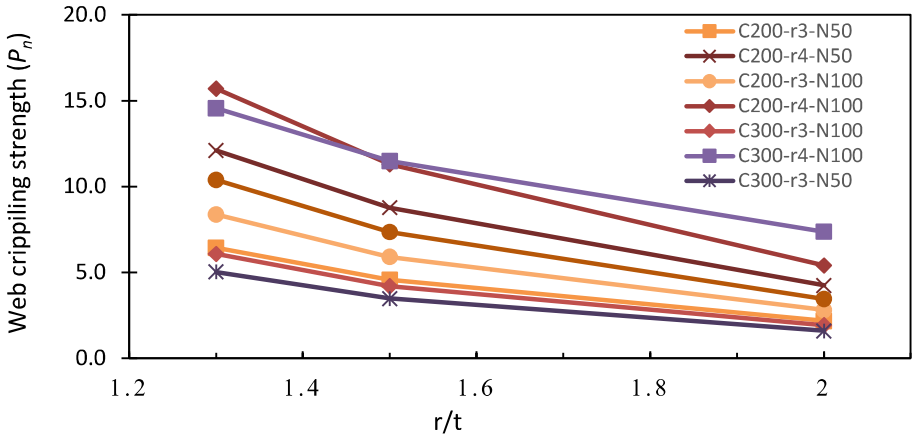

a. CFSS austenitic channel section

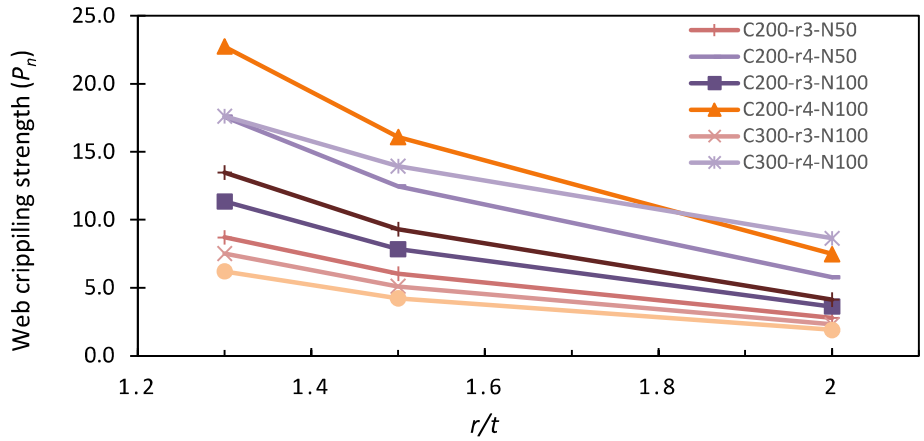

b. CFSS duplex channel section

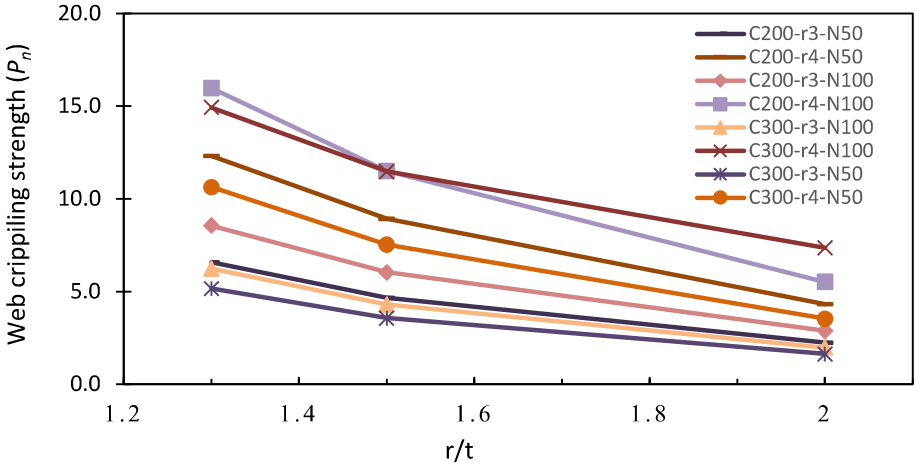

c. CFSS ferritic channel section

Figure 4.4: Web crippling strength against *r/t* for plain web sections with unfastened flange under ETF loading conditions.

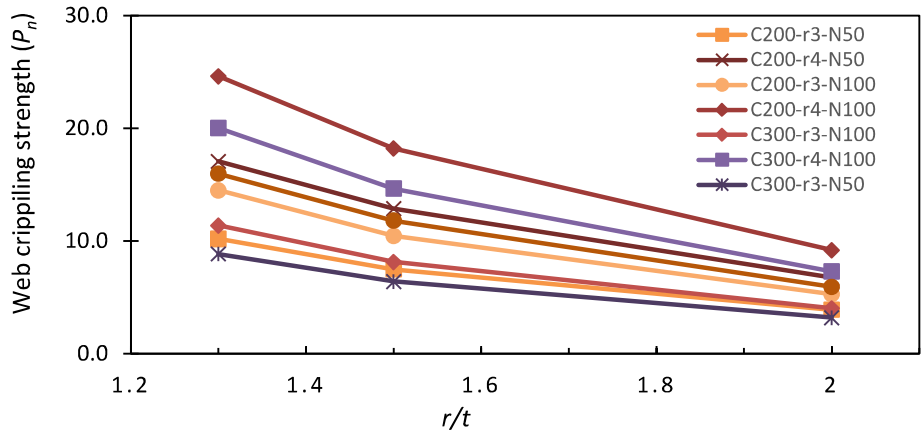

a. CFSS austenitic channel section

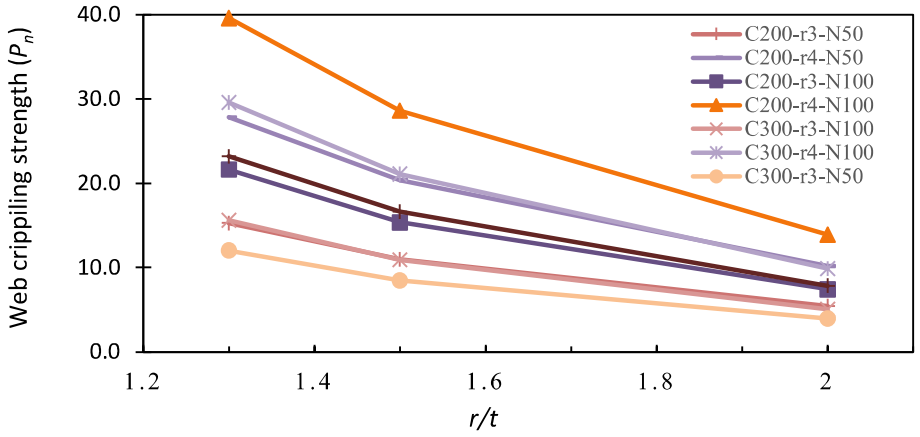

b. CFSS duplex channel section

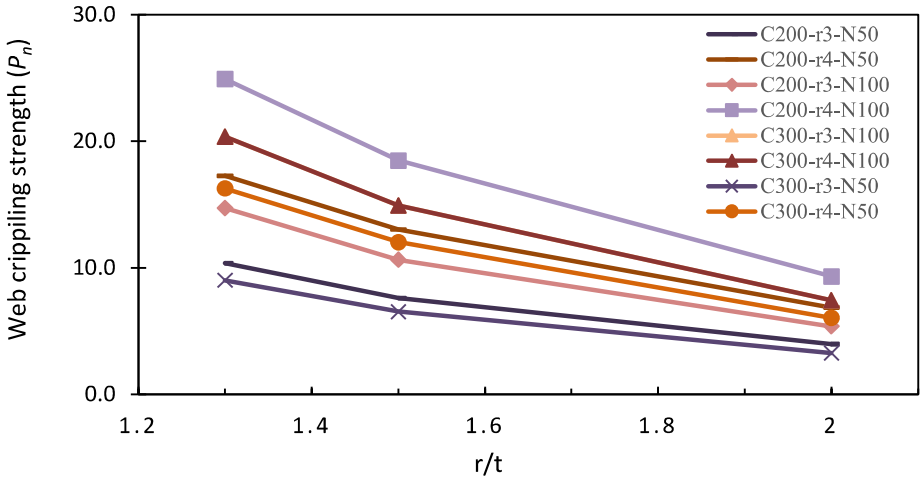

c. CFSS ferritic channel section

Figure 4.5: Web crippling strength against *r/t* for plain web sections with fastened flange under ETF loading condition

4.2.2 Effects of *N/t* ratio on the web crippling strength (P_n)

The influence of the *N/t* ratio on web crippling strength under ITF loading conditions is illustrated in Figures 4.6a-4.6c and Figures 4.7a-4.7c for channel sections with unfastened and fastened flanges, respectively. As depicted in these figures, as the *N/t* ratio rises, the web crippling strength of channel sections under ITF loading conditions experiences an average increase of 5% for sections with unfastened flanges. Moreover, for sections with fastened flanges, the average increase is more pronounced at 22%, 5%, and 23% observed for austenitic, duplex, and ferritic channel sections, respectively.

Similarly, for channel sections under ETF loading conditions, the effects of the *N/t* ratio are shown in Figures 4.8a-4.8c and Figures 4.9a-4.9c for sections with unfastened and fastened flanges, respectively. Here too, an increase in web crippling strength is evident as the *N/t* ratio increases. The average increase is 25% for sections with unfastened flanges and 33% for sections with fastened flanges.

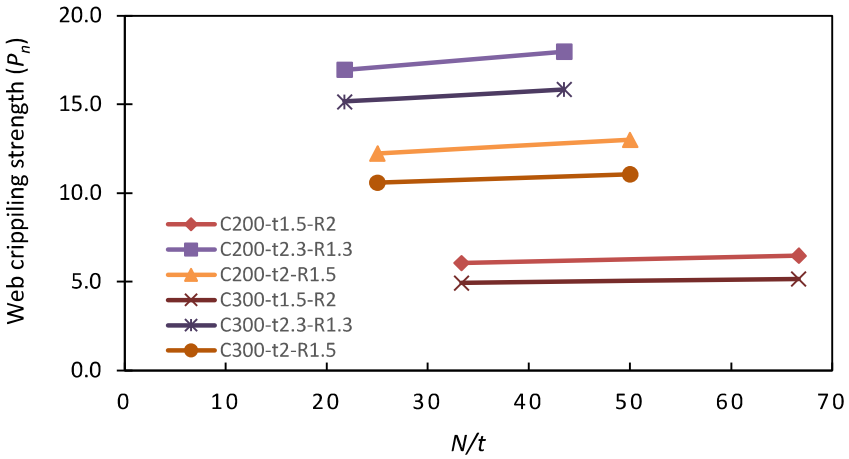

a. CFSS austenitic channel section

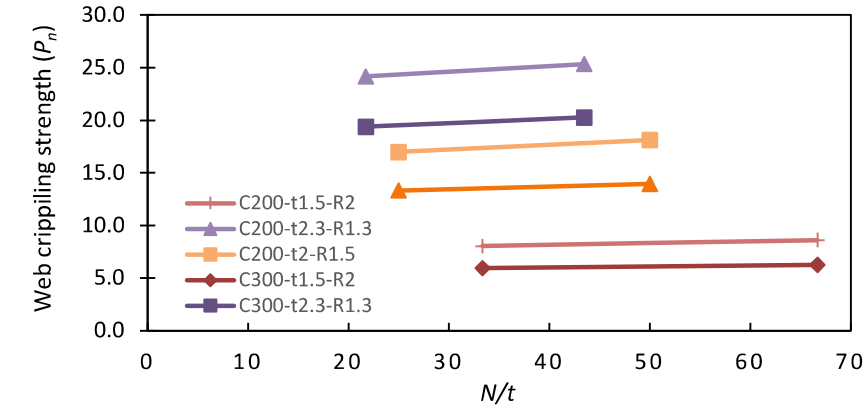

b. CFSS duplex channel section

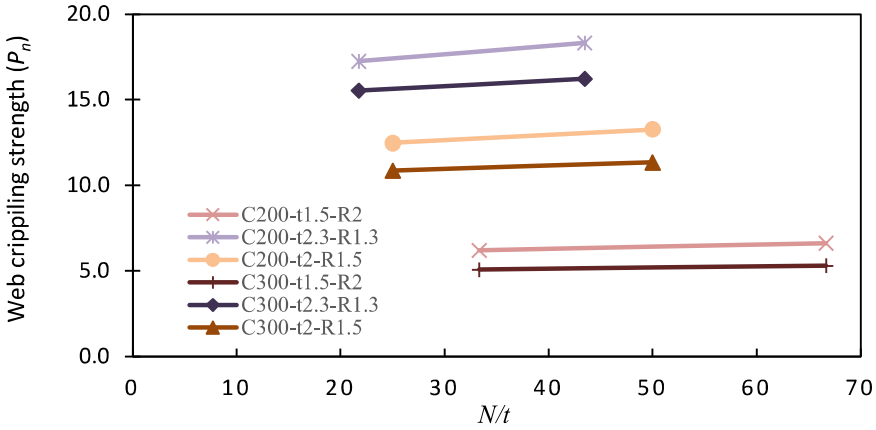

c. CFSS ferritic channel section

Figure 4.6: Web crippling strength against *N/t* for plain web sections with unfastened flange under ITF loading condition

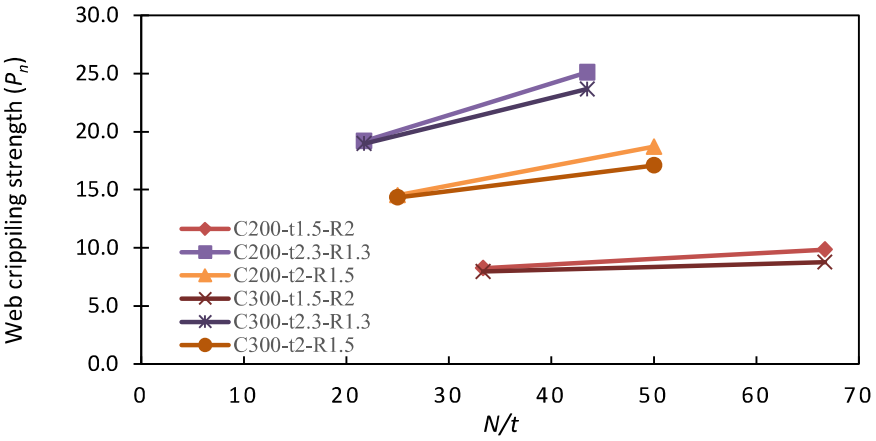

a. CFSS austenitic channel section

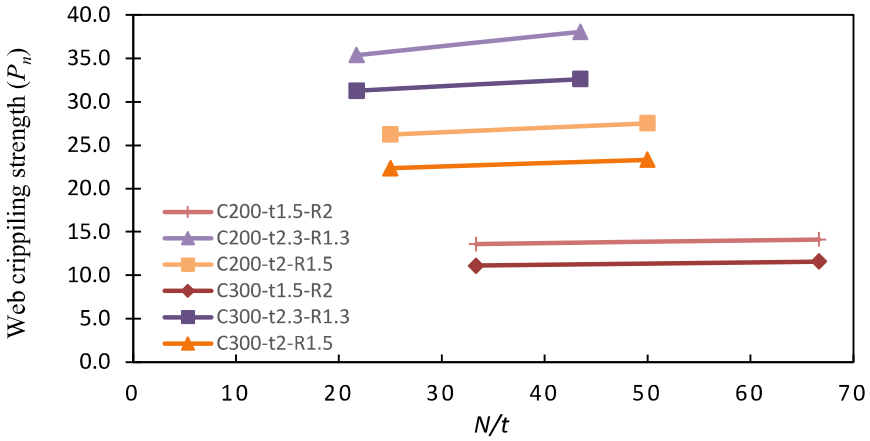

b. CFSS duplex channel section

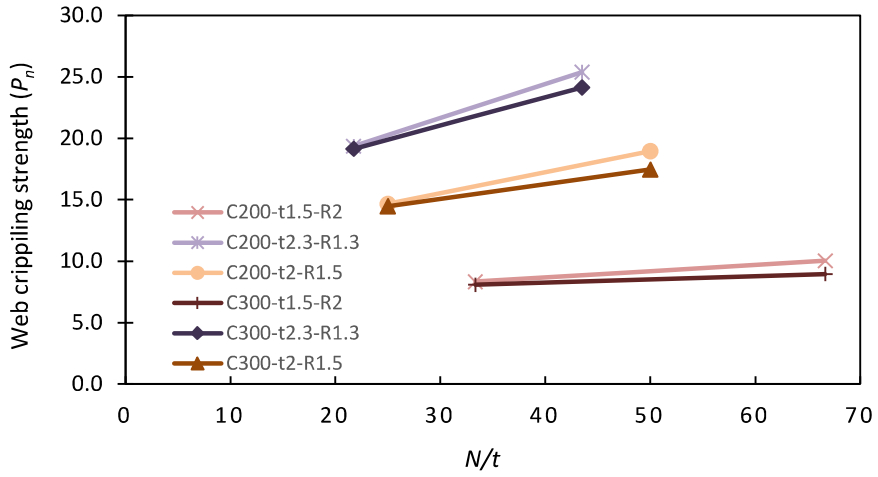

c. CFSS ferritic channel section

Figure 4.7: Web crippling strength against *N/t* for plain web sections with fastened flange under ITF loading condition

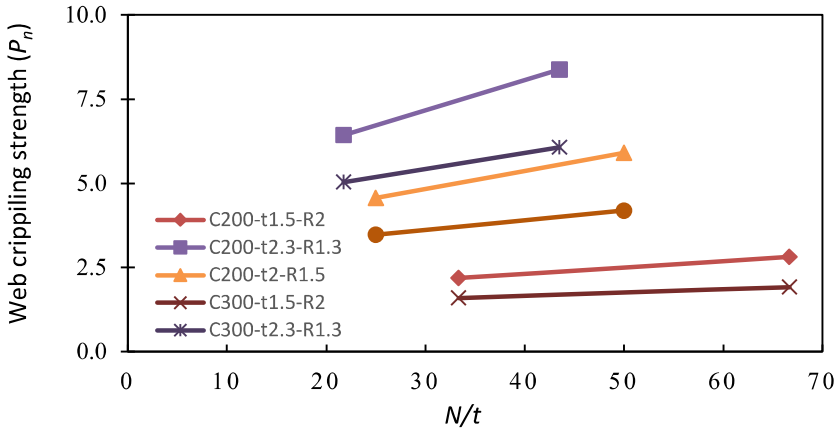

a. CFSS austenitic channel section

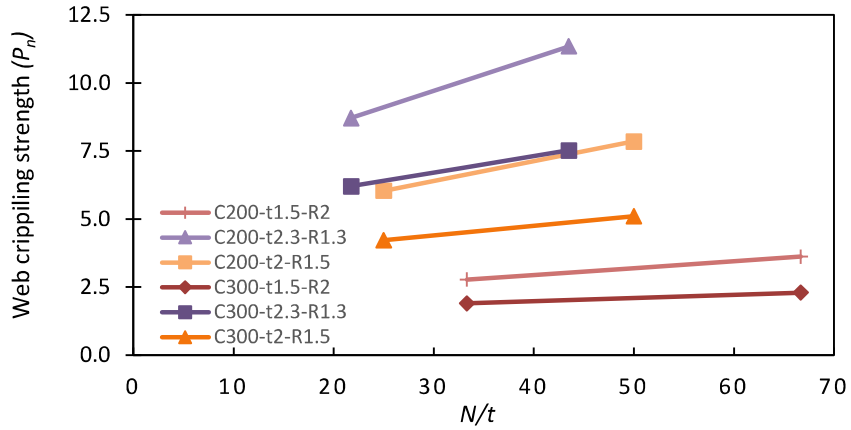

b. CFSS duplex channel section

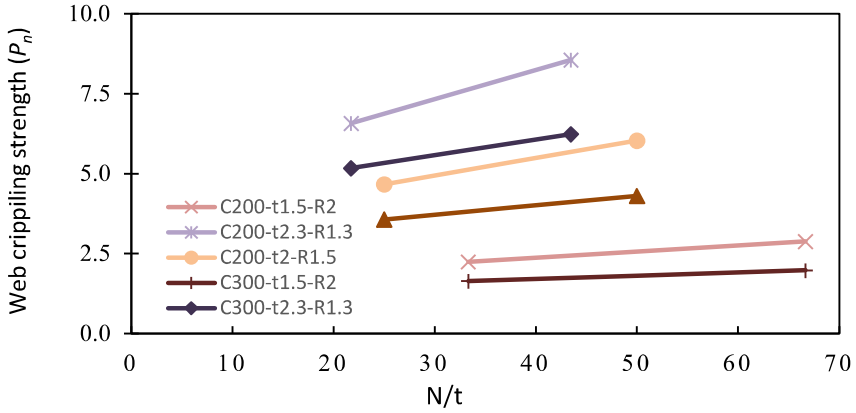

c. CFSS ferritic channel section

Figure 4.8: Web crippling strength against *N/t* for plain web sections with unfastened flange under ETF loading condition

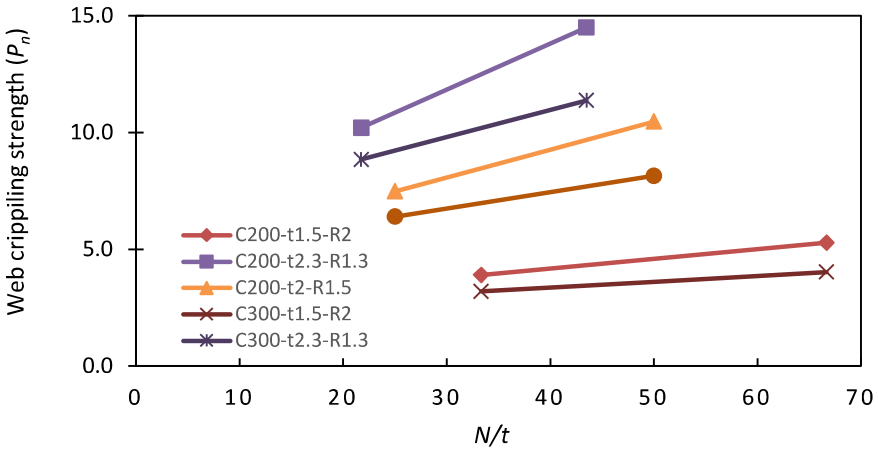

a. CFSS austenitic channel section

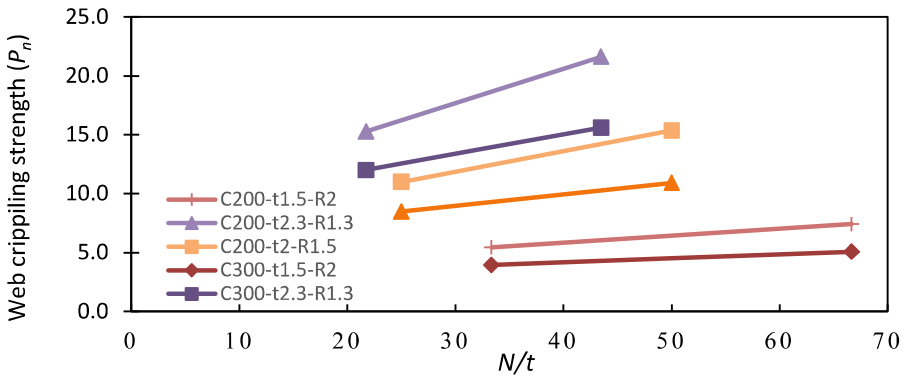

b. CFSS duplex channel section

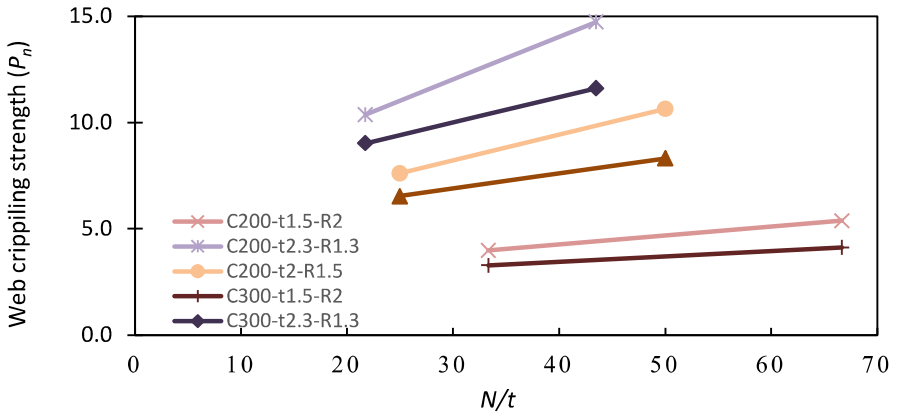

c. CFSS ferritic channel section

Figure 4.9: Web crippling strength against *N/t* for plain web sections with fastened flange under ETF loading condition

4.2.3 Effects of *h/t* ratio on the web crippling strength (P_n)

Figures 4.10a-4.10c and Figures 4.11a-4.11c illustrates the impact of the *h/t* ratio on the web crippling strength of CFSS channel sections under ITF and ETF loading conditions, respectively. Figures 4.10a-4.10c and Figures 4.11a-4.11c demonstrate that as the *h/t* ratio increases, the web crippling strength tends to decrease.

For instance, consider the duplex channel section C200-N50 with an unfastened flange. As the *h/t* ratio increases from 87 to 133, the web crippling strength experiences a reduction of 67% under both ITF and ETF loading conditions. Similarly, for the same section with a fastened flange, there is a decrease of 63% for both ITF and ETF loading conditions.

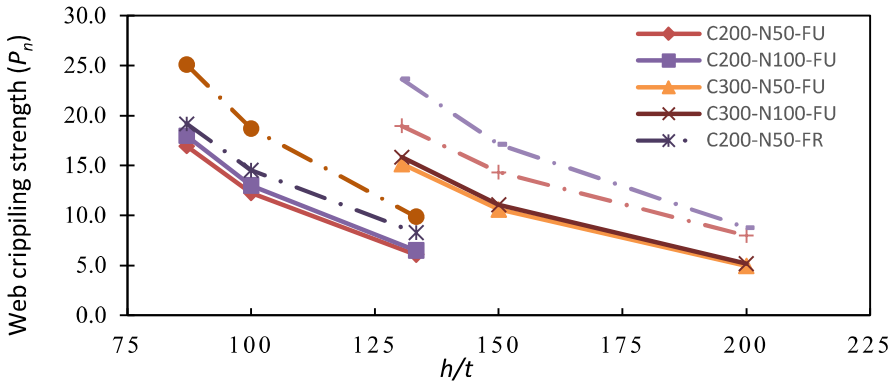

a. CFSS austenitic channel section

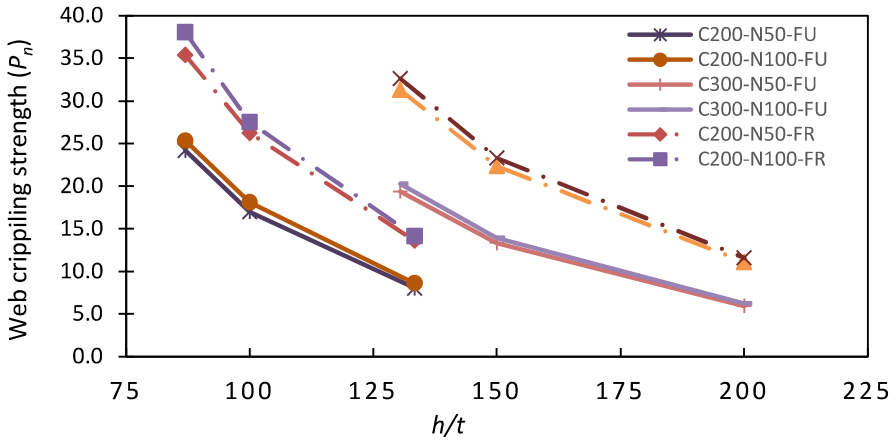

b. CFSS duplex channel section

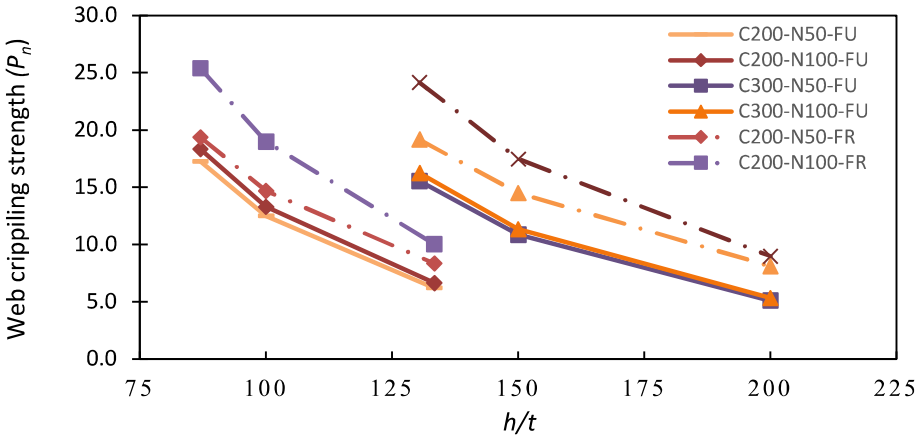

c. CFSS ferritic channel section

Figure 4.10: Web crippling strength against *h/t* for plain web sections under ITF loading condition.

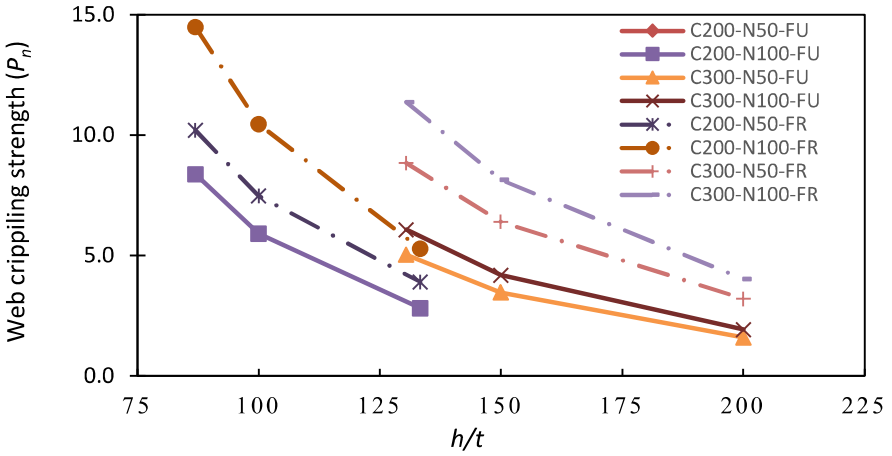

a. CFSS austenitic channel section

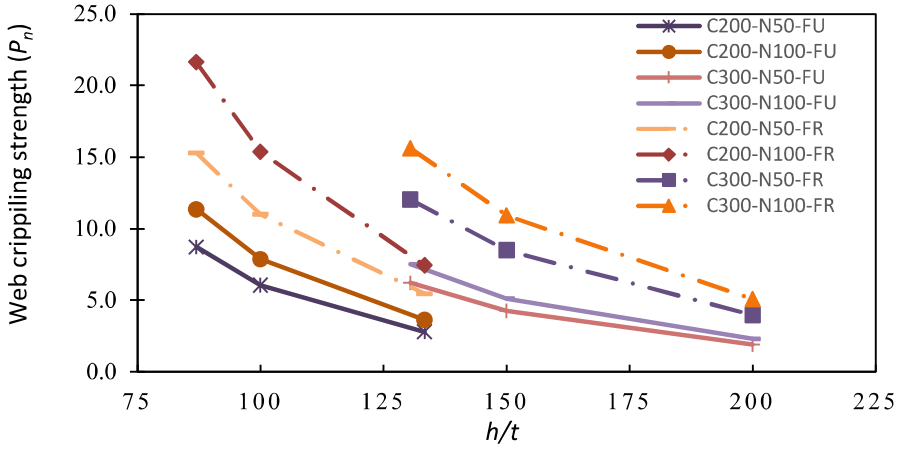

b. CFSS duplex channel section

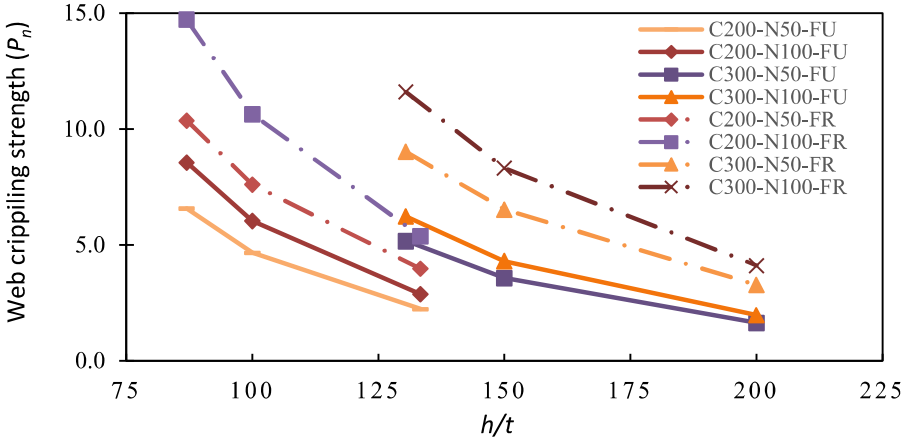

c. CFSS ferritic channel section

Figure 4.11: Web crippling strength against *h/t* for plain web sections under ETF loading condition.

4.2.4 Effects of fastened flanges on the web crippling strength (P_n)

The data presented in Tables 4.3a-4.3d and 4.4a-4.4d indicates a consistent trend. On average, CFSS austenitic, duplex, and ferritic channel sections with fastened flanges exhibit higher web crippling strength compared to those with unfastened flanges. Specifically, sections with fastened flanges are on average 40% and 71% higher than channels with unfastened flanges for ITF and ETF loading conditions, respectively.

4.3 Parametric study on the effect of unstiffened web holes on the web crippling strength reduction factor (R_U)

The available studies [13, 20, 29, 35] have shown that the impact of web holes on channel sections depends on the following variables: the ratio of hole diameter to web flat depth (a/h), the ratio of hole distance to web flat depth (x/h), the ratio of bearing length to web flat depth (N/h), and the condition of the flange (fastened or unfastened). This study conducted a detailed investigation to understand the effects of these variables more comprehensively.

4.3.1 Effects of a/h on the web crippling strength reduction factor (R_U)

The influence of the a/h ratio on the web crippling strength reduction factor (R_U) for unstiffened web holes is depicted in Figures 4.12a-4.12c and Figures 4.13a-4.13c for CFSS channel sections subjected to ITF and ETF loading conditions, respectively. As the a/t ratio increases from 0.2 to 0.6, there is a noticeable decrease in the web crippling strength reduction factors, as illustrated in the figures.

Specifically, in Figure 4.12a-4.12c, it is evident that under ITF loading conditions, R_U for CFSS channel sections decreases from an average of 0.75 to 0.55 for sections with unfastened flanges, and from 0.79 to 0.64 for sections with fastened flanges. Likewise, in Figure 4.13a-4.13c, under ETF loading conditions,

R_U for CFSS channel sections decreases from an average of 0.76 to 0.59 for sections with unfastened flanges, and from 0.78 to 0.69 for sections with fastened flanges.

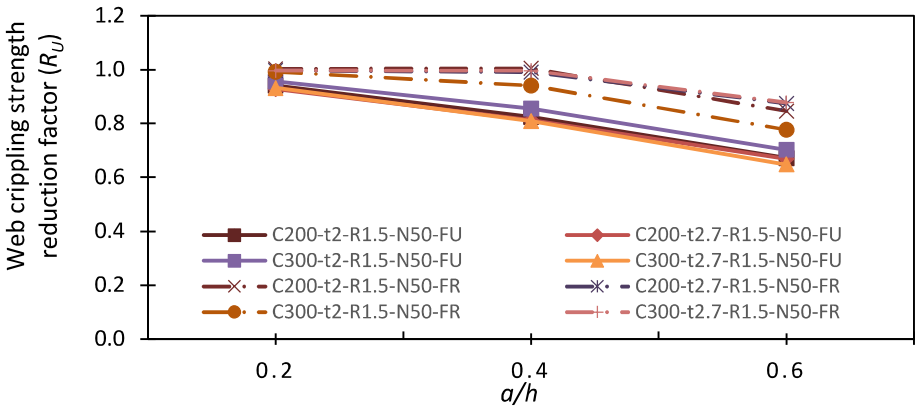

a. CFSS austenitic channel section

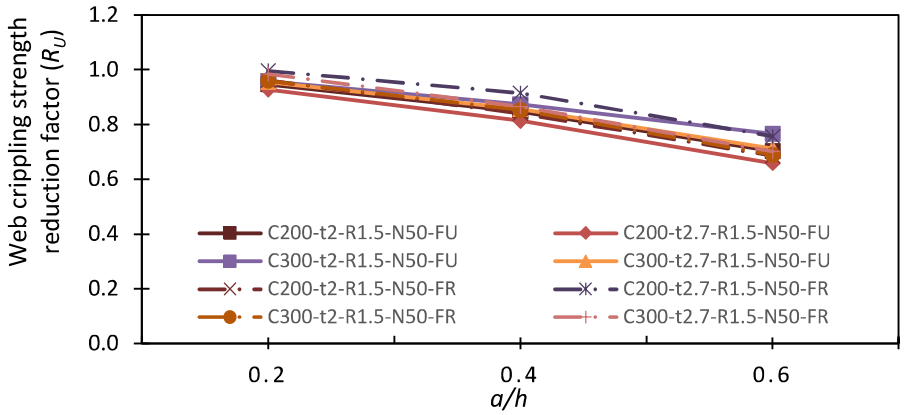

b. CFSS duplex channel section

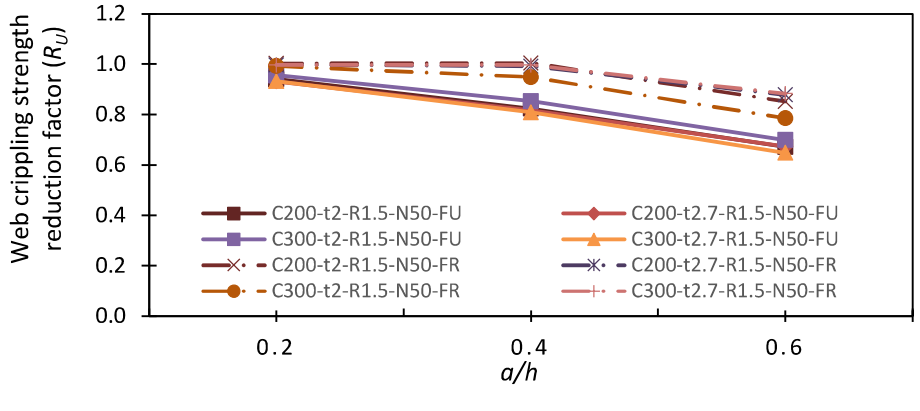

c. CFSS ferritic channel section

Figure 4.12: Web crippling strength reduction factor against a/h for CFSS channel section with unstiffened web holes under ITF loading condition

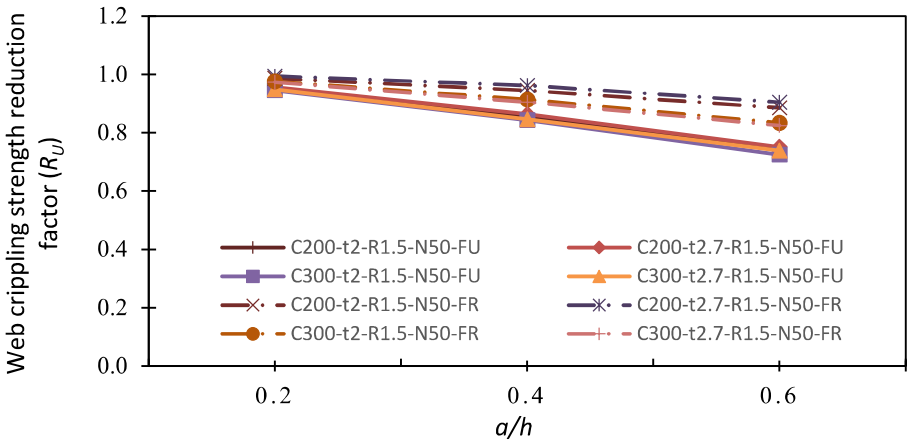

a. CFSS austenitic channel section

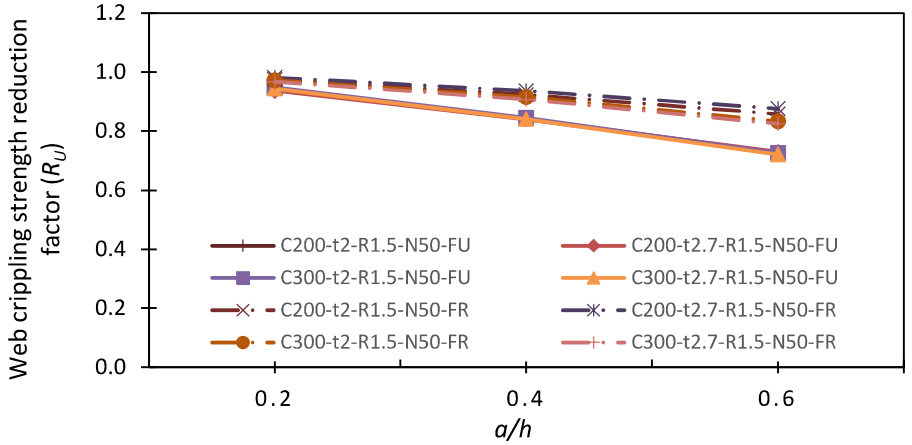

b. CFSS duplex channel section

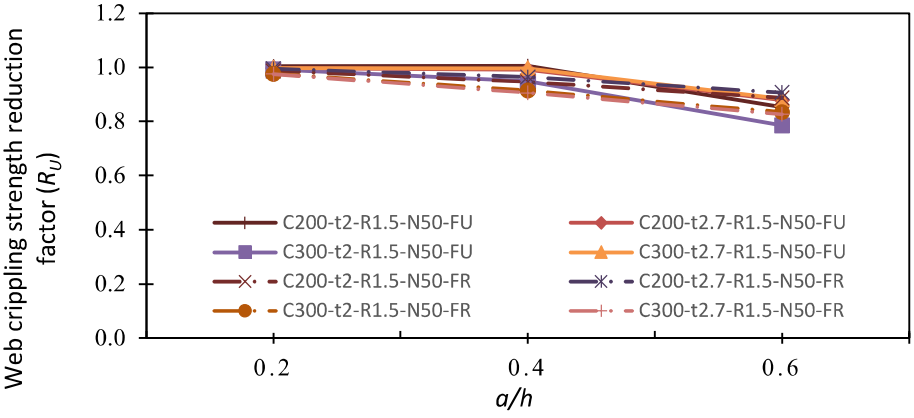

c. CFSS ferritic channel section

Figure 4.13: Web crippling strength reduction factor against *a/h* for CFSS channel section with unstiffened web holes under ETF loading condition

4.3.2 Effects of *x/h* on the web crippling strength reduction factor (R_U)

Figures 4.14a-4.14b illustrate the impact of the *x/h* ratio on the web crippling strength reduction factor for CFSS channel sections subjected to ETF loading conditions. These figures reveal a consistent effect across CFSS austenitic, duplex, and ferritic channel sections. As the *x/h* ratio increases from 0.2 to 0.6, there is a notable increase in the web crippling strength reduction factor. Specifically, for channel sections with unfastened flanges, the reduction factor experiences a linear trend increase of 48%, while for sections with fastened flanges, the linear trend increase is at 26%.

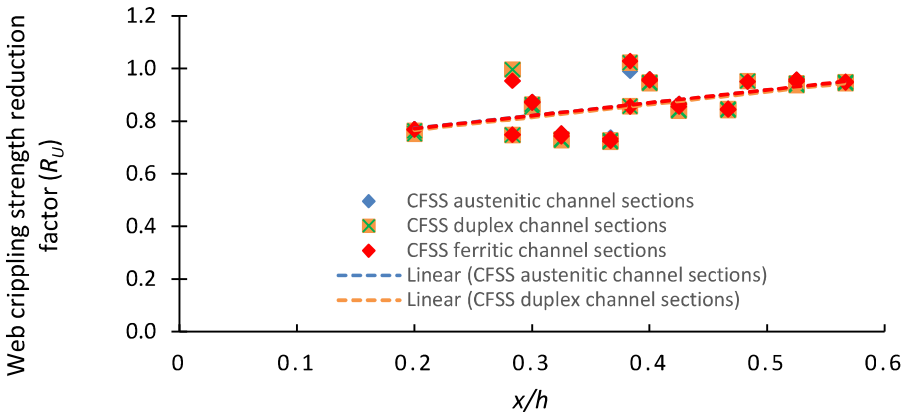

a. Sections with unfastened flange

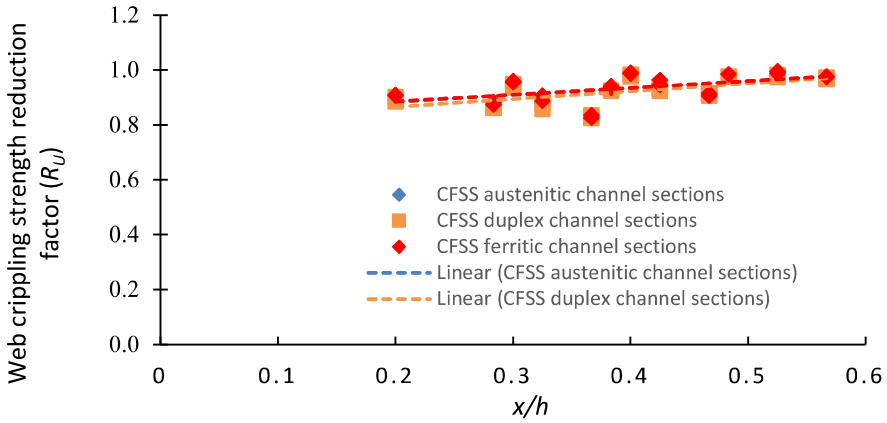

(b) Sections with fastened flange

Figure 4.14: Web crippling strength reduction factor against x/h for CFSS channel section with unstiffened web holes under ETF loading condition

4.3.3 Effects of *N/h* on the web crippling strength reduction factor (R_U)

The effects of *N/h* ratio on the web crippling strength reduction factor (R_U) were investigated. The findings, based on channel sections with an inner radius of 4, *a/h* ratio of 0.4, and *N* values of 50 and 100, were presented in Figures 4.15a-4.15c and Figures 4.16a-4.16c for CFSS channel sections subjected to ITF and ETF loading conditions, respectively. As per the figures, the increase in *N/h* ratio affects only the austenitic and ferritic channel sections with fastened flanges under ITF loading condition, and the reduction factor undergoes an average decrease of 11%.

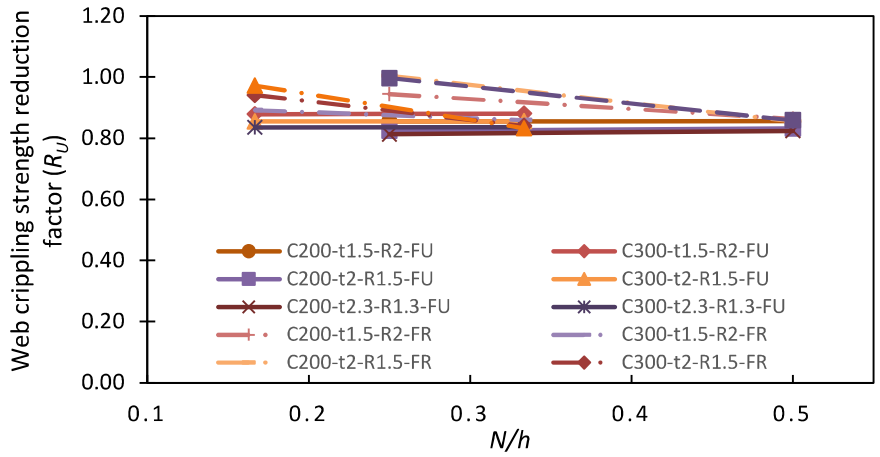

a. CFSS austenitic channel section

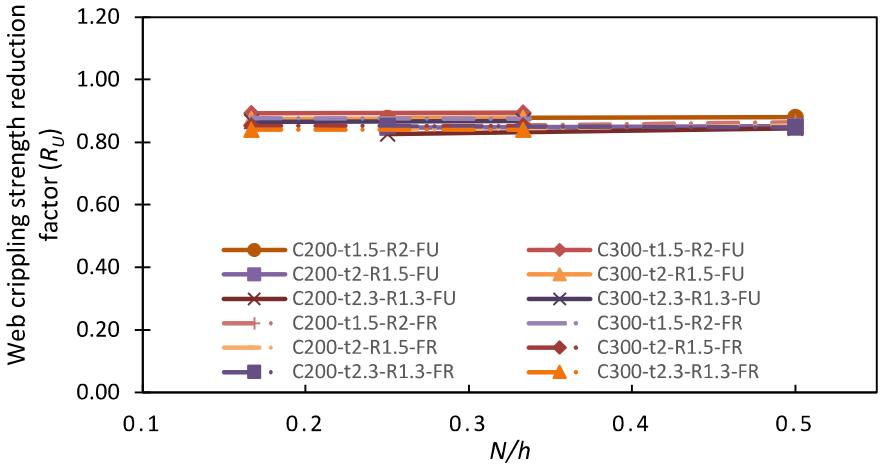

b. CFSS duplex channel section

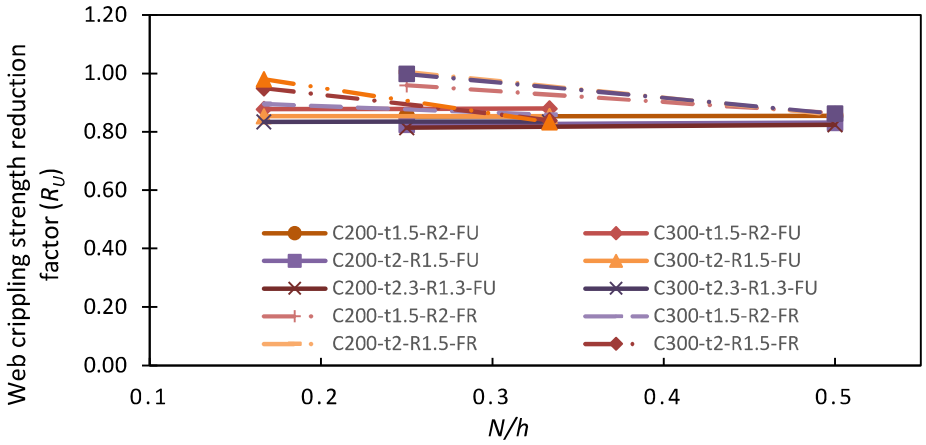

c. CFSS ferritic channel section

Figure 4.15: Web crippling strength reduction factor against *N/h* for CFSS channel section with unstiffened web holes under ITF loading condition

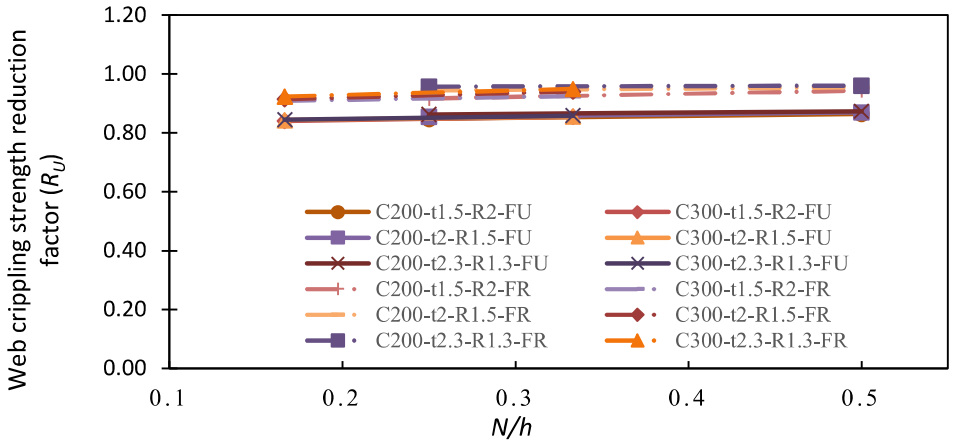

a. CFSS austenitic channel section

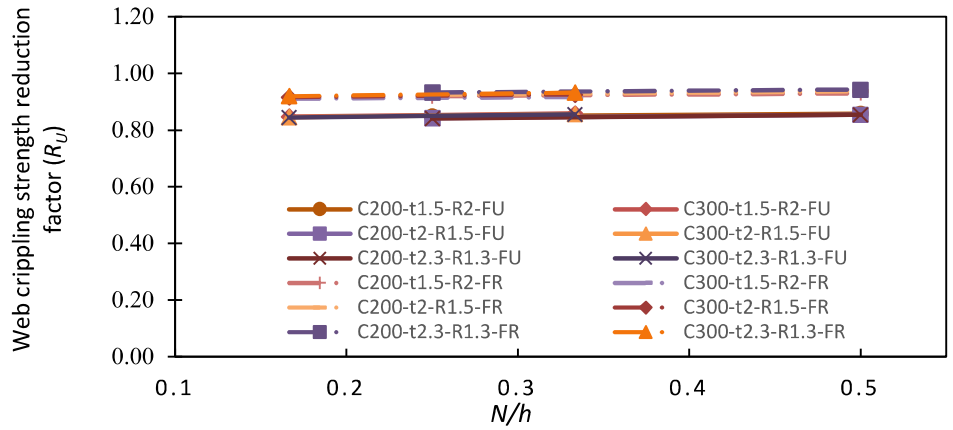

b. CFSS duplex channel section

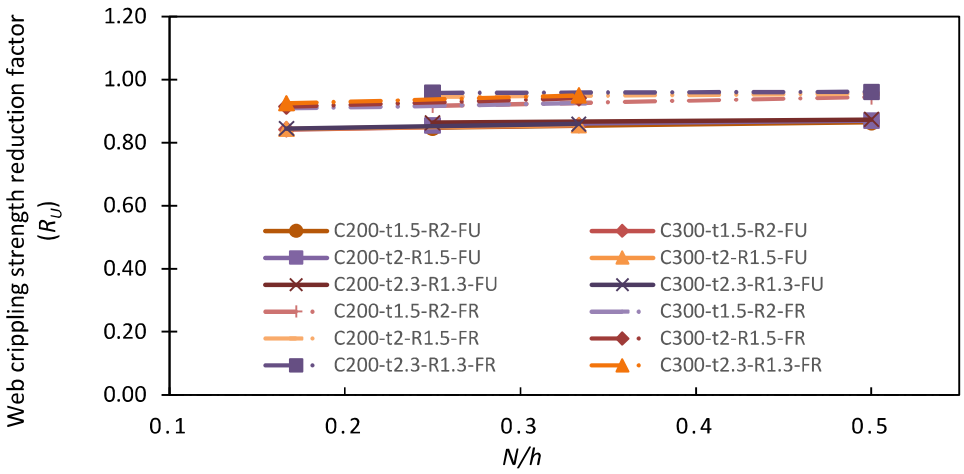

c. CFSS ferritic channel section

Figure 4.16: Web crippling strength reduction factor against *N/h* for CFSS channel section with unstiffened web holes under ETF loading condition

4.3.4 Effects of fastened flange on the web crippling strength reduction factor (R_U)

The data from Tables 4.3a-4.3d and 4.4a-4.4d consistently indicates that CFSS channel sections with fastened flanges exhibit higher web crippling strength compared to those with unfastened flanges. Specifically, web crippling strength of CFSS channel sections with fastened flanges under ITF loading condition is 41%, 55%, and 41% higher than with unstiffened flanges for CFSS austenitic, duplex, and ferritic sections, respectively. Conversely, under ETF loading conditions, web crippling strength of channel sections with fastened flanges is on the average higher by 78%, 96%, and 78% for CFSS austenitic, duplex, and ferritic sections, respectively.

4.4 Parametric study on the effect of edge-stiffened web holes on the web crippling strength reduction factor (R_S)

This study investigated the effect of edge-stiffened holes on the web crippling strength reduction factor (R_S) of CFSS channel sections. This investigation considered the following parameters: the ratio of inside bend radius to web thickness (*r/t*), the ratio of web flat depth to web thickness (*h/t*), the ratio of hole diameter to web flat depth (*a/h*), the ratio of bearing length to web flat depth (*N/h*), the ratio of hole distance to web flat depth (*x/h*), the ratio of stiffener length to web flat depth (*q/h*), and the condition of the flange (fastened or unfastened).

4.4.1 Effects of *r/t* on the web crippling strength reduction factor (R_S)

The effect of the *r/t* ratio on the web crippling strength reduction factor for CFSS channel sections with edge-stiffened web holes was investigated. This analysis involved two channel sections (C200 and C300) with an *a/h* ratio equal to 0.4, a bearing length of 50mm, two inner radius values (*r* = 3mm, 4mm), and three edge-stiffener lengths (*q* = 3mm, 5mm, 7mm). The results were graphically represented in Figures 4.17a-4.17f and Figures 4.18a-4.18f for channel sections subjected to ITF and ETF loading conditions, respectively.

According to the figures, when the *r/t* ratio increases from 1.3 to 2.0, the web crippling strength reduction factor for CFSS channel sections either remains relatively constant or increases up to 12% and 24% for sections under ITF and ETF loading conditions, respectively.

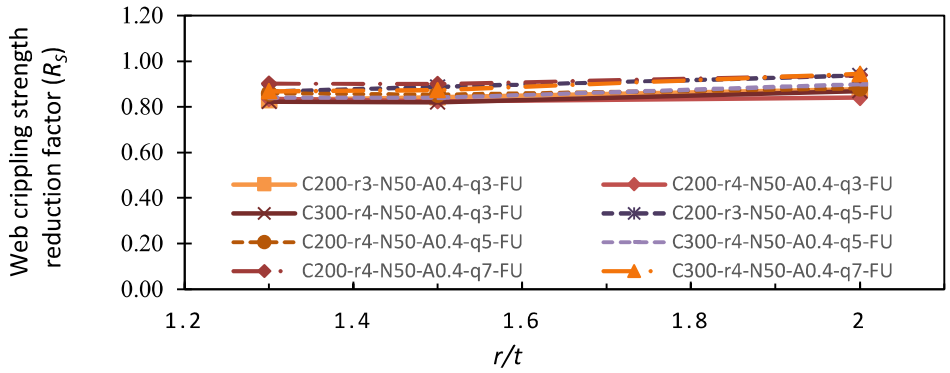

a. CFSS austenitic channel section with unfastened flange

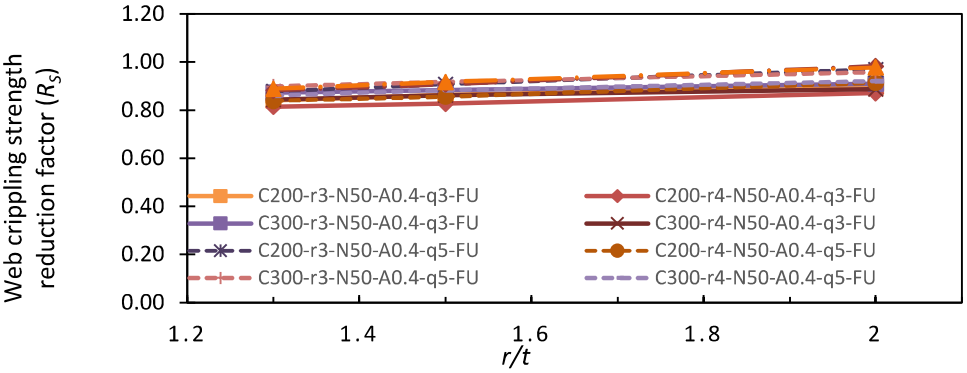

b. CFSS duplex channel section with unfastened flange

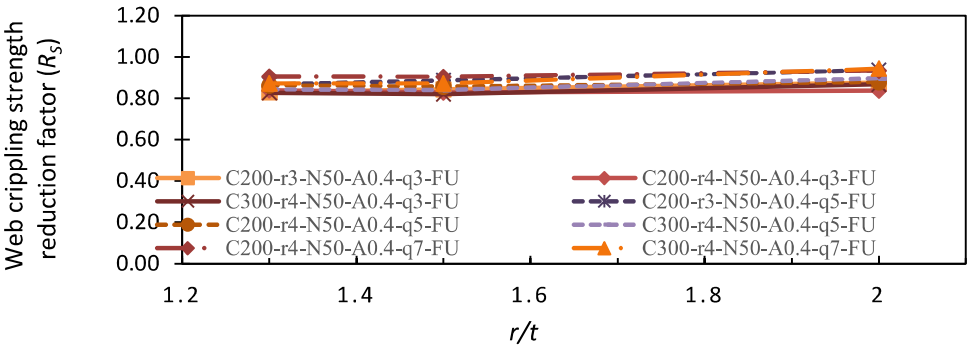

c. CFSS ferritic channel section with unfastened flange

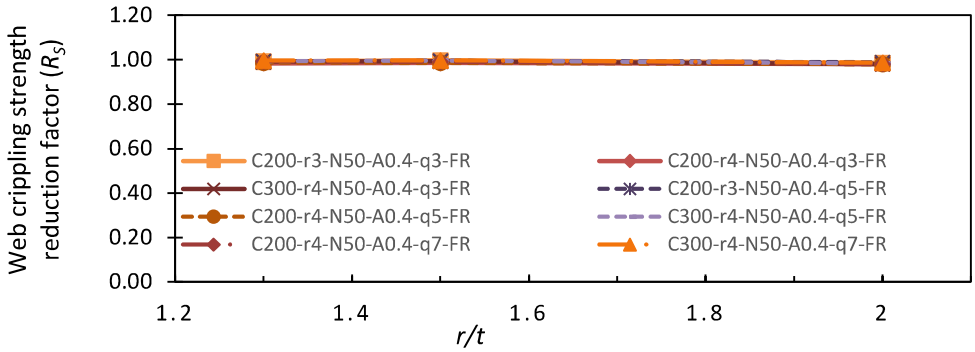

d. CFSS austenitic channel section with fastened flange

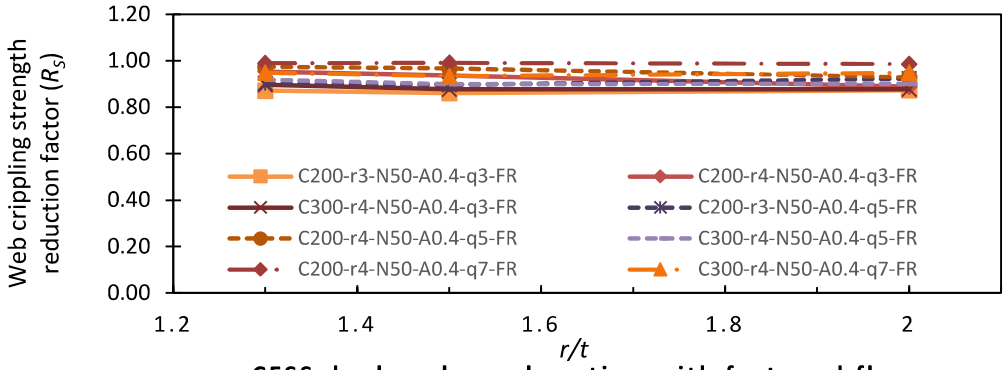

e. CFSS duplex channel section with fastened flange

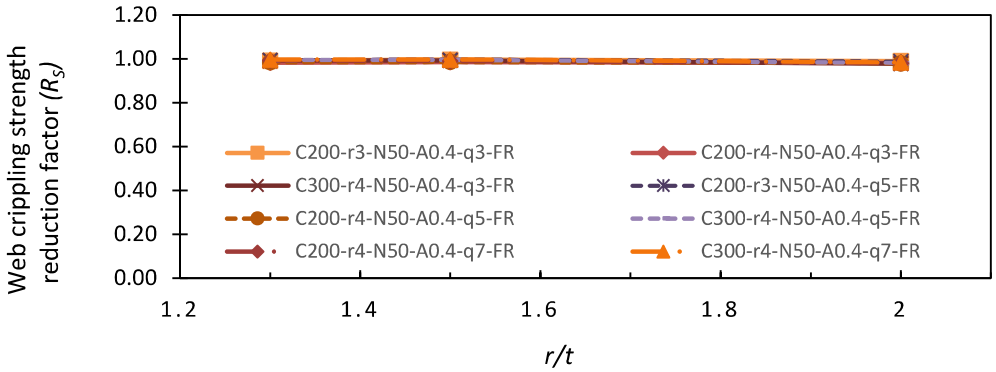

f. CFSS ferritic channel section with fastened flange

Figure 4.17: Web crippling strength reduction factor against *r/t* for CFSS channel section with edge-stiffened web holes under ITF loading condition

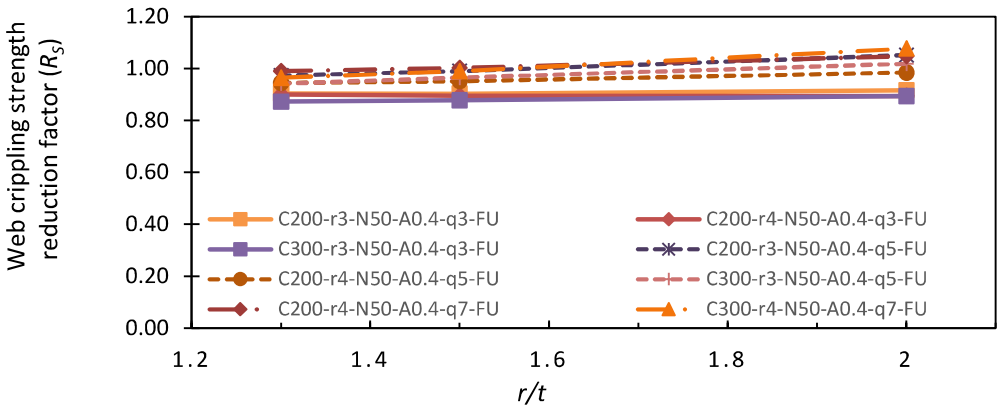

a. CFSS austenitic channel section with unfastened flange

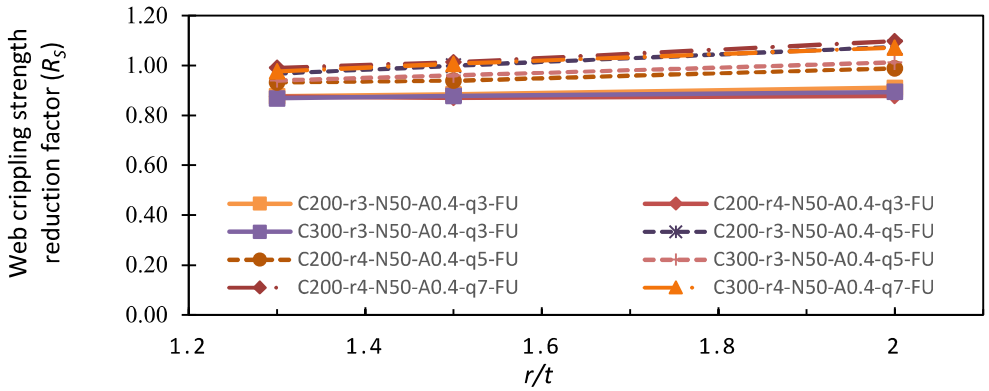

b. CFSS duplex channel section with unfastened flange

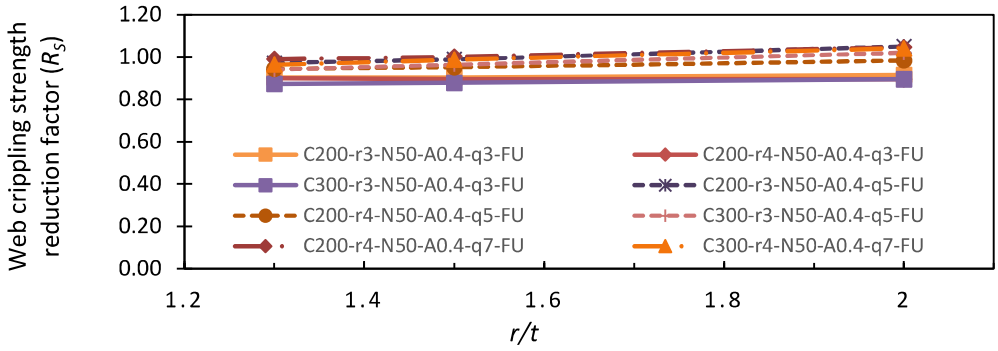

c. CFSS ferritic channel section with unfastened flange

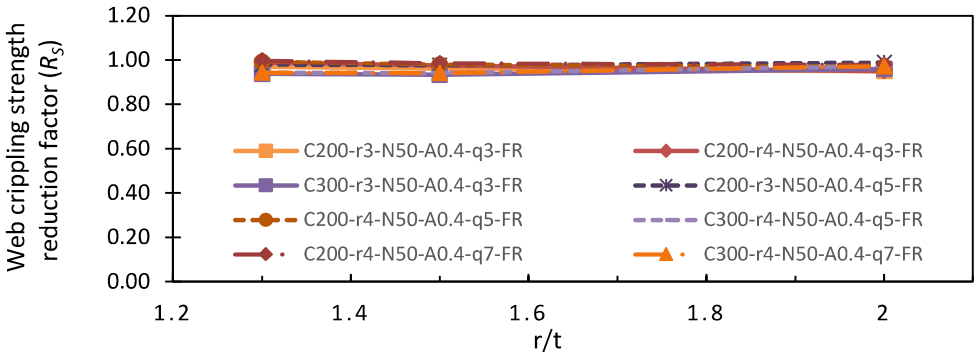

d. CFSS austenitic channel section with fastened flange

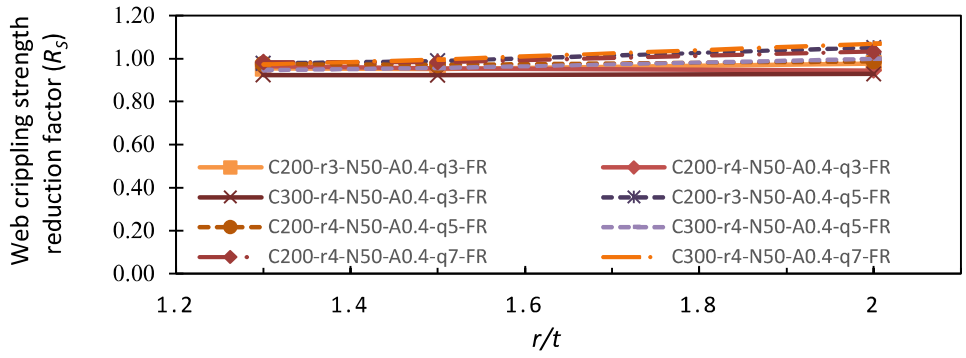

e. CFSS duplex channel section with fastened flange

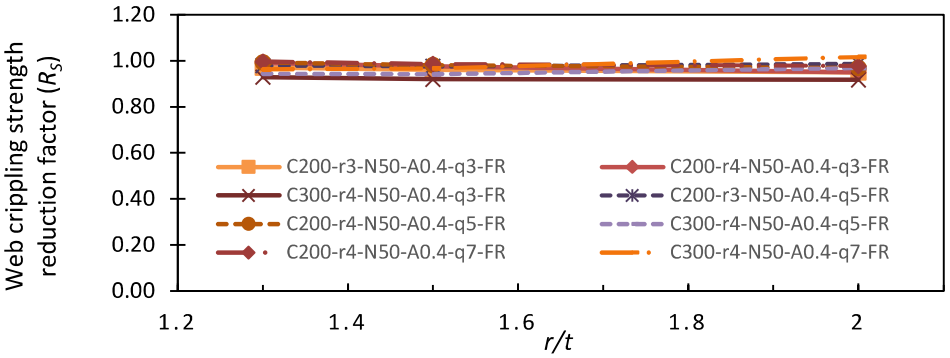

f. CFSS ferritic channel section with fastened flange

Figure 4.18: Web crippling strength reduction factor against *r/t* for CFSS channel section with edge-stiffened web holes under ETF loading condition

4.4.2 Effects of *h/t* on the web crippling strength reduction factor (R_S)

Figure 4.19a-4.19f and Figures 4.20a-4.20f illustrates the effects of *h/t* on the web crippling strength reduction factor for CFSS channel sections under ITF and ETF loading conditions, respectively. The investigation considered the following parameters: two channel sections (C200 and C300), two edge-stiffener lengths (3mm and 5mm), two bearing lengths (50mm and 100mm), inner radius equal to 3mm, and *a/h* ratio equal to 0.4.

Upon examination of the figures, it is evident that the *h/t* ratio does not significantly affect the web crippling strength reduction factor, as the graph tends to remain nearly flat for both ITF and ETF loading conditions.

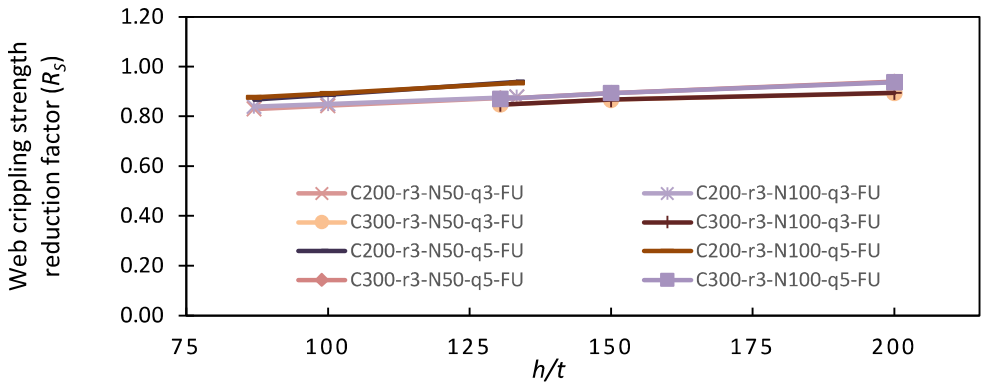

a. CFSS austenitic channel section with unfastened flange

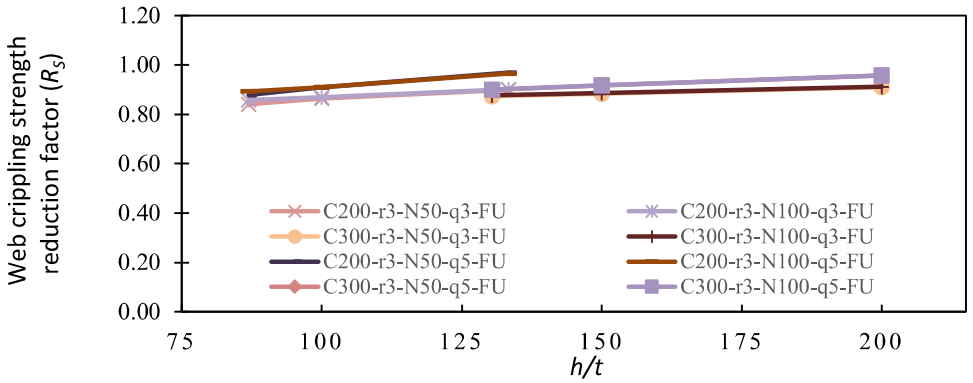

b. CFSS duplex channel section with unfastened flange

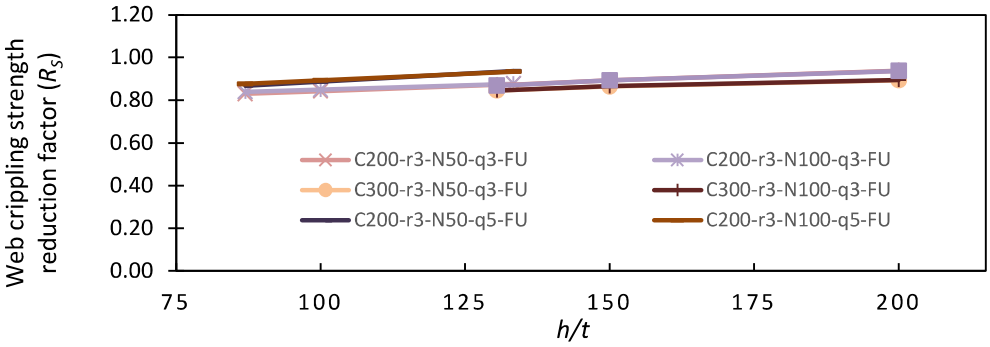

c. CFSS ferritic channel section with unfastened flange

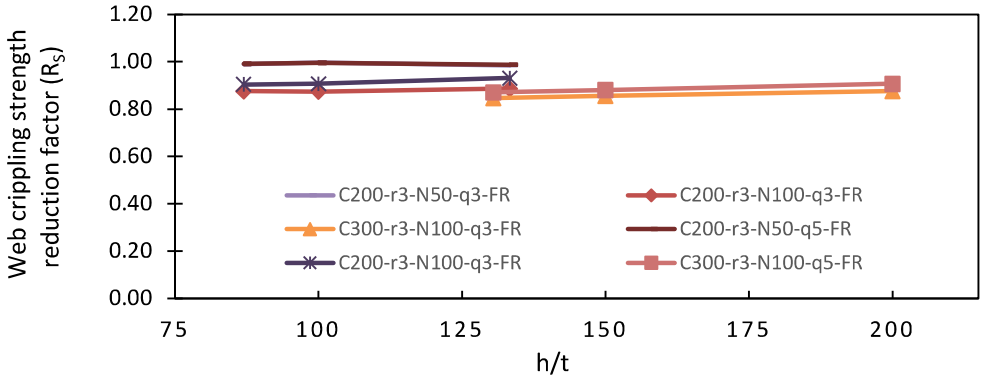

d. CFSS austenitic channel section with fastened flange

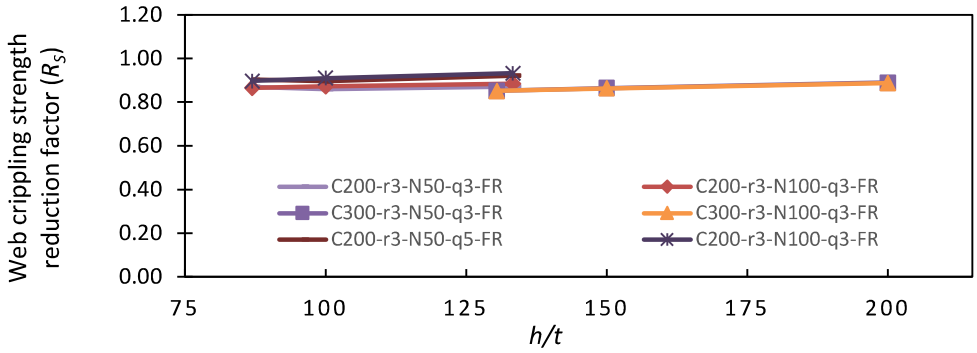

e. CFSS duplex channel section with fastened flange

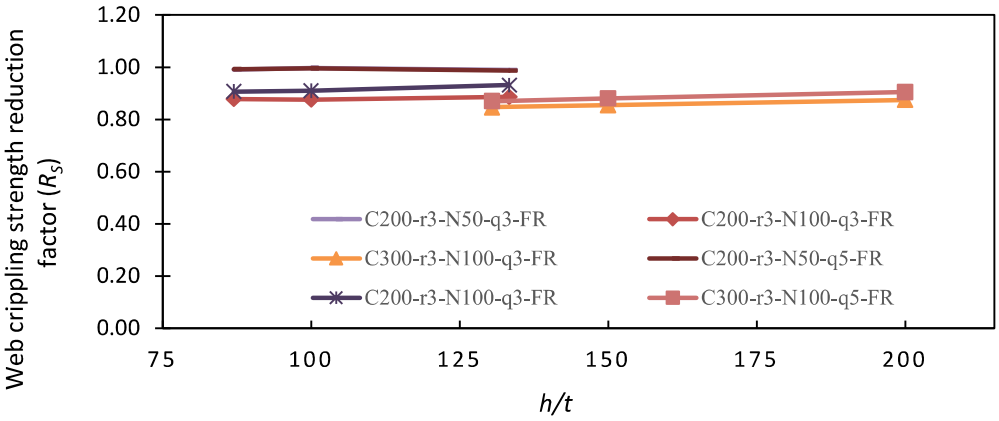

f. CFSS ferritic channel section with fastened flange

Figure 4.19: Web crippling strength reduction factor against *h/t* for CFSS channel section with edge-stiffened web holes under ITF loading condition

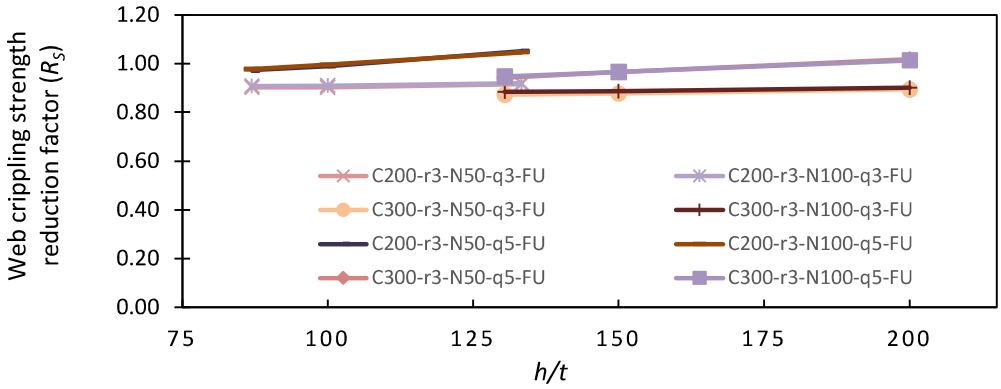

a. CFSS austenitic channel section with unfastened flange

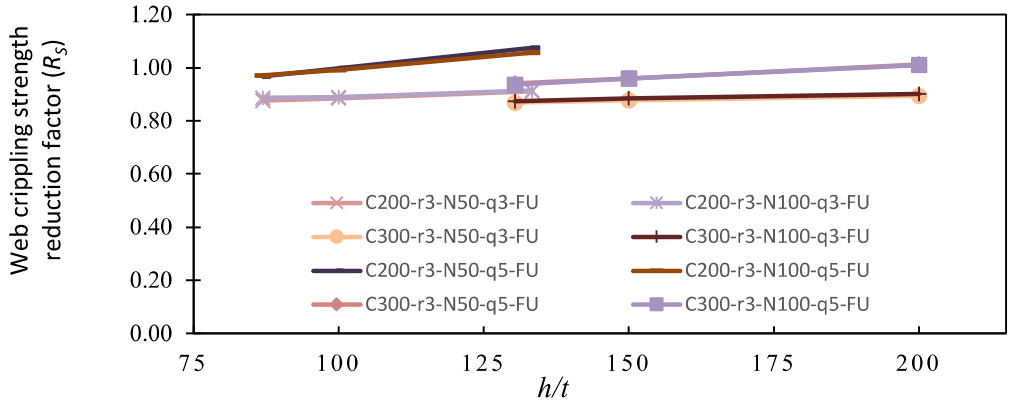

b. CFSS duplex channel section with unfastened flange

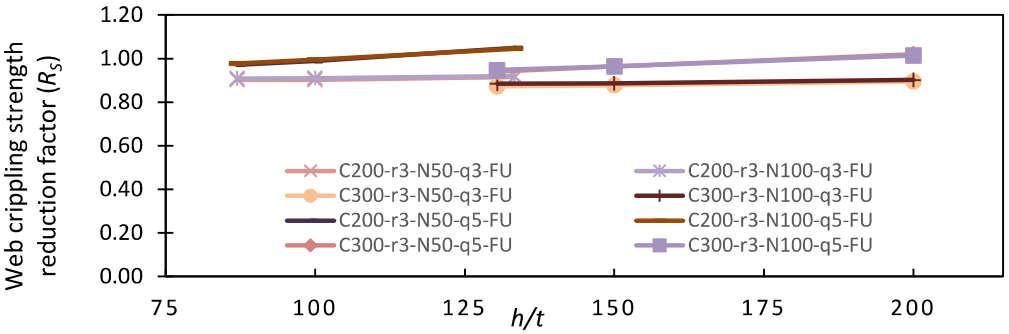

c. CFSS ferritic channel section with unfastened flange

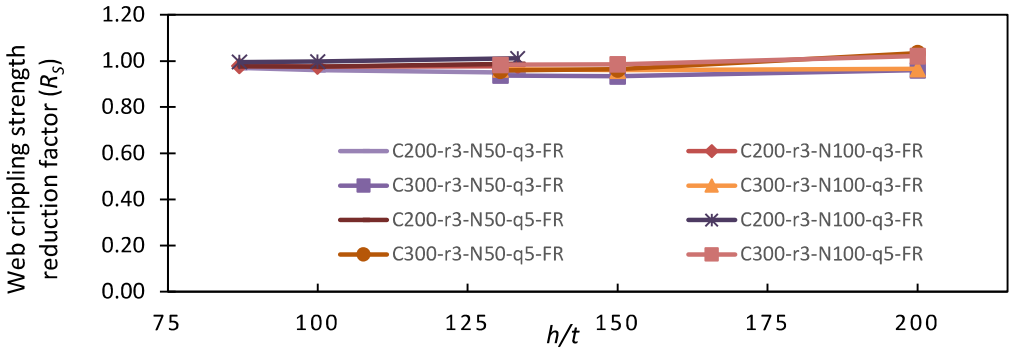

d. CFSS austenitic channel section with fastened flange

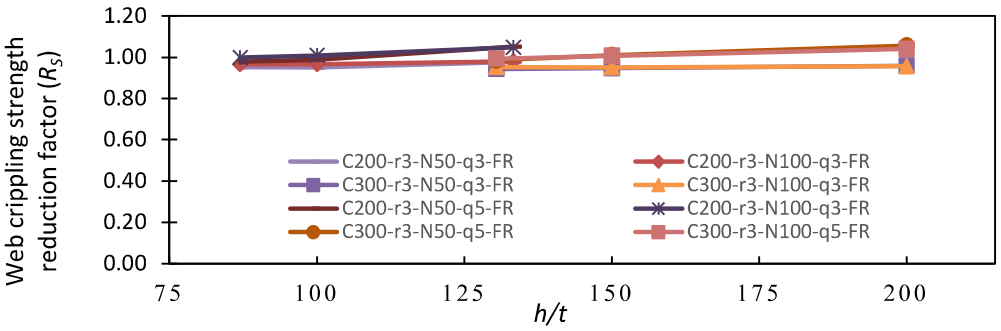

e. CFSS duplex channel section with fastened flange

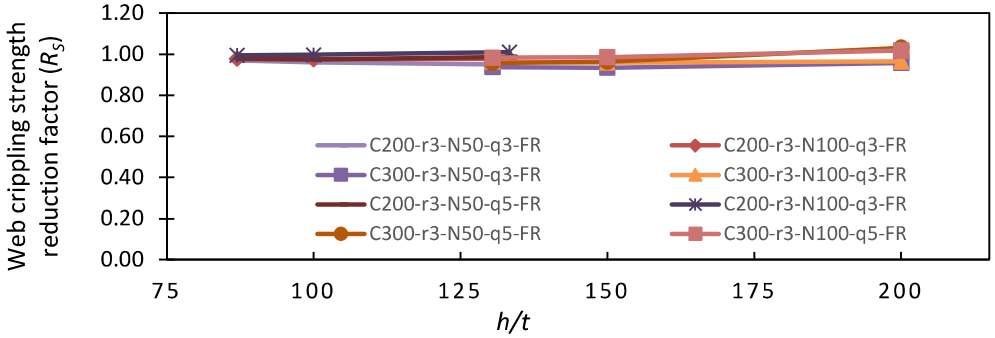

f. CFSS ferritic channel section with fastened flange

Figure 4.20: Web crippling strength reduction factor against *h/t* for CFSS channel section with edge-stiffened web holes under ETF loading condition

4.4.3 Effects of *a/h* on the web crippling strength reduction factor (R_S)

The effect of *a/h* on the web crippling strength factor of CFSS channel sections under ITF and ETF loading conditions is depicted in Figures 4.21a-4.21f and Figures 4.22a-4.22f, respectively. The parameters considered in the figures include two channel sections (C200 and C300), three edge-stiffener lengths (3mm, 5mm, and 7mm), an *r/t* ratio of 1.5, and a bearing length of 50mm.

From the provided figures, it is evident that as *the a/h* ratio increases, the web crippling strength reduction factor decreases. Specifically, for channel sections with unfastened flanges under ITF loading conditions, there is an average decrease of 26% across all stainless steel grades. For channel sections with fastened flanges, there is an initial decrease of 3% as the *a/h* ratio increases from 0.2 to 0.4. This reduction escalates to 12% as the *a/h* ratio further increases from 0.4 to 0.6.

For channel sections subjected to ETF loading conditions, there is an average decrease in the web crippling strength reduction factor of 15% for channels with unfastened flanges and 9% for channels with fastened flanges as the *a/h* ratio increases from 0.2 to 0.6.

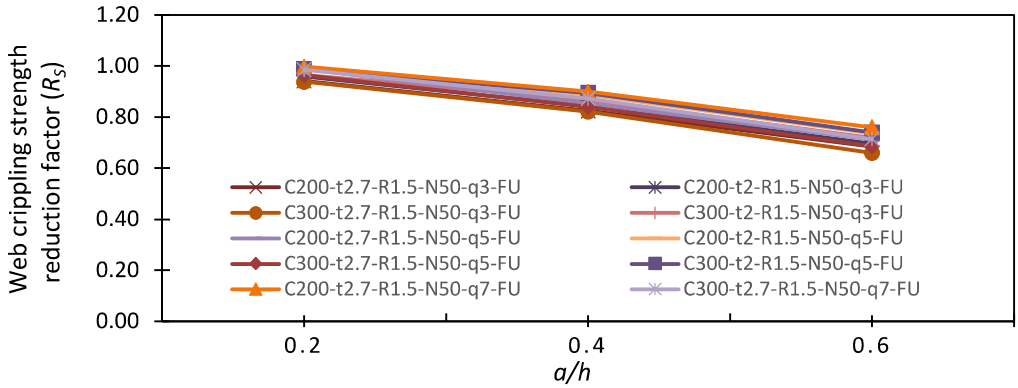

a. CFSS austenitic channel section with unfastened flange

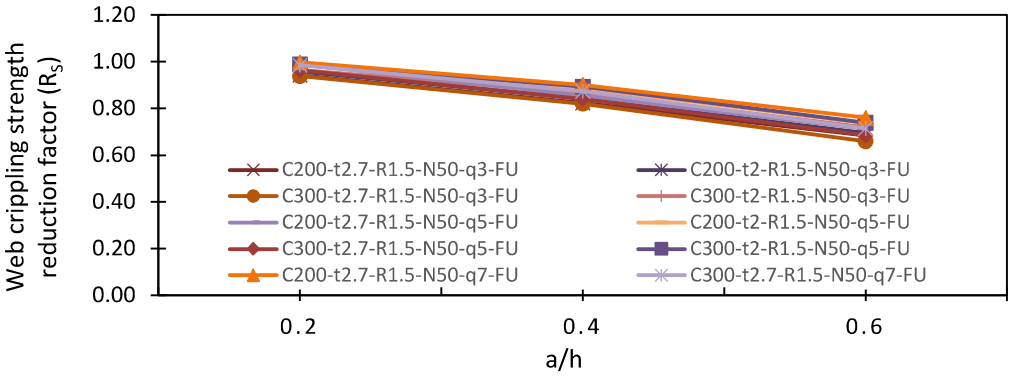

b. CFSS duplex channel section with unfastened flange

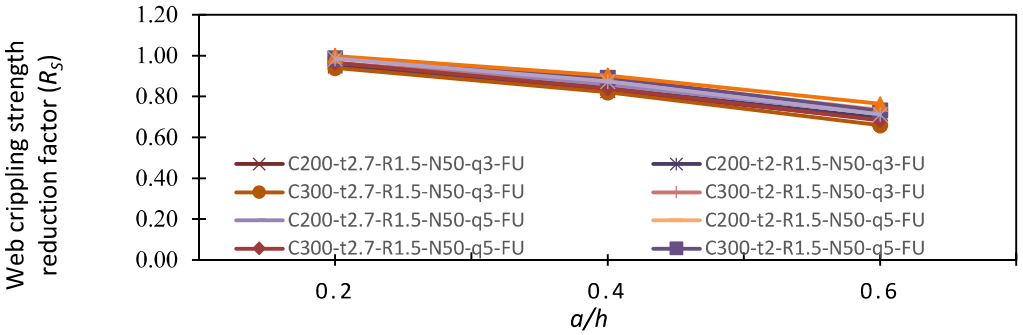

c. CFSS ferritic channel section with unfastened flange

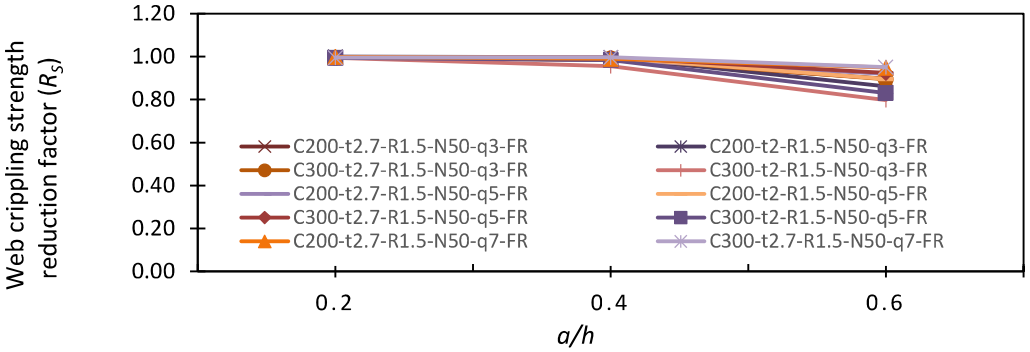

d. CFSS austenitic channel section with fastened flange

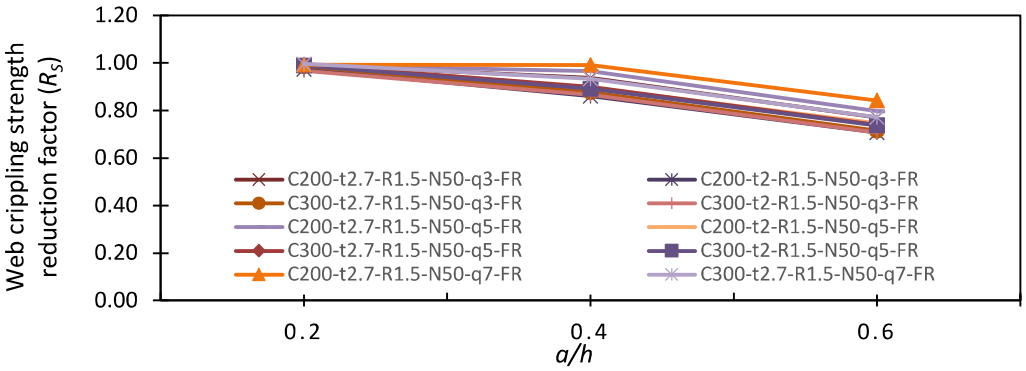

e. CFSS duplex channel section with fastened flange

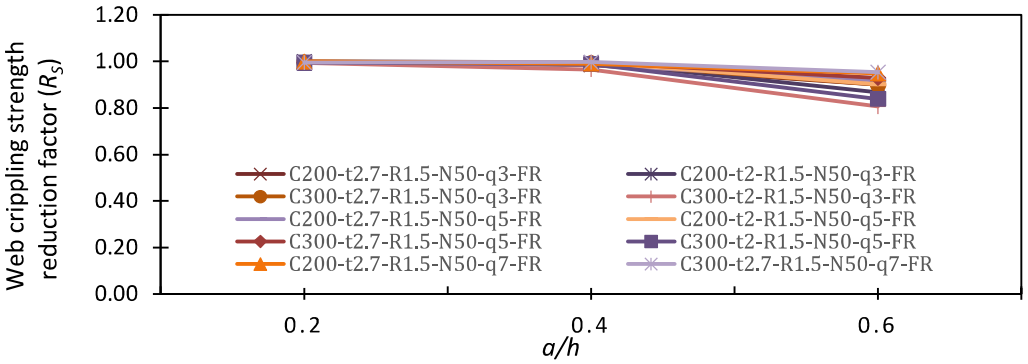

f. CFSS ferritic channel section with fastened flange

Figure 4.21: Web crippling strength reduction factor against *a/h* for CFSS channel section with edge-stiffened web holes under ITF loading condition

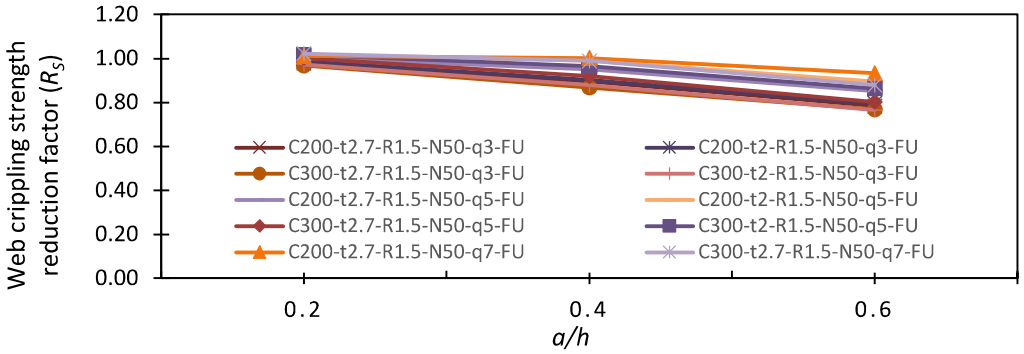

a. CFSS austenitic channel section with unfastened flange

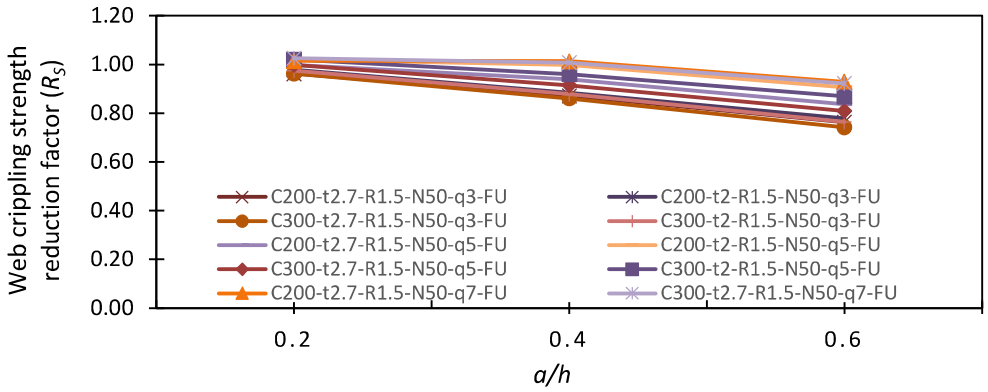

b. CFSS duplex channel section with unfastened flange

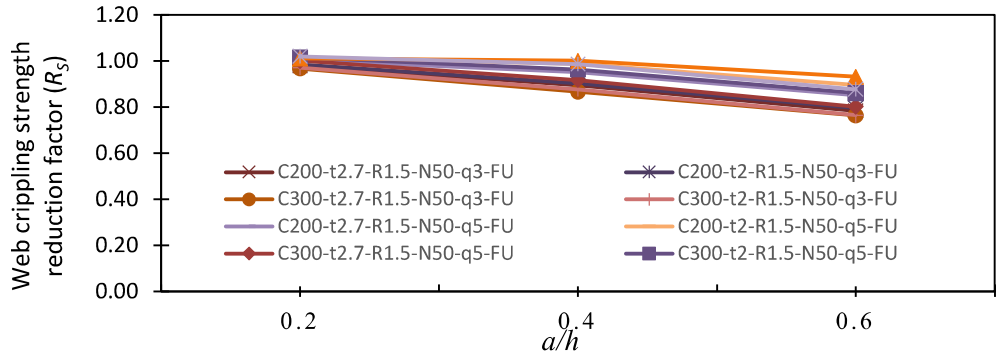

c. CFSS ferritic channel section with unfastened flange

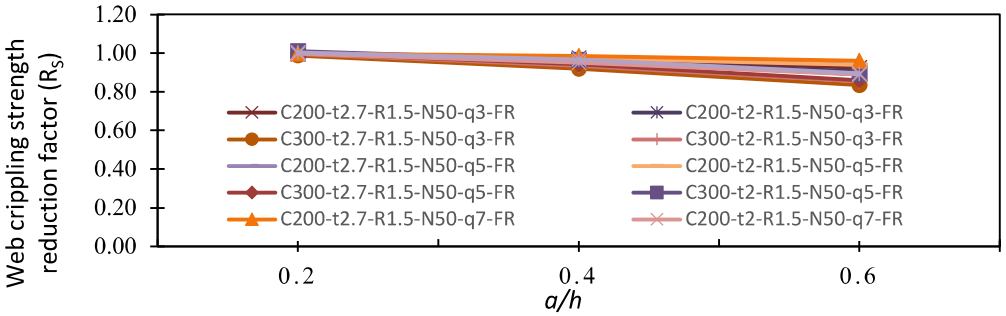

d. CFSS austenitic channel section with fastened flange

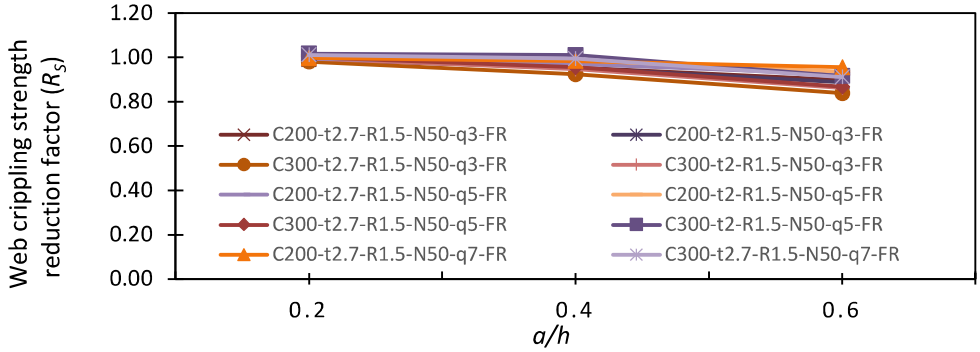

e. CFSS duplex channel section with fastened flange

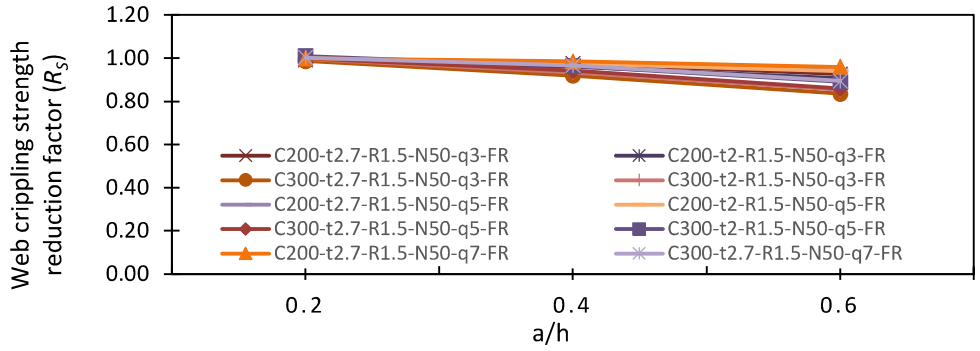

f. CFSS ferritic channel section with fastened flange

Figure 4.22: Web crippling strength reduction factor against *a/h* for CFSS channel section with edge-stiffened web holes under ETF loading condition

4.4.4 Effects of *N/h* on the web crippling strength reduction factor (R_S)

Effects of *N/h* on the web crippling strength reduction factor were analysed considering two types of channel sections (C200 and C300), two bearing lengths (50mm and 100mm), two values of edge-stiffener lengths (3mm and 5mm), channels with an inner radius of 3mm, and an *a/h* ratio of 0.4. The findings are visually represented in Figures 4.23a-4.23f and Figures 4.24a-4.24f for channel sections subjected to ITF and ETF loading conditions, respectively.

Based on Figures 4.23a-4.23f and Figures 4.24a-4.24f, it is evident that for channel sections with unfastened flanges under both ITF and ETF loading conditions, the web crippling strength reduction factor is not significantly affected by the change in *N/h* ratio, as it remains relatively constant. The trend is consistent for channel sections with fastened flanges, except for austenitic and ferritic sections under ITF loading conditions, where the web crippling strength reduction factor decreases by an average of 9%.

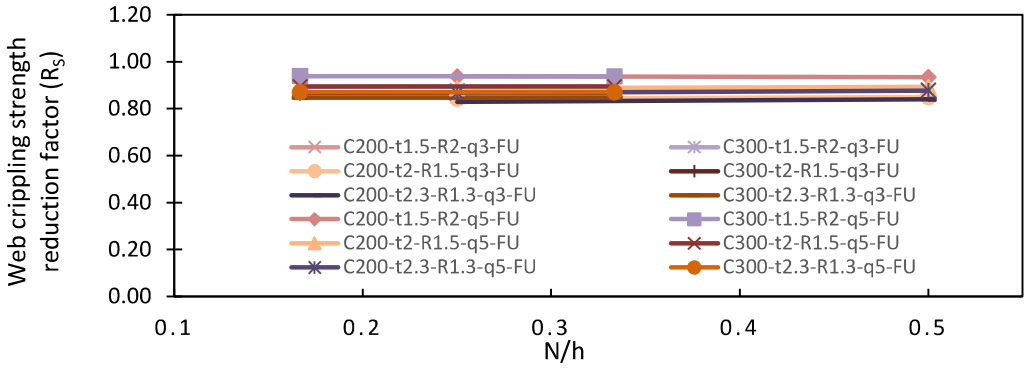

a. CFSS austenitic channel section with unfastened flange

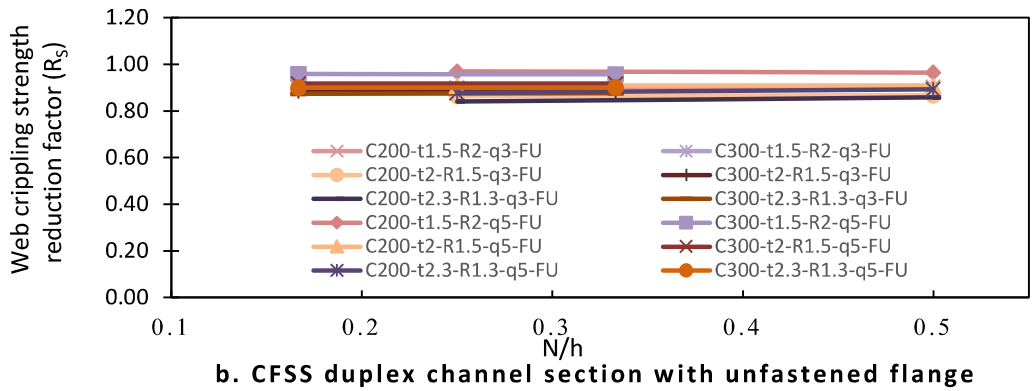

b. CFSS duplex channel section with unfastened flange

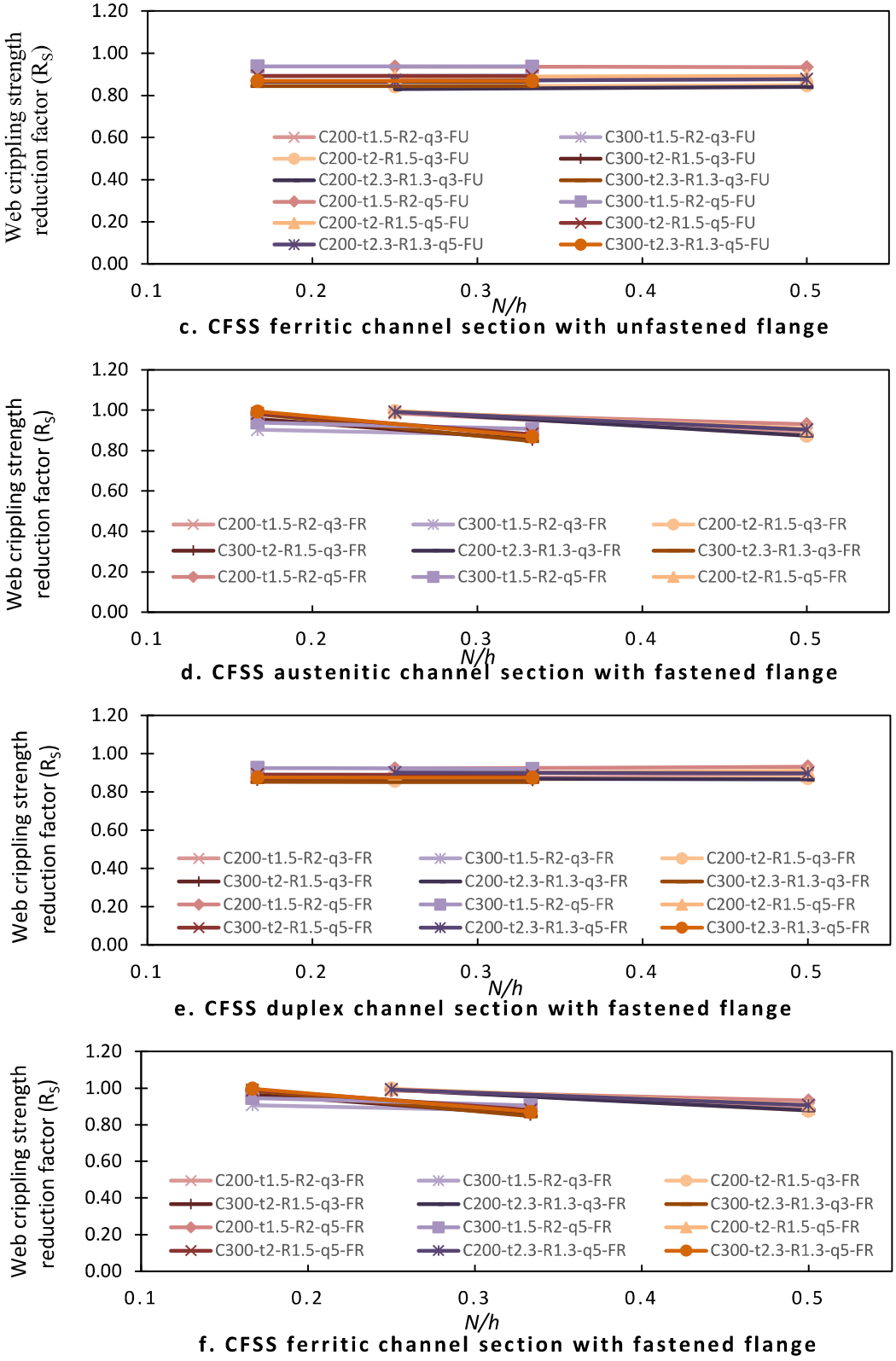

Figure 4.23: Web crippling strength reduction factor against *N/h* for CFSS channel section with edge-stiffened web holes under ITF loading condition

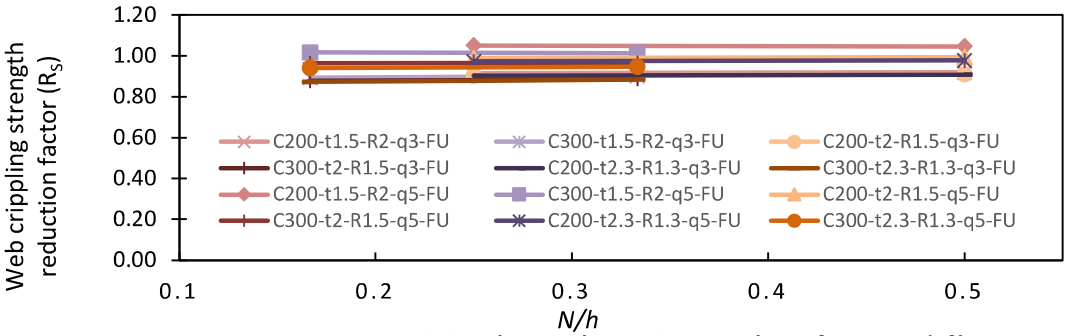

a. CFSS austenitic channel section with unfastened flange

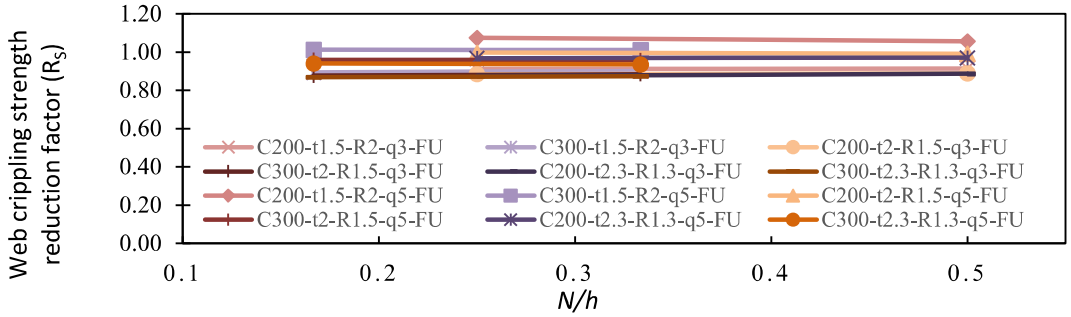

b. CFSS duplex channel section with unfastened flange

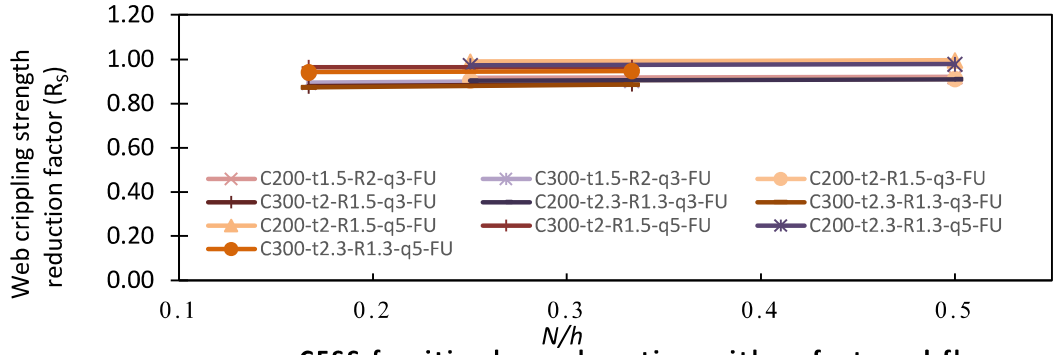

c. CFSS ferritic channel section with unfastened flange

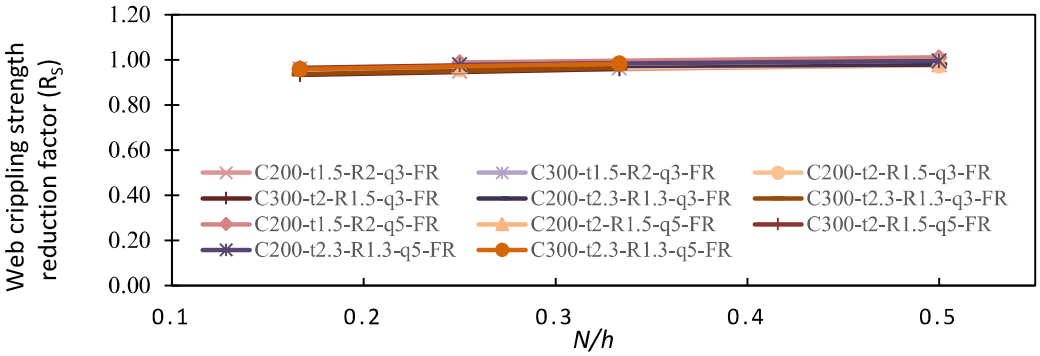

d. CFSS austenitic channel section with fastened flange

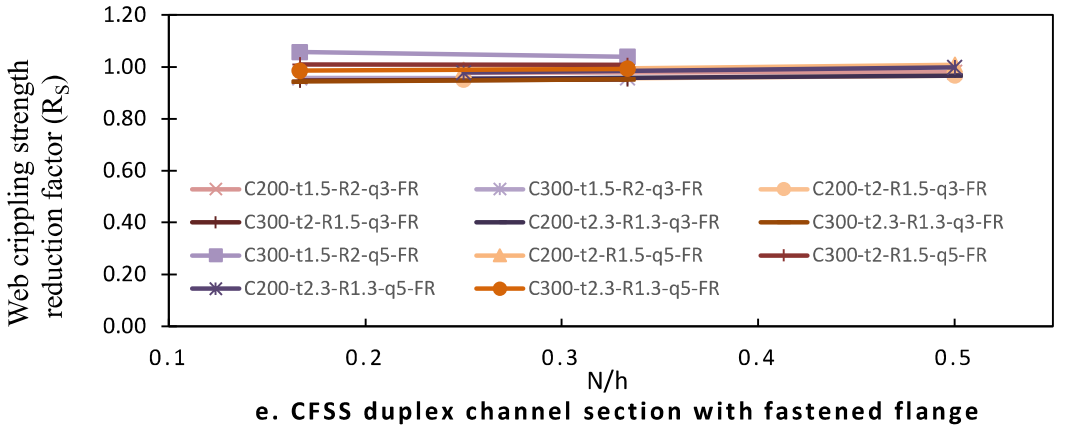

e. CFSS duplex channel section with fastened flange

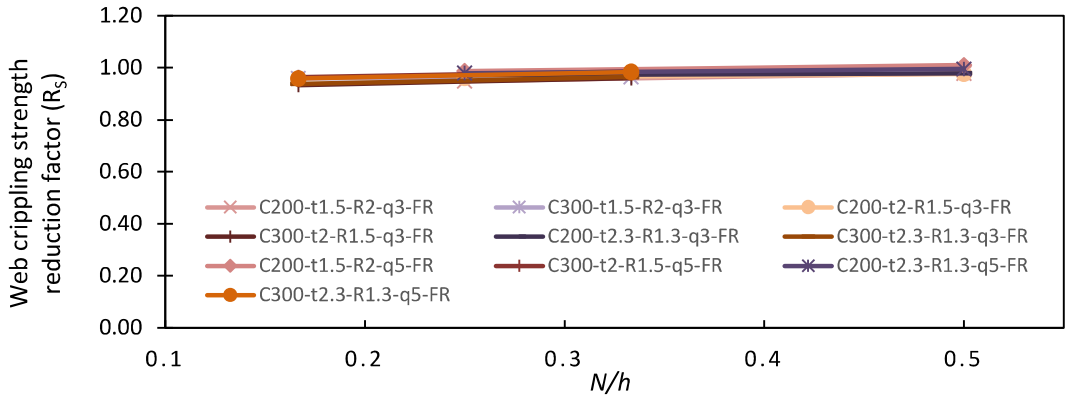

f. CFSS ferritic channel section with fastened flange

Figure 4.24: Web crippling strength reduction factor against *N/h* for CFSS channel section with edge-stiffened web holes under ETF loading condition

4.4.5 Effects of *q/h* on the web crippling strength reduction factor (R_S)

Figures 4.25a-4.25f and Figures 4.26a-4.26f depict the impact of *q/h* on the web crippling strength reduction factor of CFSS channel sections under ITF and ETF loading conditions, respectively. The parameters considered in this analysis include two types of channel sections (C200 and C300), three different edge-stiffener lengths (3mm, 5mm, and 7mm), a bearing plate length of 50mm, an inner radius of 3mm, and an *a/h* ratio of 0.4.

Figures 4.25a-4.25f and Figures 4.26a-4.26f demonstrate a steady rise in the web crippling strength factor as *q* increases from 3mm to 5mm. Then a sharp increase is observed as *q* further increases to

7mm. In detail, for channel sections under ITF loading conditions, as q increases from 3mm to 5mm, R_S increases at an average of 5% and 2% for channels with unfastened and fastened flanges, respectively. As q further increases to 7mm, the average increase of R_S spikes to 98% and 75% for channels with fastened and unfastened flanges, respectively.

Similarly, for channel sections under ETF loading conditions, as q increases from 3mm to 5mm, R_S increases at an average of 10% and 4% for channels with unfastened and fastened flanges, respectively. As q further increases to 7mm, the average increase of R_S spikes to 112% and 82% for channels with fastened and unfastened flanges, respectively.

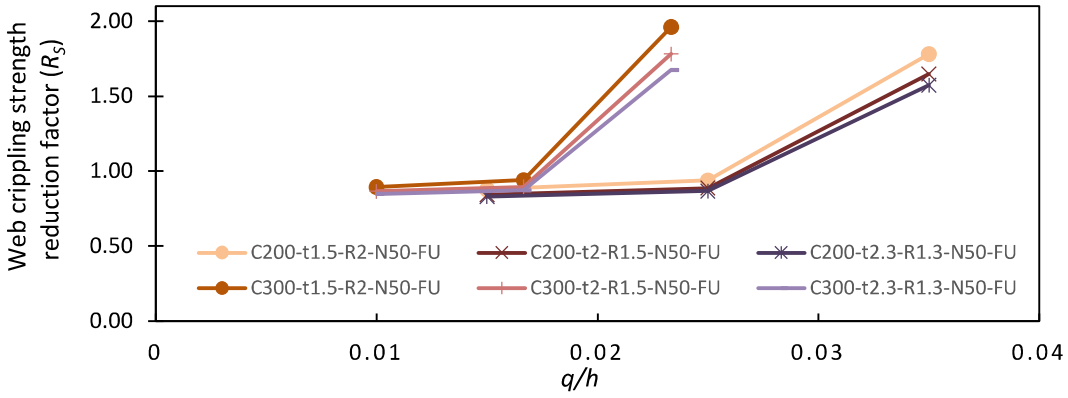

a. CFSS austenitic channel section with unfastened flange

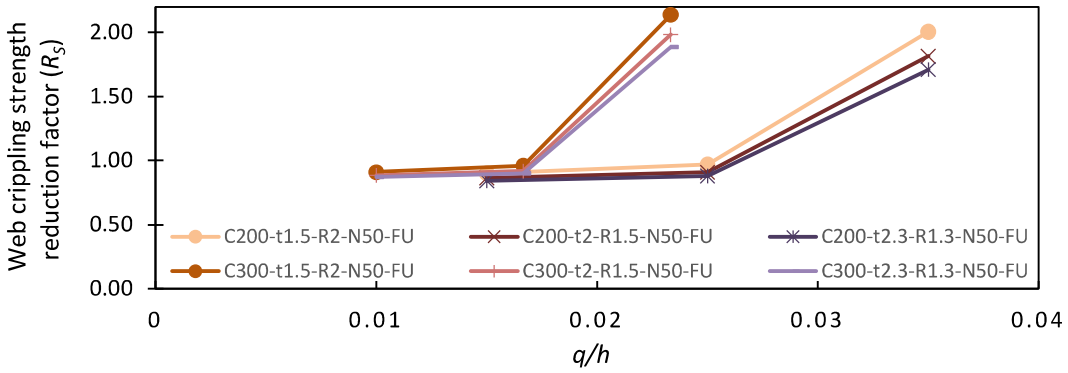

b. CFSS duplex channel section with unfastened flange

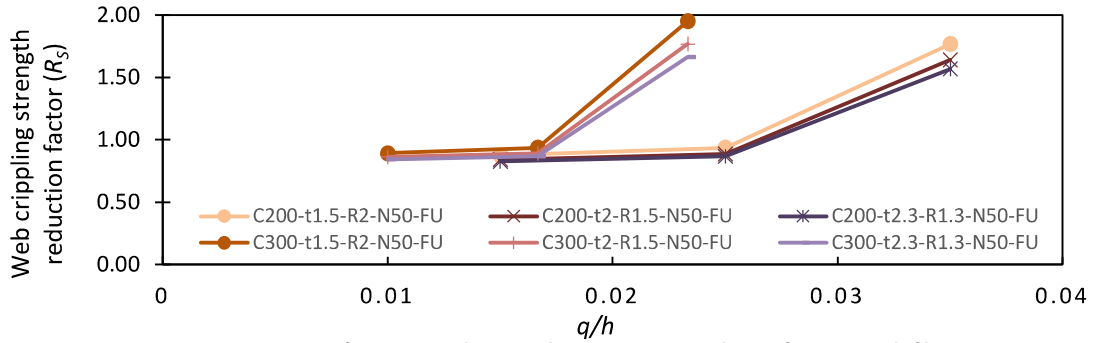

c. CFSS ferritic channel section with unfastened flange

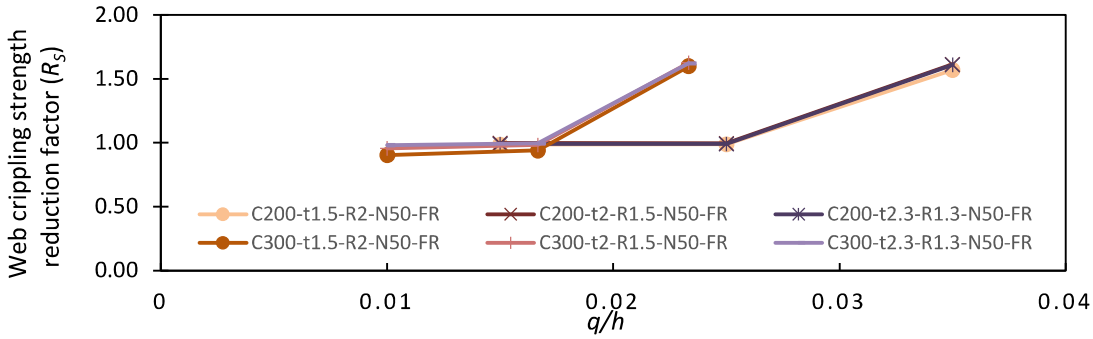

d. CFSS austenitic channel section with fastened flange

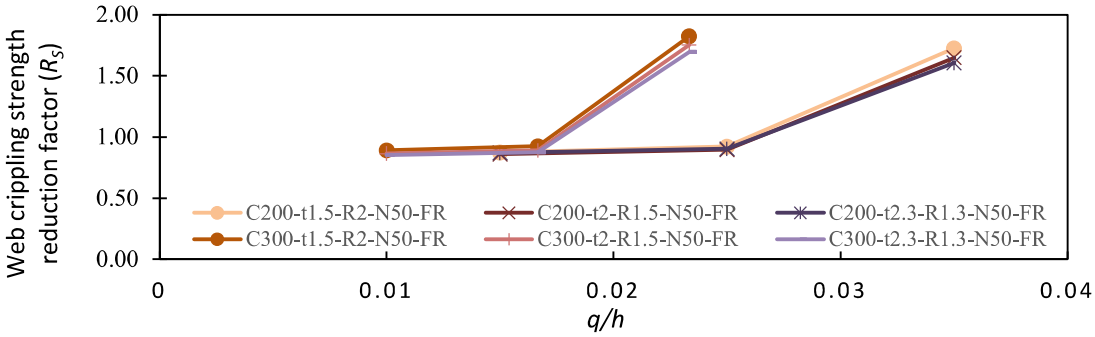

e. CFSS duplex channel section with fastened flange

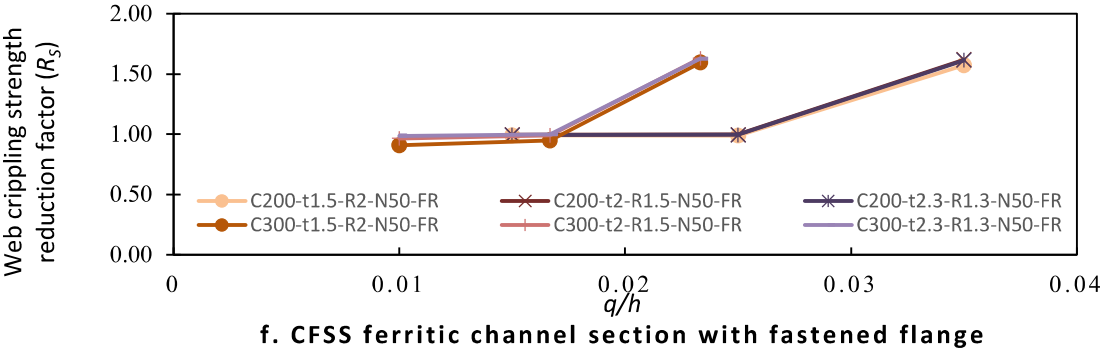

f. CFSS ferritic channel section with fastened flange

Figure 4.25: Web crippling strength reduction factor against *q/h* for CFSS channel section with edge-stiffened web holes under ITF loading condition

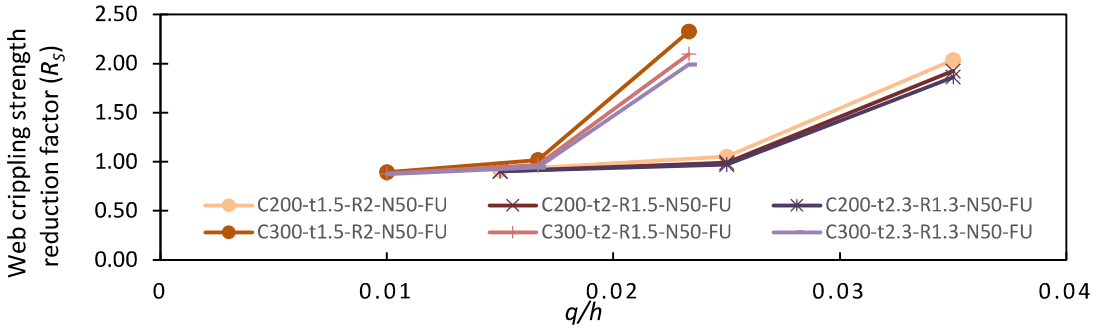

a. CFSS austenitic channel section with unfastened flange

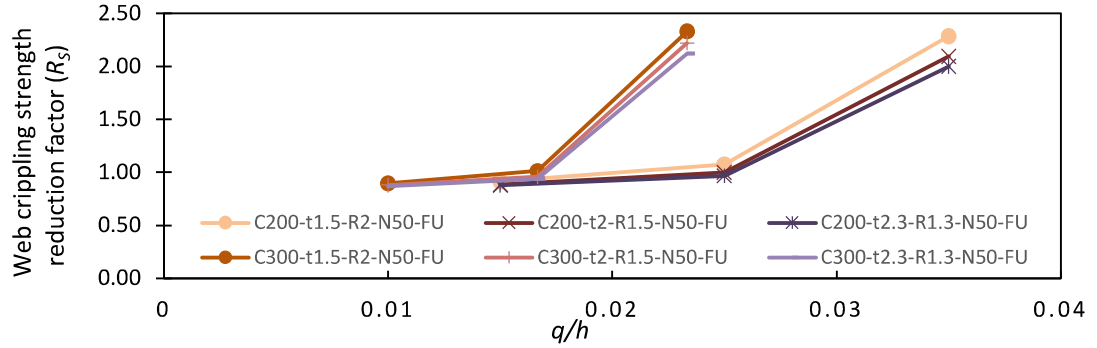

b. CFSS duplex channel section with unfastened flange

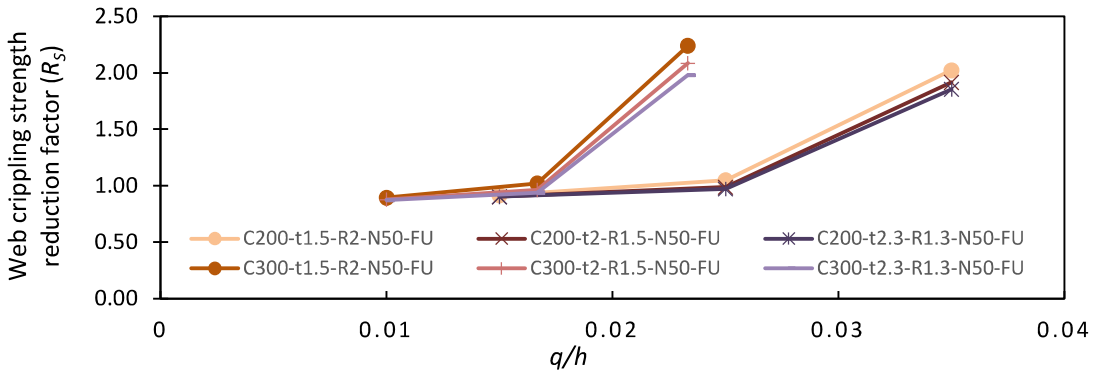

c. CFSS ferritic channel section with unfastened flange

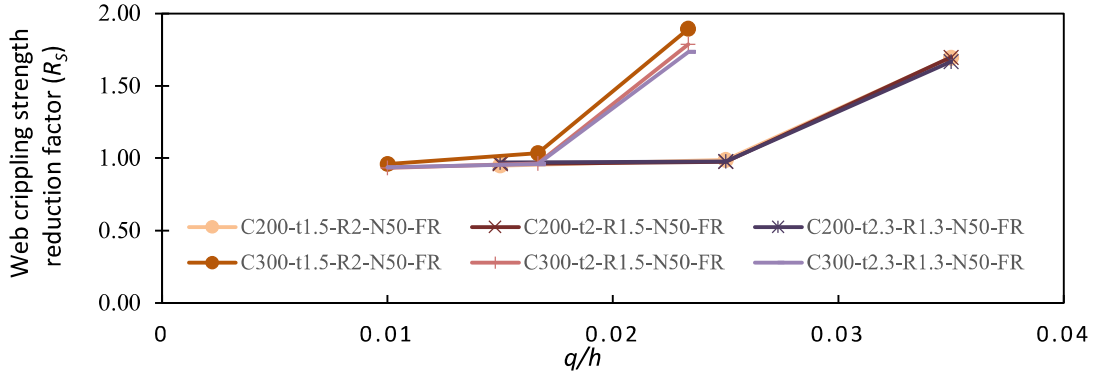

d. CFSS austenitic channel section with fastened flange

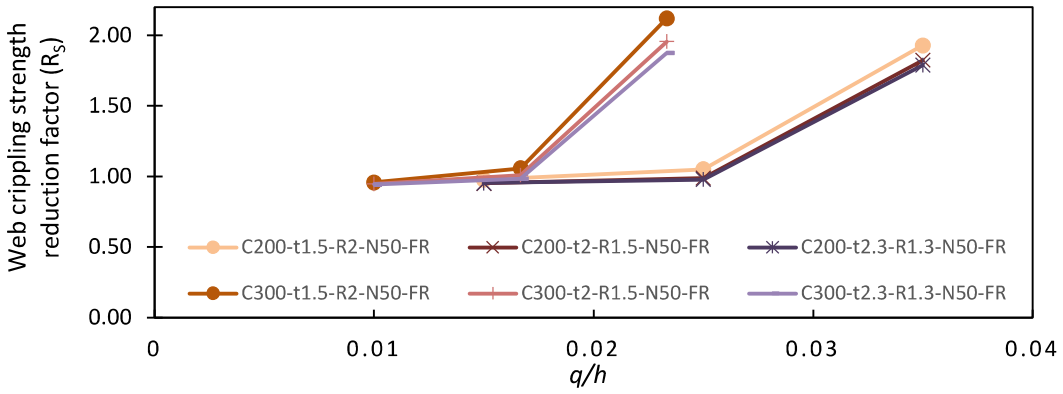

e. CFSS duplex channel section with fastened flange

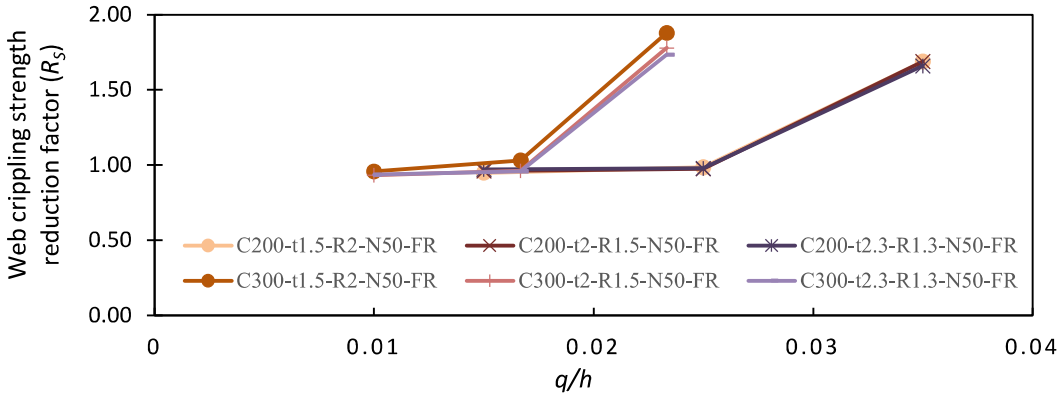

f. CFSS ferritic channel section with fastened flange

Figure 4.26: Web crippling strength reduction factor against *q/h* for CFSS channel section with edge-stiffened web holes under ETF loading condition

4.4.6 Effects of *x/h* on the web crippling strength reduction factor (R_S)

The result for the effect of the *x/h* ratio on the web crippling strength reduction factor for CFSS channel sections subjected to ETF loading condition is visually presented in Figs. 27a-27f. These figures reveal a consistent effect across CFSS austenitic, duplex, and ferritic channel sections. With an increase in the *x/h* ratio, the web crippling strength reduction factor increases by an average of 22% and 12% for channels with unfastened and fastened flanges, respectively.

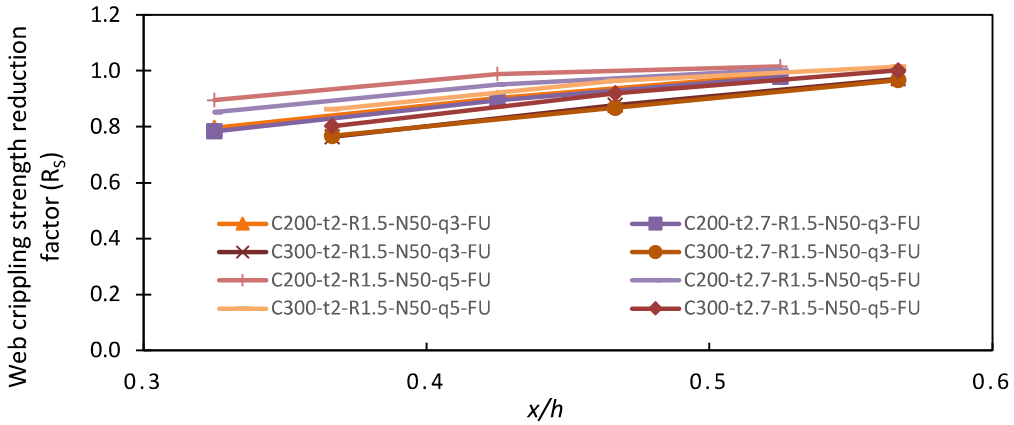

a. CFSS austenitic channel section with unfastened flange

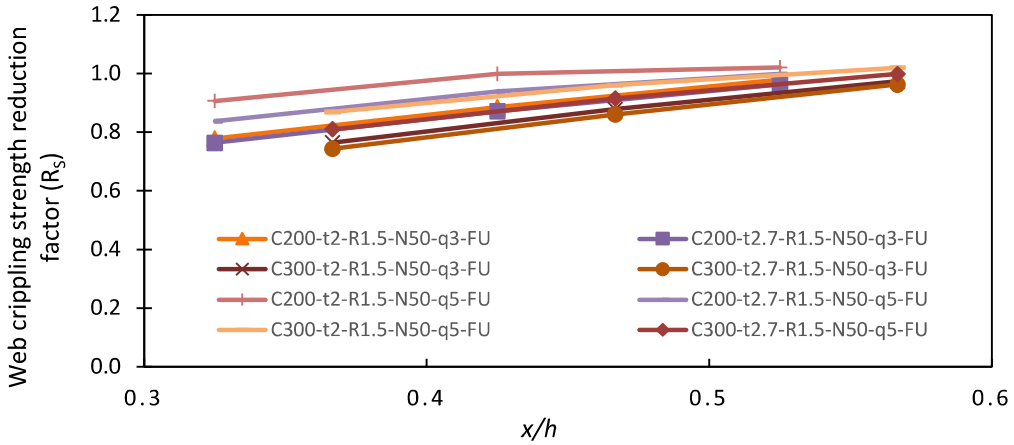

b. CFSS duplex channel section with unfastened flange

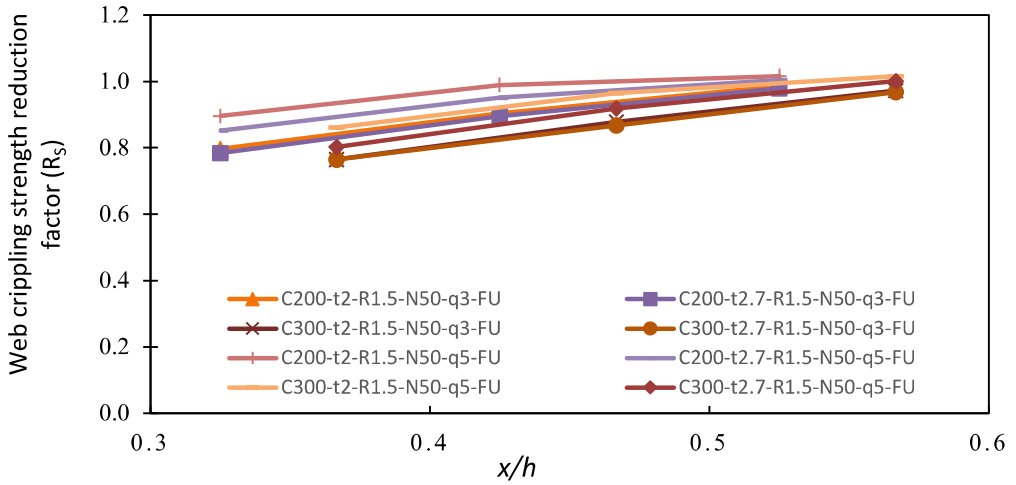

c. CFSS ferritic channel section with unfastened flange

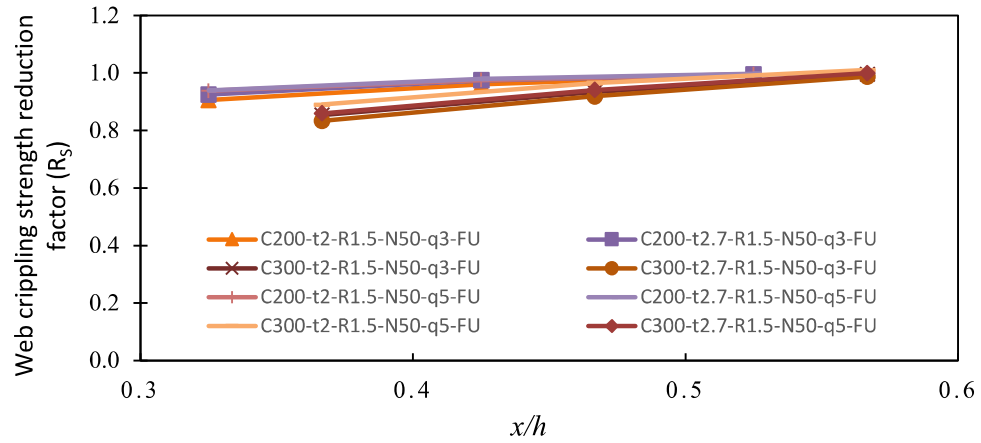

d. CFSS austenitic channel section with fastened flange

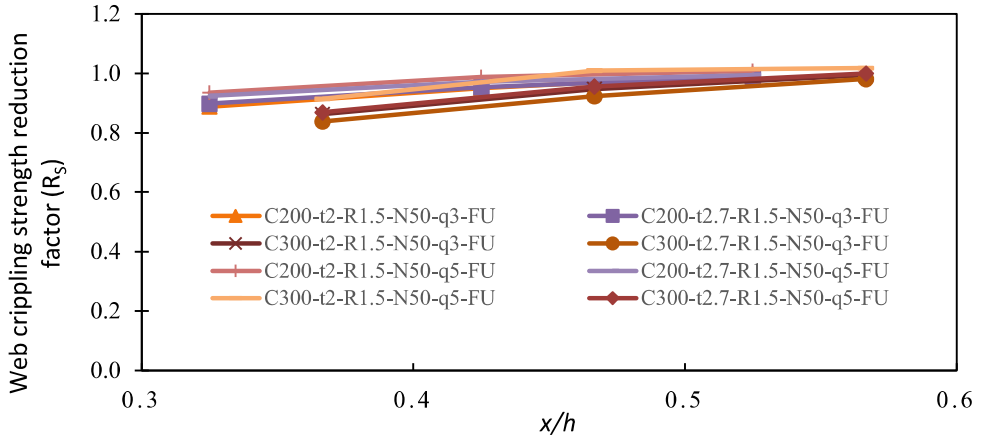

(e) CFSS duplex channel section with fastened flange

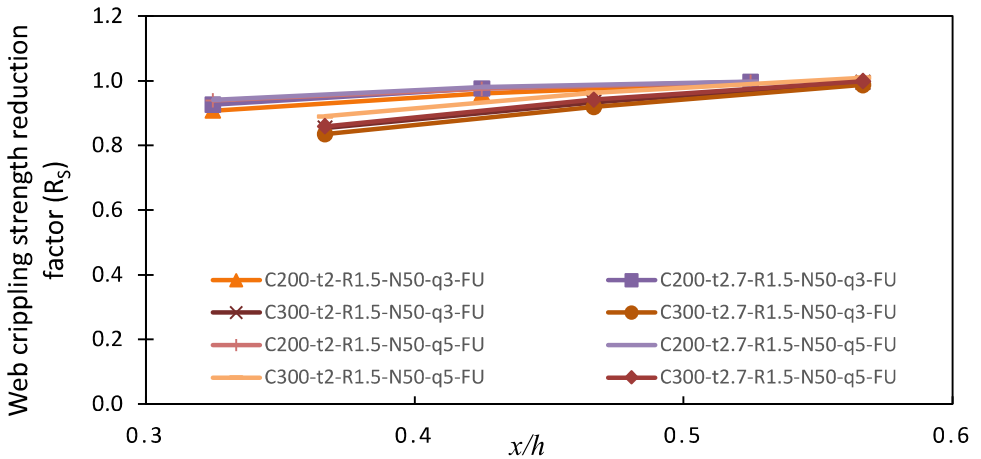

(f) CFSS ferritic channel section with fastened flange

Figure 4.27: Web crippling strength reduction factor against *x/h* for CFSS channel section with edge-stiffened web holes under ETF loading condition

4.4.7 Effects of the fastened flange on web crippling strength (P_n)

The result for the effect of the x/h ratio on the web crippling strength reduction factor for CFSS channel sections subjected to ETF loading condition is visually presented in Figs. 32a-32f. These figures reveal a consistent effect across CFSS austenitic, duplex, and ferritic channel sections. With an increase in the *x/h* ratio, the web crippling strength reduction factor increases by an average of 22% and 12% for channels with unfastened and fastened flanges, respectively.

Chapter 5: Current design rules

5.1 Design equations for web crippling strength of channel sections without web holes

Web crippling strength calculation for CFSS channel sections without web holes is available in ASCE 8-02 [3] and AS/NZS 4673:2001 [4]. For CFCS channel sections, the web crippling strength calculation is available in AISC&AS/NZS [2, 5], EN 1993-1-3 [9], and other current design standards. However, the effects of section geometry are not comprehensively considered in the equations from these design standards [2-5, 8].

5.1.1 ASCE 8-02 [3]

Design equations for web crippling strength calculation of CFSS channels are available in ASCE 8-02 [3]. Equations (3) and (4) show the formulas given for ETF and ITF loading cases, respectively.

$$P_{ASCE} = t^2 C_3 C_4 C_\theta \; x \left(244 + 0.57 \frac{h}{t}\right) x \left(1 + 0.01 \frac{N}{t}\right) x \; C_t \qquad (3)$$

$$P_{ASCE} = t^2 C_1 C_2 C_\theta \; x \left(771 + 2.26 \frac{h}{t}\right) x \left(1 + 0.0013 \frac{N}{t}\right) x \; C_t \qquad (4)$$

where: $C_t = 6.9$

$$C_1 = (1.22 - 0.22k)k \quad when \; \frac{F_y}{91.5C_t} \leq 1.0 \qquad (5)$$

$$= 1.69 \qquad when \; \frac{F_y}{91.5C_t} > 1.0$$

$$C_2 = \left(1.06 - \frac{0.06}{t}\right) \leq 1.0 \qquad (6)$$

$$C_3 = (1.33 - 0.33k)k \quad when \; \frac{F_y}{66.5C_t} \leq 1.0 \qquad (7)$$

$$= 1.34 \qquad when\ \frac{F_y}{66.5C_t} > 1.0$$

$$C_4 = \left(1.15 - \frac{0.15R}{t}\right) \leq 1.0\ but\ not\ less\ than\ 0.50 \qquad (8)$$

$$C_\theta = 0.7 + 0.3(\frac{\theta}{90})^2 \qquad (9)$$

$$k = \frac{F_y}{33C_t} \qquad (10)$$

θ = angle between the web plane and the bearing surface

5.1.2 AS/NZS 4673:2001 [4]

AS/NZS 4673:2001 [4] provided a design equation for web crippling strength calculation of CFSS channels as shown in equations (11) and (12) for ETF and ITF loading cases, respectively. These equations are limited to sections with ratios $\frac{N}{t} \leq 210, \frac{N}{h} \leq 3.5, and\ \frac{r}{t} \leq 6.$

$$P_{AS/NZS} = t^2 C_3 C_4 C_\theta\ x\ \left(1.68 - 0.004\ \frac{h}{t}\right) x\ \left(1 + 0.01\ \frac{N}{t}\right) \qquad (11)$$

$$P_{AS/NZS} = t^2 C_1 C_2 C_\theta\ x\ \left(5.32 - 0.016\ \frac{h}{t}\right) x\ \left(1 + 0.0013\ \frac{N}{t}\right) \qquad (12)$$

where: $C_1 = (1.22 - 0.22k)k \quad when\ f_y \leq 631\ MPa \qquad (13)$

$$= 1.69 \qquad when\ f_y > 631\ MPa$$

$$C_2 = \left(1.06 - \frac{0.06R}{t}\right) \leq 1.0 \qquad (14)$$

$$C_3 = (1.33 - 0.33k)k \quad when\ f_y \leq 459\ MPa \qquad (15)$$

$$= 1.34 \qquad when\ f_y > 459\ MPa$$

$$C_4 = \left(1.15 - \frac{0.15R}{t}\right) \leq 1.0 \; but \; not \; less \; than \; 0.50 \quad (16)$$

$$C_\theta = 0.7 + 0.3(\frac{\theta}{90})^2 \quad (17)$$

$$k = \frac{F_y}{228} \quad (18)$$

5.1.3 AISI&AS/NZS [2, 5]

Design equations with different coefficients for unified web crippling strength for CFCS plain sections can be obtained from AISI&AS/NZS [2, 5] as shown in equation (19) below. The effect of fastened support was also incorporated into the design rules.

$$P_{AISI\&AS/NZS} = Ct^2 f_y sin\theta \left(1 - C_h\sqrt{\frac{h}{t}}\right)\left(1 - C_r\sqrt{\frac{r}{t}}\right)\left(1 + C_N\sqrt{\frac{N}{t}}\right) \quad (19)$$

Where C is a coefficient; N is the bearing length; and C_r, C_N and C_h are the coefficients of inside bent radius, bearing length and web slenderness, respectively. Coefficient values are given in Table 5.1. Equation (19) imited to sections with ratios of $\frac{r}{t} \leq 12 \; and \frac{r}{t} \leq 3$ for fastened and un-fastened flange to support, respectively.

Table 5.1: Web crippling coefficients from AISI&AS/NZS [2, 5]

Support condition	Load Cases	Coefficients				Limitations			
		C	C_r	C_N	C_h	r/t	d/t	N/t	N/d
Fastened flange	ITF	20	0.10	0.08	0.031	≤ 12	≤ 200	≤ 210	≤ 2
	ETF	7.5	0.08	0.12	0.049	≤ 12			
Unfastened	ITF	24	0.52	0.15	0.001	≤ 3			
	ETF	13	0.32	0.05	0.04	≤ 3			

5.1.4 Eurocode 3 [9]

Eurocode 3 (EC3) provides web crippling strength design equations of CFCS plain channel sections. Equations (20) and (21) show the formula given for ETF and ITF loading conditions, respectively. These equations are limited to CFCS channel sections with ratios of $\frac{r}{t} \leq 6\ and \frac{d}{t} \leq 300$.

$$P_{EC} = k_1 k_2 k_3 \left(6.66 - \frac{d/t}{64}\right) \left(1 + 0.01\frac{N}{t}\right) t^2 f_y \quad (20)$$

$$P_{EC} = k_3 k_4 k_5 \left(21.0 - \frac{d/t}{16.3}\right) \left(1 + 0.0013\frac{N}{t}\right) t^2 f_y \quad (21)$$

Where: $k_1 = 1.33 - 0.33k$ (22)

$$k_2 = 0.5 \leq 1.15 - 0.15\frac{r}{t} \leq 1.0 \quad (23)$$

$$k_3 = 0.7 + 0.3\ (\frac{\theta}{90})^2 \quad (24)$$

$$k_4 = 1.22 - 0.22k \quad (25)$$

$$k_5 = 1.06 - 0.06\ r/t \leq 1.0 \quad (26)$$

$$k = \frac{f_y}{228} \quad (27)$$

5.1.5 Fang et. al [11, 12]

Fang et. al [11, 12] proposed a design equation for the web crippling strength of CFSS channel sections for ETF and ITF loading conditions. Proposed equations are based on AISI&AS/NZS [2, 5]. However, the equation for fastened sections considers the effect of lip slenderness as shown in Equation (28). Limits of the proposed equations for ETF loading condition are channel sections with ratios $\frac{h}{t} \leq\ 600, \frac{N}{t} \leq$

$200, \frac{r}{t} \leq 12.0, \frac{N}{h} \leq 1.15, \frac{a}{h} \leq 0.8$ *and* $\theta = 90º$. While the limit for the proposed equation for ITF are $\frac{h}{t} \leq 600, \frac{N}{t} \leq 200, \frac{r}{t} \leq 12.0, \frac{N}{h} \leq 1.15, \frac{a}{h} \leq 0.6$ and $\theta = 90º$. Proposed coefficients are shown in Table 5.2.

$$P_{FANG} = Ct^2 f_y sin\theta \left(1 - C_R\sqrt{\frac{r}{t}}\right)\left(1 + C_N\sqrt{\frac{N}{t}}\right)\left(1 - C_h\sqrt{\frac{h}{t}}\right)\left(1 + C_l\sqrt{\frac{b_l}{t}}\right) \quad > 0 \quad (28)$$

Table 5.2: Web crippling coefficients as proposed by Fang et al [11, 12]

Loading condition	Support condition	Stainless Steel Material	*C*	C_R	C_N	C_h	C_l
ITF	Unfastened flange	Ferritic	19.243	0.335	0.041	0.029	
		Duplex	19.763	0.237	0.041	0.047	
		Austenitic	18.882	0.304	0.039	0.030	
	Fastened flange	Ferritic	23.968	0.306	0.063	0.001	0.016
		Duplex	21.598	0.244	0.042	0.028	0.022
		Austenitic	24.112	0.298	0.053	0.002	0.014
ETF	Unfastened flange	Ferritic	5.126	0.258	0.215	0.046	
		Duplex	3.143	0.177	0.183	0.050	
		Austenitic	4.727	0.261	0.217	0.046	
	Fastened flange	Ferritic	5.124	0.237	0.306	0.038	0.022
		Duplex	3.307	0.220	0.422	0.048	0.005
		Austenitic	4.746	0.235	0.324	0.039	0.020

5.2 Design equations for web crippling strength of channel sections with unstiffened web holes

Fang et. al [11, 12] proposed design equations for ferritic, duplex, and austenitic CFSS lipped channel sections with unfastened and fastened flanges. These design equations were developed in the form of web crippling strength reduction factors (R_{FANG}), and it is about the ratios *a/h*, *x/h*, and *N/h*. Equations (29) and (30) shows the proposed reduction factors for sections with centred hole and sections with offset web hole, respectively.

$$R_{FANG} = \alpha - \gamma\frac{\alpha}{h} + \lambda\frac{N}{h} \quad \leq 1.0 \tag{29}$$

$$R_{FANG} = ß - \mu\frac{\alpha}{h} + \zeta\frac{N}{h} + \xi\frac{x}{h} \quad \leq 1.0 \tag{30}$$

The $\alpha, \gamma, \lambda, ß, \mu, \zeta, \xi$ are equation coefficients and values are tabulated in Table 5.3.

Table 5.3: Web crippling reduction coefficients as proposed by Fang et al [11, 12]

Loading condition	Support condition	Stainless Steel Material	α	γ	λ	ß	μ	ζ	ξ
ITF	Unfastened flange	Ferritic	1.069	0.521	0.010	0.530	0.090	0.130	0.660
		Duplex	1.066	0.487	0.010	0.944	0.368	0.044	0.105
		Austenitic	1.064	0.526	0.024	0.620	0.150	0.117	0.535
	Fastened flange	Ferritic	1.046	0.474	0.033	0.938	0.557	0.081	0.127
		Duplex	1.046	0.428	0.014	1.019	0.610	0.059	0.027
		Austenitic	1.047	0.480	0.036	0.983	0.585	0.069	0.070
ETF	Unfastened flange	Ferritic	0.966	-0.689	0.095	0.446	0.785	-0.161	-0.544
		Duplex	0.961	-0.684	0.103	1.045	0.525	0.084	-0.018
		Austenitic	0.973	-0.692	0.098	1.588	0.871	-0.254	-0.723
	Fastened flange	Ferritic	0.985	-0.636	0.139	0.415	0.001	0.498	0.765
		Duplex	0.974	-0.650	0.138	0.583	0.070	0.358	0.557
		Austenitic	0.985	-0.633	0.139	0.406	0.001	0.507	0.774

5.3 Design equations for web crippling strength of channel sections with edge-stiffened web holes

Uzzaman et. al [27, 29] proposed design equations for the calculation of strength reduction factor (R_{UZZ}) of CFCS lipped channel sections with unfastened flange. The proposed equations as shown in Equations (31) and (32) are applicable for channels under ITF and ETF loading conditions, respectively, with the following dimensional limitations: $\frac{h}{t} \leq 118, \frac{N}{h} \leq 0.44, \frac{x}{h} \leq 0.6, \frac{a}{h} \leq 0.8,$ and $\frac{q}{h} \leq 0.08.$

$$R_{UZZ} = 1.02 - 0.39\frac{\alpha}{h} + 0.02\frac{N}{h} + 0.04\frac{rq}{t} + 0.49\frac{q}{h} \quad \leq 1.0 \tag{31}$$

$$R_{UZZ} = 0.98 - 0.11\frac{\alpha}{h} + 0.01\frac{x}{h} + 0.05\frac{rq}{t} + 0.41\frac{q}{h} \quad \leq 1.0 \tag{32}$$

Chapter 6: Proposed design equations

6.1 General

In total, 3,744 validated FE models would be used to propose design equations for the web crippling strength of CFSS channels with web holes. Therefore, the results of FEA were used to propose design equations (33) – (37) in the forms of web crippling strength and web crippling strength reduction factors for plain channels and channels with unstiffened and edge-stiffened web holes. The related coefficients were obtained from non-linear regression analysis using SPSS [16] software. Limitations of the proposed design equations are $\frac{h}{t} \leq\ 200, \frac{N}{t} \leq\ 70, \frac{r}{t} \leq\ 2.0, \frac{N}{h} \leq 0.5, \frac{a}{h} \leq\ 0.6, \frac{q}{t} < 3\ and\ \theta\ =\ 90º$.

6.2. Proposed design equations for CFSS channel sections without web holes

The proposed design equation for web crippling strength (P_{PROP}) of CFSS lipped channels considers three different grades of stainless steel and two different flange types. It is given as:

$$P_{PROP} = Ct^2 f_y sin\theta \left(1 - C_r\sqrt{\frac{r}{t}}\right)\left(1 + C_N\sqrt{\frac{N}{t}}\right)\left(1 - C_h\sqrt{\frac{h}{t}}\right) \qquad (33)$$

Where *C* is a coefficient, C_r is the inside bend radius coefficient, C_N is the bearing length coefficient, and C_h is the web slenderness coefficient. The values of these coefficients are tabulated in Table 6.1.

It was shown from Tables 11a-11b and 12a-12b, that the calculated web crippling strength (P_{PROP}) closely matches the FEA results (P_{FEA}). For both unfastened and fastened channels, under ITF and ETF loading conditions, the average ratios are close to 1.0, with *COV* ranging from 0.01 to 0.05. This highlights the high accuracy of the proposed equation, surpassing current design standards and those recommended by Fang et al [11, 12].

Table 6.1: Proposed web crippling coefficients

Loading Condition	Flange Condition	Stainless Steel Material	*C*	*Cr*	*Cn*	*Ch*
ITF	Unfastened flange	Austenitic	23.793	0.255	0.040	0.026
		Duplex	19.591	0.185	0.030	0.047
		Ferritic	23.762	0.257	0.043	0.025
	Fastened flange	Austenitic	7.706	0.399	0.668	-0.004
		Duplex	17.473	0.272	0.124	0.029
		Ferritic	7.594	0.400	0.678	-0.006
ETF	Unfastened flange	Austenitic	3.391	0.253	0.757	0.047
		Duplex	2.502	0.161	0.647	0.058
		Ferritic	3.635	0.266	0.727	0.047
	Fastened flange	Austenitic	2.707	0.306	1.728	0.045
		Duplex	1.815	0.278	2.108	0.056
		Ferritic	2.734	0.309	1.726	0.044

Examining Table 6.2a-6.2b under ITF loading condition, the ratios of web crippling strengths obtained from FEA to current design standards (ASCE 8-02 [3], AS/NZS 4673:2001 [4], AISI&AS/NZS [2, 5], Eurocode 3 [9]) and the proposed equation by Fang et al [11, 12] range from 0.59 to 1.51 with *COVs* ranging from 0.01 to 0.15 for channels with unfastened flanges. For channels with fastened flanges, ratios range from 0.81 to 1.28 with *COVs* ranging from 0.04 to 0.19. Under ETF loading condition, as shown in Table 6.3a-6.3b, for channels with unfastened flanges, the ratios vary from 0.59 to 2.89 with *COVs* ranging from 0.09 to 0.20. For channels with fastened flanges, ratios are from 0.84 to 2.95 with *COVs* ranging from 0.09 to 0.32. These ratios with corresponding *COVs* are higher compared to those obtained from the proposed equations in this study.

Table 6.2a: Comparison of web crippling strength obtained from FEA results with proposed equation and with other calculation methods under ITF loading condition for channel sections with unfastened flange.

Specimen	*h/t*	*N/t*	*r/t*	*Fy (Mpa)*	P_{FEA} *(kN)*	P_{FEA}/P_{PROP}	P_{FEA}/P_{ASCE}	$P_{FEA}/P_{AS/NZS}$	$P_{FEA}/P_{AIS\&AS/NZS}$	P_{FEA}/P_{EURO}	P_{FEA}/P_{FANG}
Cold-formed austenitic stainless steel											
C200-t2.3-R1.3-N50-A0-FU	84.4	21.7	1.3	205.6	16.94	0.97	0.86	0.87	0.92	0.94	1.43
C200-t2.3-R1.3-N100-A0-FU	84.4	43.5	1.3	205.6	17.97	0.98	0.89	0.90	0.84	0.97	1.43
C200-t2.7-R1.5-N50-A0-FU	71.1	18.5	1.5	205.6	22.41	1.00	0.82	0.80	1.05	0.89	1.44
C200-t2.7-R1.5-N100-A0-FU	71.1	37.0	1.5	205.6	23.80	0.99	0.85	0.83	0.95	0.92	1.44
C300-t2.3-R1.3-N50-A0-FU	127.8	21.7	1.3	205.6	15.16	1.01	0.96	0.94	0.85	1.05	1.46
C300-t2.3-R1.3-N100-A0-FU	127.8	43.5	1.3	205.6	15.84	1.03	1.00	0.96	0.78	1.08	1.46
C300-t2.7-R1.5-N50-A0-FU	108.1	18.5	1.5	205.6	21.59	0.96	0.89	0.90	0.98	0.97	1.46
C300-t2.7-R1.5-N100-A0-FU	108.1	37.0	1.5	205.6	22.49	0.98	0.92	0.92	0.89	1.00	1.46
Average						**0.99**	**0.90**	**0.89**	**0.91**	**0.98**	**1.45**
COV						**0.02**	**0.07**	**0.06**	**0.09**	**0.07**	**0.01**
Cold-formed duplex stainless steel											
C200-t2.3-R1.3-N50-A0-FU	84.4	21.7	1.3	451.9	24.18	1.00	0.79	0.73	0.61	0.81	1.03
C200-t2.3-R1.3-N100-A0-FU	84.4	43.5	1.3	451.9	25.34	1.00	0.81	0.75	0.55	0.83	1.02
C200-t2.7-R1.5-N50-A0-FU	71.1	18.5	1.5	451.9	33.96	1.01	0.79	0.72	0.73	0.81	1.04
C200-t2.7-R1.5-N100-A0-FU	71.1	37.0	1.5	451.9	35.34	1.01	0.81	0.73	0.66	0.83	1.03
C300-t2.3-R1.3-N50-A0-FU	127.8	21.7	1.3	451.9	19.39	1.03	0.79	0.71	0.51	0.81	1.03
C300-t2.3-R1.3-N100-A0-FU	127.8	43.5	1.3	451.9	20.26	1.03	0.81	0.73	0.46	0.83	1.02
C300-t2.7-R1.5-N50-A0-FU	108.1	18.5	1.5	451.9	28.77	1.01	0.78	0.71	0.62	0.80	1.04
C300-t2.7-R1.5-N100-A0-FU	108.1	37.0	1.5	451.9	29.93	1.02	0.80	0.72	0.56	0.82	1.03
Average						**1.01**	**0.80**	**0.73**	**0.59**	**0.82**	**1.03**
COV						**0.01**	**0.02**	**0.02**	**0.15**	**0.01**	**0.01**

Cold-formed ferritic stainless steel											
C200-t2.3-R1.3-N50-A0-FU	84.4	21.7	1.3	205.6	17.25	0.98	0.88	0.88	0.94	0.96	1.49
C200-t2.3-R1.3-N100-A0-FU	84.4	43.5	1.3	205.6	18.32	0.98	0.92	0.91	0.86	1.00	1.49
C200-t2.7-R1.5-N50-A0-FU	71.1	18.5	1.5	205.6	22.65	1.01	0.84	0.81	1.07	0.91	1.51
C200-t2.7-R1.5-N100-A0-FU	71.1	37.0	1.5	205.6	24.19	1.00	0.87	0.85	0.98	0.95	1.51
C300-t2.3-R1.3-N50-A0-FU	127.8	21.7	1.3	205.6	15.53	1.01	0.99	0.96	0.88	1.08	1.51
C300-t2.3-R1.3-N100-A0-FU	127.8	43.5	1.3	205.6	16.23	1.03	1.03	0.98	0.80	1.12	1.52
C300-t2.7-R1.5-N50-A0-FU	108.1	18.5	1.5	205.6	22.00	0.97	0.91	0.92	1.00	0.99	1.53
C300-t2.7-R1.5-N100-A0-FU	108.1	37.0	1.5	205.6	22.95	0.99	0.94	0.94	0.92	1.03	1.53
Average						**1.00**	**0.92**	**0.91**	**0.93**	**1.00**	**1.51**
COV						**0.02**	**0.07**	**0.06**	**0.09**	**0.07**	**0.01**

Table 6.2b: Comparison of web crippling strength obtained from FEA results with proposed equation and with other calculation methods under ITF loading condition for channel sections with fastened flange.

Specimen	*h/t*	*N/t*	*r/t*	*Fy (Mpa)*	P_{FEA} (kN)	P_{FEA}/P_{PROP}	P_{FEA}/P_{ASCE}	$P_{FEA}/P_{AS/NZS}$	$P_{FEA}/P_{AIS\&AS/NZS}$	P_{FEA}/P_{EURO}	P_{FEA}/P_{FANG}
Cold-formed austenitic stainless steel											
C200-t2.3-R1.3-N50-A0-FR	84.4	21.7	1.3	205.6	19.44	0.99	1.00	1.00	1.01	1.09	0.87
C200-t2.3-R1.3-N100-A0-FR	84.4	43.5	1.3	205.6	25.54	0.98	1.28	1.27	1.19	1.39	1.05
C200-t2.7-R1.5-N50-A0-FR	71.1	18.5	1.5	205.6	23.60	1.00	0.87	0.85	0.91	0.95	0.82
C200-t2.7-R1.5-N100-A0-FR	71.1	37.0	1.5	205.6	30.85	0.97	1.07	1.08	1.03	1.17	0.97
C300-t2.3-R1.3-N50-A0-FR	127.8	21.7	1.3	205.6	19.60	0.97	1.19	1.22	1.10	1.30	0.85
C300-t2.3-R1.3-N100-A0-FR	127.8	43.5	1.3	205.6	25.74	0.92	1.45	1.55	1.24	1.58	0.99
C300-t2.7-R1.5-N50-A0-FR	108.1	18.5	1.5	205.6	23.78	0.98	0.99	0.99	0.97	1.08	0.81
C300-t2.7-R1.5-N100-A0-FR	108.1	37.0	1.5	205.6	31.08	1.09	1.41	1.27	1.28	1.54	1.10
Average						**0.99**	**1.16**	**1.15**	**1.09**	**1.26**	**0.93**
COV						**0.05**	**0.18**	**0.19**	**0.12**	**0.18**	**0.12**

Cold-formed duplex stainless steel											
C200-t2.3-R1.3-N50-A0-FR	84.4	21.7	1.3	451.9	33.54	1.06	1.17	1.02	0.85	1.19	0.87
C200-t2.3-R1.3-N100-A0-FR	84.4	43.5	1.3	451.9	38.63	0.99	1.22	1.14	0.82	1.25	0.93
C200-t2.7-R1.5-N50-A0-FR	71.1	18.5	1.5	451.9	44.69	0.98	1.01	0.95	0.76	1.03	0.81
C200-t2.7-R1.5-N100-A0-FR	71.1	37.0	1.5	451.9	51.13	1.00	1.15	1.06	0.80	1.18	0.94
C300-t2.3-R1.3-N50-A0-FR	127.8	21.7	1.3	451.9	30.78	1.02	1.24	1.13	0.83	1.27	0.76
C300-t2.3-R1.3-N100-A0-FR	127.8	43.5	1.3	451.9	35.45	0.92	1.26	1.27	0.78	1.29	0.79
C300-t2.7-R1.5-N50-A0-FR	108.1	18.5	1.5	451.9	41.38	1.01	1.12	1.02	0.80	1.15	0.77
C300-t2.7-R1.5-N100-A0-FR	108.1	37.0	1.5	451.9	47.34	1.01	1.26	1.14	0.82	1.29	0.87
Average						**1.00**	**1.18**	**1.09**	**0.81**	**1.21**	**0.84**
COV						**0.04**	**0.07**	**0.09**	**0.04**	**0.07**	**0.08**
Cold-formed ferritic stainless steel											
C200-t2.3-R1.3-N50-A0-FR	84.4	21.7	1.3	205.6	19.66	0.98	1.01	1.01	1.02	1.10	0.85
C200-t2.3-R1.3-N100-A0-FR	84.4	43.5	1.3	205.6	25.85	0.98	1.29	1.29	1.21	1.41	1.03
C200-t2.7-R1.5-N50-A0-FR	71.1	18.5	1.5	205.6	23.83	1.01	0.88	0.85	0.92	0.96	0.82
C200-t2.7-R1.5-N100-A0-FR	71.1	37.0	1.5	205.6	31.18	0.97	1.08	1.09	1.04	1.18	0.95
C300-t2.3-R1.3-N50-A0-FR	127.8	21.7	1.3	205.6	19.88	0.96	1.21	1.23	1.11	1.31	0.84
C300-t2.3-R1.3-N100-A0-FR	127.8	43.5	1.3	205.6	26.14	0.92	1.48	1.58	1.26	1.61	0.97
C300-t2.7-R1.5-N50-A0-FR	108.1	18.5	1.5	205.6	24.08	0.98	1.01	1.01	0.99	1.10	0.80
C300-t2.7-R1.5-N100-A0-FR	108.1	37.0	1.5	205.6	31.51	1.10	1.44	1.29	1.30	1.57	1.08
Average						**0.99**	**1.17**	**1.17**	**1.11**	**1.28**	**0.92**
COV						**0.05**	**0.18**	**0.19**	**0.13**	**0.18**	**0.11**

Table 6.3a: Comparison of web crippling strength obtained from FEA results with proposed equation and with other calculation methods under ETF loading condition for channel sections with unfastened flange

Specimen	*h/t*	*N/t*	*r/t*	*Fy (Mpa)*	P_{FEA} (kN)	P_{FEA}/P_{PROP}	P_{FEA}/P_{ASCE}	$P_{FEA}/P_{AS/NZS}$	$P_{FEA}/P_{AIS\&AS/NZS}$	P_{FEA}/P_{EURO}	P_{FEA}/P_{FANG}
Cold-formed austenitic stainless steel											
C200-t2.3-R1.3-N50-A0-FU	84.4	21.7	1.3	205.6	6.44	0.95	0.83	0.84	0.92	1.78	0.91
C200-t2.3-R1.3-N100-A0-FU	84.4	43.5	1.3	205.6	8.38	0.94	0.92	0.92	1.11	1.96	0.99
C200-t2.7-R1.5-N50-A0-FU	71.1	18.5	1.5	205.6	8.76	0.97	0.84	0.84	0.92	1.74	0.96
C200-t2.7-R1.5-N100-A0-FU	71.1	37.0	1.5	205.6	11.30	0.95	0.93	0.94	1.10	1.94	1.04
C300-t2.3-R1.3-N50-A0-FU	127.8	21.7	1.3	205.6	5.03	0.91	0.74	0.75	0.83	1.59	0.71
C300-t2.3-R1.3-N100-A0-FU	127.8	43.5	1.3	205.6	6.07	0.83	0.76	0.77	0.93	1.63	0.71
C300-t2.7-R1.5-N50-A0-FU	108.1	18.5	1.5	205.6	7.36	0.97	0.79	0.79	0.88	1.63	0.80
C300-t2.7-R1.5-N100-A0-FU	108.1	37.0	1.5	205.6	11.49	1.15	1.06	1.07	1.27	2.20	1.05
Average						**0.96**	**0.86**	**0.87**	**0.99**	**1.81**	**0.90**
COV						**0.09**	**0.12**	**0.12**	**0.15**	**0.12**	**0.16**
Cold-formed duplex stainless steel											
C200-t2.3-R1.3-N50-A0-FU	84.4	21.7	1.3	451.9	8.71	0.95	0.78	0.79	0.57	1.67	0.80
C200-t2.3-R1.3-N100-A0-FU	84.4	43.5	1.3	451.9	11.35	0.95	0.86	0.87	0.68	1.85	0.89
C200-t2.7-R1.5-N50-A0-FU	71.1	18.5	1.5	451.9	12.47	0.98	0.83	0.83	0.59	1.72	0.88
C200-t2.7-R1.5-N100-A0-FU	71.1	37.0	1.5	451.9	16.09	0.97	0.93	0.93	0.71	1.92	0.97
C300-t2.3-R1.3-N50-A0-FU	127.8	21.7	1.3	451.9	6.21	0.92	0.64	0.64	0.47	1.37	0.57
C300-t2.3-R1.3-N100-A0-FU	127.8	43.5	1.3	451.9	7.52	0.85	0.66	0.66	0.52	1.40	0.59
C300-t2.7-R1.5-N50-A0-FU	108.1	18.5	1.5	451.9	9.32	0.94	0.69	0.70	0.50	1.43	0.66
C300-t2.7-R1.5-N100-A0-FU	108.1	37.0	1.5	451.9	13.96	1.08	0.90	0.90	0.70	1.86	0.84
Average						**0.96**	**0.79**	**0.79**	**0.59**	**1.65**	**0.77**
COV						**0.07**	**0.14**	**0.14**	**0.16**	**0.13**	**0.20**

Cold-formed ferritic stainless steel											
C200-t2.3-R1.3-N50-A0-FU	84.4	21.7	1.3	205.6	6.57	0.95	0.85	0.86	0.94	1.81	0.85
C200-t2.3-R1.3-N100-A0-FU	84.4	43.5	1.3	205.6	8.56	0.94	0.94	0.94	1.13	2.00	0.93
C200-t2.7-R1.5-N50-A0-FU	71.1	18.5	1.5	205.6	8.93	0.97	0.85	0.86	0.94	1.77	0.90
C200-t2.7-R1.5-N100-A0-FU	71.1	37.0	1.5	205.6	11.51	0.96	0.95	0.96	1.12	1.97	0.98
C300-t2.3-R1.3-N50-A0-FU	127.8	21.7	1.3	205.6	5.17	0.91	0.76	0.77	0.85	1.64	0.67
C300-t2.3-R1.3-N100-A0-FU	127.8	43.5	1.3	205.6	6.23	0.83	0.78	0.79	0.95	1.67	0.67
C300-t2.7-R1.5-N50-A0-FU	108.1	18.5	1.5	205.6	7.54	0.97	0.80	0.81	0.90	1.67	0.76
C300-t2.7-R1.5-N100-A0-FU	108.1	37.0	1.5	205.6	11.48	1.12	1.06	1.07	1.27	2.20	0.97
Average						**0.96**	**0.87**	**0.88**	**1.01**	**1.84**	**0.84**
COV						**0.09**	**0.12**	**0.11**	**0.14**	**0.11**	**0.15**

Table 6.3b: Comparison of web crippling strength obtained from FEA results with proposed equation and with other calculation methods under ETF loading condition for channel sections with fastened flange

Specimen	*h/t*	*N/t*	*r/t*	*Fy (Mpa)*	P_{FEA} *(kN)*	P_{FEA}/P_{PROP}	P_{FEA}/P_{ASCE}	$P_{FEA}/P_{AS/NZS}$	$P_{FEA}/P_{AIS\&AS/NZS}$	P_{FEA}/P_{EURO}	P_{FEA}/P_{FANG}
Cold-formed austenitic stainless steel											
C200-t2.3-R1.3-N50-A0-FR	84.4	21.7	1.3	205.6	10.20	1.00	1.32	1.33	1.58	2.81	1.05
C200-t2.3-R1.3-N100-A0-FR	84.4	43.5	1.3	205.6	14.49	1.04	1.59	1.60	1.95	3.39	1.20
C200-t2.7-R1.5-N50-A0-FR	71.1	18.5	1.5	205.6	12.88	0.97	1.23	1.24	1.41	2.55	1.04
C200-t2.7-R1.5-N100-A0-FR	71.1	37.0	1.5	205.6	18.22	1.00	1.51	1.52	1.74	3.12	1.20
C300-t2.3-R1.3-N50-A0-FR	127.8	21.7	1.3	205.6	8.84	1.03	1.31	1.32	1.67	2.80	0.90
C300-t2.3-R1.3-N100-A0-FR	127.8	43.5	1.3	205.6	11.37	0.97	1.43	1.44	1.87	3.05	0.93
C300-t2.7-R1.5-N50-A0-FR	108.1	18.5	1.5	205.6	11.81	1.03	1.26	1.27	1.53	2.62	0.94
C300-t2.7-R1.5-N100-A0-FR	108.1	37.0	1.5	205.6	14.65	0.94	1.35	1.36	1.67	2.81	0.95
Average						**1.00**	**1.37**	**1.39**	**1.68**	**2.89**	**1.03**
COV						**0.04**	**0.09**	**0.09**	**0.11**	**0.10**	**0.12**

Cold-formed duplex stainless steel											
C200-t2.3-R1.3-N50-A0-FR	84.4	21.7	1.3	451.9	15.29	0.98	1.37	1.38	1.08	2.93	0.88
C200-t2.3-R1.3-N100-A0-FR	84.4	43.5	1.3	451.9	21.63	1.01	1.65	1.66	1.33	3.52	0.99
C200-t2.7-R1.5-N50-A0-FR	71.1	18.5	1.5	451.9	20.37	0.97	1.36	1.36	1.01	2.81	0.92
C200-t2.7-R1.5-N100-A0-FR	71.1	37.0	1.5	451.9	28.63	0.99	1.65	1.66	1.25	3.41	1.03
C300-t2.3-R1.3-N50-A0-FR	127.8	21.7	1.3	451.9	12.03	1.02	1.24	1.25	1.04	2.65	0.69
C300-t2.3-R1.3-N100-A0-FR	127.8	43.5	1.3	451.9	15.61	0.96	1.36	1.38	1.17	2.91	0.71
C300-t2.7-R1.5-N50-A0-FR	108.1	18.5	1.5	451.9	16.67	1.01	1.24	1.25	0.98	2.57	0.75
C300-t2.7-R1.5-N100-A0-FR	108.1	37.0	1.5	451.9	21.09	0.93	1.35	1.37	1.09	2.81	0.75
Average						**0.98**	**1.40**	**1.41**	**1.12**	**2.95**	**0.84**
COV						**0.03**	**0.12**	**0.11**	**0.11**	**0.12**	**0.16**
Cold-formed ferritic stainless steel											
C200-t2.3-R1.3-N50-A0-FR	84.4	21.7	1.3	205.6	10.37	1.00	1.34	0.97	1.60	2.86	1.02
C200-t2.3-R1.3-N100-A0-FR	84.4	43.5	1.3	205.6	14.73	1.04	1.61	1.59	1.98	3.45	1.17
C200-t2.7-R1.5-N50-A0-FR	71.1	18.5	1.5	205.6	13.05	0.97	1.25	1.95	1.43	2.59	1.01
C200-t2.7-R1.5-N100-A0-FR	71.1	37.0	1.5	205.6	18.48	1.00	1.53	2.34	1.77	3.17	1.17
C300-t2.3-R1.3-N50-A0-FR	127.8	21.7	1.3	205.6	9.02	1.03	1.33	1.17	1.71	2.86	0.88
C300-t2.3-R1.3-N100-A0-FR	127.8	43.5	1.3	205.6	11.61	0.97	1.46	1.28	1.91	3.12	0.91
C300-t2.7-R1.5-N50-A0-FR	108.1	18.5	1.5	205.6	12.05	1.04	1.29	1.16	1.56	2.67	0.92
C300-t2.7-R1.5-N100-A0-FR	108.1	37.0	1.5	205.6	14.93	0.94	1.38	1.24	1.70	2.86	0.93
Average						**1.00**	**1.40**	**1.46**	**1.71**	**2.95**	**1.00**
COV						**0.04**	**0.09**	**0.32**	**0.11**	**0.10**	**0.12**

6.3. Proposed design equations for CFSS channel sections with unstiffened web holes

The FEA results were also used to propose design equations for CFSS channel sections with unstiffened web holes under ITF and ETF loading conditions. These equations as presented in Equations (34) and (35) are in the form of web crippling strength reduction factor ($R_{U,PROP}$) to the following ratios: *α/h*, *N/h*, and *x/h*.

For ITF loading condition,

$$R_{U,PROP} = \alpha - \gamma\frac{\alpha}{h} + \lambda\frac{N}{h} \qquad \leq 1.0 \tag{34}$$

For ETF loading condition,

$$R_{U,PROP} = \alpha - \gamma\frac{\alpha}{h} + \lambda\frac{N}{h} + \xi\frac{x}{h} \qquad \leq 1.0 \tag{35}$$

where $\alpha, \gamma, \lambda, \xi$ are equation coefficients. The coefficient values are tabulated in Table 6.4 for each stainless steel material type (austenitic, duplex, and ferritic) considering fastened and unfastened flange.

Table 6.4: Coefficient values for the proposed web crippling reduction factors for CFSS channel sections with unstiffened web holes

Loading condition	Support condition	Stainless Steel Material	α	γ	λ	ξ
ITF	Unfastened flange	Austenitic	1.074	0.631	0.006	
		Duplex	1.075	0.557	-0.027	
		Ferritic	1.074	0.630	0.005	
	Fastened flange	Austenitic	1.163	0.517	-0.187	
		Duplex	1.110	0.641	-0.025	
		Ferritic	1.167	0.517	-0.192	
ETF	Unfastened flange	Austenitic	1.144	0.510	0.046	-0.125
		Duplex	1.174	0.531	0.048	-0.169
		Ferritic	1.144	0.512	0.045	-0.123
	Fastened flange	Austenitic	0.968	0.244	0.092	0.049
		Duplex	0.986	0.270	0.080	0.028
		Ferritic	0.968	0.239	0.093	0.047

The proposed equations exhibit a notable level of predictive accuracy, as demonstrated in Table 6.5a-6.5b and Table 6.6a-6.6b. The reduction factors obtained from the proposed equations ($R_{U,PROP}$) closely match those obtained from the FEA results (R_U). Under ITF loading conditions, the average ratios are 0.99 with a *COV* of 0.03 for channels with unfastened flanges, and 1.0 with a *COV* of 0.04 for channels with fastened flanges. For ETF loading conditions, the average ratios are 0.97 and 0.98 for channels with unfastened and fastened flanges, respectively, with a *COV* of 0.02.

In comparison, the reduction factors from Fang et al.'s proposed equation (R_{FANG}) indicate average ratios of 0.95 with a *COV* of 0.03, and 0.99 with a *COV* of 0.04 for channels under ITF loading conditions with unfastened and fastened flanges, respectively. For channels under ETF loading conditions, the average ratios are 0.89 with a *COV* of 0.09 and 0.97 with a *COV* of 0.07 for unfastened and fastened flanges, respectively. It's worth noting that the *COV* for Fang et al.'s proposed equation is higher compared to the one presented in this thesis.

Table 6.5a: Comparison of web crippling strength reduction factor obtained from FEA results with proposed equation and with other calculation methods for CFSS channel sections with unstiffened web hole and unfastened flange under ITF loading condition

Specimen	*N/h*	P_{FEA} *(kN)*	$P_{FEA,UH}$ *(kN)*	R_U $[P_{FEA,UH}/ P_{FEA}]$	$R_{U,PROP}$	R_{FANG}	$R_U/ R_{U,PROP}$	R_U/ R_{FANG}
Cold-formed austenitic stainless steel								
C200-t2.7-R1.5-N100-A0.2-FU	0.26	16.94	15.82	0.93	0.95	0.96	0.98	0.97
C200-t2.7-R1.5-N100-A0.4-FU	0.26	16.94	13.78	0.81	0.82	0.86	0.99	0.95
C200-t2.7-R1.5-N100-A0.6-FU	0.26	16.94	11.24	0.66	0.70	0.75	0.95	0.88
C200-t2.7-R1.5-N100-A0.2-FU	0.52	17.97	16.76	0.93	0.95	0.97	0.98	0.96
C200-t2.7-R1.5-N100-A0.4-FU	0.52	17.97	14.81	0.82	0.82	0.87	1.00	0.95
C200-t2.7-R1.5-N100-A0.6-FU	0.52	17.97	12.41	0.69	0.70	0.76	0.99	0.91
C200-t2.7-R1.5-N50-A0.2-FU	0.17	15.16	14.37	0.95	0.95	0.96	1.00	0.98
C200-t2.7-R1.5-N50-A0.4-FU	0.17	15.16	12.67	0.84	0.82	0.86	1.02	0.97
C200-t2.7-R1.5-N50-A0.6-FU	0.17	15.16	10.22	0.67	0.70	0.75	0.97	0.90
C200-t2.7-R1.5-N50-A0.2-FU	0.34	15.84	14.96	0.94	0.95	0.97	0.99	0.98
C200-t2.7-R1.5-N50-A0.4-FU	0.34	15.84	14.96	0.94	0.95	0.97	0.99	0.98
C200-t2.7-R1.5-N50-A0.6-FU	0.34	15.84	13.24	0.84	0.70	0.76	1.20	1.10
Average							**1.03**	**0.99**
COV							**0.09**	**0.08**
Cold-formed duplex stainless steel								
C200-t2.7-R1.5-N100-A0.2-FU	0.26	25.34	23.90	0.94	0.95	0.97	0.99	0.97
C200-t2.7-R1.5-N100-A0.4-FU	0.26	25.34	21.41	0.84	0.84	0.88	1.01	0.96
C200-t2.7-R1.5-N100-A0.6-FU	0.26	25.34	17.92	0.71	0.73	0.78	0.97	0.91
C200-t2.7-R1.5-N100-A0.2-FU	0.52	33.96	31.50	0.93	0.96	0.97	0.97	0.96
C200-t2.7-R1.5-N100-A0.4-FU	0.52	33.96	27.60	0.81	0.85	0.87	0.96	0.93

C200-t2.7-R1.5-N100-A0.6-FU	0.52	33.96	22.38	0.66	0.73	0.78	0.90	0.85
C200-t2.7-R1.5-N50-A0.2-FU	0.17	20.26	19.35	0.96	0.95	0.97	1.00	0.98
C200-t2.7-R1.5-N50-A0.4-FU	0.17	20.26	19.35	0.96	0.95	0.97	1.00	0.98
C200-t2.7-R1.5-N50-A0.6-FU	0.17	20.26	17.58	0.87	0.84	0.87	1.03	0.99
C200-t2.7-R1.5-N50-A0.2-FU	0.34	28.77	27.45	0.95	0.96	0.97	0.99	0.98
C200-t2.7-R1.5-N50-A0.4-FU	0.34	28.77	24.61	0.86	0.85	0.87	1.01	0.98
C200-t2.7-R1.5-N50-A0.6-FU	0.34	28.77	20.50	0.71	0.74	0.78	0.97	0.92
Average							**1.00**	**0.97**
COV							**0.02**	**0.03**
Cold-formed ferritic stainless steel								
C200-t2.7-R1.5-N100-A0.2-FU	0.26	17.25	16.11	0.93	0.95	0.97	0.98	0.97
C200-t2.7-R1.5-N100-A0.4-FU	0.26	17.25	14.03	0.81	0.82	0.86	0.99	0.94
C200-t2.7-R1.5-N100-A0.6-FU	0.26	17.25	11.45	0.66	0.70	0.76	0.95	0.87
C200-t2.7-R1.5-N100-A0.2-FU	0.52	18.32	17.08	0.93	0.95	0.97	0.98	0.96
C200-t2.7-R1.5-N100-A0.4-FU	0.52	18.32	15.09	0.82	0.82	0.87	1.00	0.95
C200-t2.7-R1.5-N100-A0.6-FU	0.52	18.32	12.64	0.69	0.70	0.76	0.99	0.91
C200-t2.7-R1.5-N50-A0.2-FU	0.17	15.53	14.71	0.95	0.95	0.97	1.00	0.98
C200-t2.7-R1.5-N50-A0.4-FU	0.17	15.53	12.95	0.83	0.82	0.86	1.01	0.97
C200-t2.7-R1.5-N50-A0.6-FU	0.17	15.53	10.44	0.67	0.70	0.76	0.97	0.89
C200-t2.7-R1.5-N50-A0.2-FU	0.34	16.23	15.31	0.94	0.95	0.97	0.99	0.97
C200-t2.7-R1.5-N50-A0.4-FU	0.34	16.23	15.31	0.94	0.95	0.97	0.99	0.97
C200-t2.7-R1.5-N50-A0.6-FU	0.34	16.23	13.53	0.83	0.82	0.86	1.01	0.97
Average							**1.00**	**0.95**
COV							**0.02**	**0.04**

Table 6.5b: Comparison of web crippling strength reduction factor obtained from FEA results with proposed equation and with other calculation methods for CFSS channel sections with unstiffened web hole and fastened flange under ITF loading condition.

Specimen	*N/h*	P_{FEA} *(kN)*	$P_{FEA,UH}$ *(kN)*	R_U $[P_{FEA,UH}/ P_{FEA}]$	$R_{U,PROP}$	R_{FANG}	$R_U/ R_{U,PROP}$	R_U/ R_{FANG}
Cold-formed austenitic stainless steel								
C200-t2.3-R1.3-N50-A0.4-FR	0.26	19.18	19.16	1.00	1.00	0.96	1.00	1.04
C200-t2.3-R1.3-N50-A0.6-FR	0.26	19.18	19.12	1.00	0.91	0.86	1.10	1.15
C200-t2.3-R1.3-N50-A0.2-FR	0.26	19.18	16.41	0.86	0.80	0.77	1.06	1.11
C200-t2.3-R1.3-N100-A0.4-FR	0.52	25.10	24.45	0.97	0.96	0.97	1.01	1.00
C200-t2.3-R1.3-N100-A0.6-FR	0.52	25.10	21.54	0.86	0.86	0.87	1.00	0.98
C200-t2.3-R1.3-N100-A0.2-FR	0.52	25.10	18.24	0.73	0.76	0.78	0.96	0.93
C300-t2.3-R1.3-N50-A0.4-FR	0.17	18.96	18.86	1.00	1.00	0.96	1.00	1.04
C300-t2.3-R1.3-N50-A0.6-FR	0.17	18.96	18.43	0.97	0.92	0.86	1.05	1.13
C300-t2.3-R1.3-N50-A0.2-FR	0.17	18.96	15.26	0.80	0.82	0.77	0.98	1.05
C300-t2.3-R1.3-N100-A0.4-FR	0.34	23.65	22.55	0.95	1.00	0.96	0.96	0.99
C300-t2.3-R1.3-N100-A0.6-FR	0.34	23.65	22.55	0.95	1.00	0.96	0.96	0.99
C300-t2.3-R1.3-N100-A0.2-FR	0.34	23.65	19.70	0.83	0.79	0.77	1.06	1.08
Average							**1.00**	**1.05**
COV							**0.05**	**0.06**
Cold-formed duplex stainless steel								
C200-t2.3-R1.3-N50-A0.4-FR	0.26	38.07	36.58	0.96	0.97	0.97	0.99	0.99
C200-t2.3-R1.3-N50-A0.6-FR	0.26	38.07	32.26	0.85	0.84	0.88	1.01	0.96
C200-t2.3-R1.3-N50-A0.2-FR	0.26	38.07	27.16	0.71	0.71	0.80	1.00	0.90
C200-t2.3-R1.3-N100-A0.4-FR	0.52	43.66	43.47	1.00	0.98	0.96	1.02	1.03
C200-t2.3-R1.3-N100-A0.6-FR	0.52	43.66	39.92	0.91	0.85	0.88	1.08	1.04

C200-t2.3-R1.3-N100-A0.2-FR	0.52	43.66	33.03	0.76	0.72	0.79	1.05	0.95
C300-t2.3-R1.3-N50-A0.4-FR	0.17	32.63	31.05	0.95	0.97	0.97	0.98	0.99
C300-t2.3-R1.3-N50-A0.6-FR	0.17	32.63	31.05	0.95	0.97	0.97	0.98	0.99
C300-t2.3-R1.3-N50-A0.2-FR	0.17	32.63	27.40	0.84	0.84	0.88	0.99	0.95
C300-t2.3-R1.3-N100-A0.4-FR	0.34	41.95	41.28	0.98	0.98	0.96	1.01	1.02
C300-t2.3-R1.3-N100-A0.6-FR	0.34	41.95	36.30	0.87	0.85	0.88	1.02	0.99
C300-t2.3-R1.3-N100-A0.2-FR	0.34	41.95	29.41	0.70	0.72	0.79	0.97	0.89
Average							**0.99**	**0.97**
COV							**0.02**	**0.05**
Cold-formed ferritic stainless steel								
C200-t2.3-R1.3-N50-A0.4-FR	0.26	19.36	19.36	1.00	1.00	0.96	1.00	1.04
C200-t2.3-R1.3-N50-A0.6-FR	0.26	19.36	19.31	1.00	0.91	0.86	1.10	1.15
C200-t2.3-R1.3-N50-A0.2-FR	0.26	19.36	16.66	0.86	0.81	0.77	1.07	1.12
C200-t2.3-R1.3-N100-A0.4-FR	0.52	25.39	24.85	0.98	0.96	0.97	1.01	1.01
C200-t2.3-R1.3-N100-A0.6-FR	0.52	25.39	21.88	0.86	0.86	0.87	1.00	0.99
C200-t2.3-R1.3-N100-A0.2-FR	0.52	25.39	18.55	0.73	0.76	0.78	0.96	0.94
C300-t2.3-R1.3-N50-A0.4-FR	0.17	19.14	19.06	1.00	1.00	0.96	1.00	1.04
C300-t2.3-R1.3-N50-A0.6-FR	0.17	19.14	18.75	0.98	0.93	0.86	1.06	1.14
C300-t2.3-R1.3-N50-A0.2-FR	0.17	19.14	15.57	0.81	0.82	0.77	0.99	1.06
C300-t2.3-R1.3-N100-A0.4-FR	0.34	24.14	23.02	0.95	1.00	0.96	0.96	0.99
C300-t2.3-R1.3-N100-A0.6-FR	0.34	24.14	23.02	0.95	1.00	0.96	0.96	0.99
C300-t2.3-R1.3-N100-A0.2-FR	0.34	24.14	20.09	0.83	0.89	0.87	0.93	0.96
Average							**0.98**	**1.03**
COV							**0.05**	**0.07**

Table 6.6a: Comparison of web crippling strength reduction factor obtained from FEA results with proposed equation and with other calculation methods for CFSS channel sections with unstiffened web hole and unfastened flange under ETF loading condition.

Specimen	N/h	P_{FEA} (kN)	$P_{FEA,UH}$ (kN)	R_U [$P_{FEA,UH}$/ P_{FEA}]	$R_{U,PROP}$	R_{FANG}	R_U/ $R_{U,PROP}$	R_U/ R_{FANG}
Cold-formed austenitic stainless steel								
C200-t2.7-R1.5-N100-A0.2-FU	0.26	6.44	6.14	0.95	0.94	1.00	1.02	0.95
C200-t2.7-R1.5-N100-A0.4-FU	0.26	6.44	5.55	0.86	0.85	1.00	1.02	0.86
C200-t2.7-R1.5-N100-A0.6-FU	0.26	6.44	4.84	0.75	0.76	1.00	0.99	0.75
C200-t2.7-R1.5-N100-A0.2-FU	0.52	8.38	8.02	0.96	0.97	1.00	0.99	0.96
C200-t2.7-R1.5-N100-A0.4-FU	0.52	8.38	7.32	0.87	0.88	1.00	1.00	0.87
C200-t2.7-R1.5-N100-A0.6-FU	0.52	8.38	6.45	0.77	0.79	1.00	0.98	0.77
C200-t2.7-R1.5-N50-A0.2-FU	0.17	5.03	4.76	0.95	0.98	1.00	0.97	0.95
C200-t2.7-R1.5-N50-A0.4-FU	0.17	5.03	4.25	0.84	0.89	1.00	0.95	0.84
C200-t2.7-R1.5-N50-A0.6-FU	0.17	5.03	3.65	0.73	0.80	1.00	0.91	0.73
C200-t2.7-R1.5-N50-A0.2-FU	0.34	6.07	5.78	0.95	1.00	1.00	0.96	0.95
C200-t2.7-R1.5-N50-A0.4-FU	0.34	6.07	5.78	0.95	1.00	1.00	0.96	0.95
C200-t2.7-R1.5-N50-A0.6-FU	0.34	6.07	5.21	0.86	0.82	1.00	1.05	0.86
Average							**0.96**	**0.87**
COV							**0.05**	**0.11**
Cold-formed duplex stainless steel								
C200-t2.7-R1.5-N100-A0.2-FU	0.26	11.35	10.70	0.94	0.96	1.00	0.98	0.94
C200-t2.7-R1.5-N100-A0.4-FU	0.26	11.35	9.70	0.85	0.87	1.00	0.98	0.85
C200-t2.7-R1.5-N100-A0.6-FU	0.26	11.35	8.57	0.75	0.78	1.00	0.97	0.75
C200-t2.7-R1.5-N100-A0.2-FU	0.52	12.47	11.68	0.94	0.92	1.00	1.02	0.94
C200-t2.7-R1.5-N100-A0.4-FU	0.52	12.47	10.47	0.84	0.83	1.00	1.01	0.84

C200-t2.7-R1.5-N100-A0.6-FU	0.52	12.47	9.10	0.73	0.74	1.00	0.98	0.73
C200-t2.7-R1.5-N50-A0.2-FU	0.17	7.52	7.16	0.95	1.00	1.00	0.95	0.95
C200-t2.7-R1.5-N50-A0.4-FU	0.17	7.52	7.16	0.95	1.00	1.00	0.95	0.95
C200-t2.7-R1.5-N50-A0.6-FU	0.17	7.52	6.44	0.86	0.91	1.00	0.94	0.86
C200-t2.7-R1.5-N50-A0.2-FU	0.34	9.32	8.80	0.94	0.98	1.00	0.97	0.94
C200-t2.7-R1.5-N50-A0.4-FU	0.34	9.32	7.84	0.84	0.89	1.00	0.95	0.84
C200-t2.7-R1.5-N50-A0.6-FU	0.34	9.32	6.72	0.72	0.80	1.00	0.90	0.72
Average							**0.94**	**0.86**
COV							**0.03**	**0.11**
Cold-formed ferritic stainless steel								
C200-t2.7-R1.5-N100-A0.2-FU	0.26	6.57	6.28	0.96	0.94	1.00	1.02	0.96
C200-t2.7-R1.5-N100-A0.4-FU	0.26	6.57	5.68	0.86	0.85	1.00	1.02	0.86
C200-t2.7-R1.5-N100-A0.6-FU	0.26	6.57	4.95	0.75	0.76	1.00	0.99	0.75
C200-t2.7-R1.5-N100-A0.2-FU	0.52	8.56	8.19	0.96	0.97	0.96	0.99	1.00
C200-t2.7-R1.5-N100-A0.4-FU	0.52	8.56	7.47	0.87	0.88	1.00	1.00	0.87
C200-t2.7-R1.5-N100-A0.6-FU	0.52	8.56	6.59	0.77	0.79	1.00	0.98	0.77
C200-t2.7-R1.5-N50-A0.2-FU	0.17	5.17	4.89	0.95	0.98	0.89	0.97	1.06
C200-t2.7-R1.5-N50-A0.4-FU	0.17	5.17	4.36	0.84	0.89	0.99	0.95	0.85
C200-t2.7-R1.5-N50-A0.6-FU	0.17	5.17	3.75	0.73	0.80	1.00	0.91	0.73
C200-t2.7-R1.5-N50-A0.2-FU	0.34	6.23	5.93	0.95	1.00	0.82	0.96	1.16
C200-t2.7-R1.5-N50-A0.4-FU	0.34	6.23	5.93	0.95	1.00	0.82	0.96	1.16
C200-t2.7-R1.5-N50-A0.6-FU	0.34	6.23	5.35	0.86	0.91	0.92	0.95	0.93
Average							**0.94**	**0.97**
COV							**0.02**	**0.20**

Table 6.6b: Comparison of web crippling strength reduction factor obtained from FEA results with proposed equation and with other calculation methods for CFSS channel sections with unstiffened web hole and fastened flange under ETF loading condition.

Specimen	N/h	P_{FEA} (kN)	$P_{FEA,UH}$ (kN)	R_U [$P_{FEA,UH}$/ P_{FEA}]	$R_{U,PROP}$	R_{FANG}	R_U/ $R_{U,PROP}$	R_U/ R_{FANG}
Cold-formed austenitic stainless steel								
C200-t2.7-R1.5-N100-A0.2-FR	0.26	10.20	10.11	0.99	0.99	1.00	1.00	0.99
C200-t2.7-R1.5-N100-A0.4-FR	0.26	10.20	9.76	0.96	0.93	1.00	1.02	0.96
C200-t2.7-R1.5-N100-A0.6-FR	0.26	10.20	9.18	0.90	0.88	1.00	1.02	0.90
C200-t2.7-R1.5-N100-A0.2-FR	0.52	14.49	14.33	0.99	1.00	1.00	0.99	0.99
C200-t2.7-R1.5-N100-A0.4-FR	0.52	14.49	13.91	0.96	0.95	1.00	1.01	0.96
C200-t2.7-R1.5-N100-A0.6-FR	0.52	14.49	13.24	0.91	0.90	1.00	1.02	0.91
C200-t2.7-R1.5-N50-A0.2-FR	0.17	8.84	8.67	0.98	0.96	0.94	1.02	1.04
C200-t2.7-R1.5-N50-A0.4-FR	0.17	8.84	8.17	0.92	0.91	0.86	1.02	1.07
C200-t2.7-R1.5-N50-A0.6-FR	0.17	8.84	7.52	0.85	0.86	0.79	0.99	1.08
C200-t2.7-R1.5-N50-A0.2-FR	0.34	11.37	11.24	0.99	0.97	0.96	1.01	1.03
C200-t2.7-R1.5-N50-A0.4-FR	0.34	11.37	11.24	0.99	0.97	0.96	1.01	1.03
C200-t2.7-R1.5-N50-A0.6-FR	0.34	11.37	10.80	0.95	0.87	0.81	1.09	1.18
Average							**1.03**	**1.08**
COV							**0.04**	**0.06**
Cold-formed duplex stainless steel								
C200-t2.7-R1.5-N100-A0.2-FR	0.26	21.63	21.20	0.98	1.00	1.00	0.98	0.98
C200-t2.7-R1.5-N100-A0.4-FR	0.26	21.63	20.39	0.94	0.94	1.00	1.00	0.94
C200-t2.7-R1.5-N100-A0.6-FR	0.26	21.63	19.30	0.89	0.88	1.00	1.01	0.89
C200-t2.7-R1.5-N100-A0.2-FR	0.52	20.37	20.00	0.98	0.98	1.00	1.00	0.98

C200-t2.7-R1.5-N100-A0.4-FR	0.52	20.37	19.09	0.94	0.92	1.00	1.02	0.94
C200-t2.7-R1.5-N100-A0.6-FR	0.52	20.37	17.85	0.88	0.87	1.00	1.01	0.88
C200-t2.7-R1.5-N50-A0.2-FR	0.17	15.61	15.29	0.98	0.97	0.97	1.01	1.01
C200-t2.7-R1.5-N50-A0.4-FR	0.17	15.61	15.29	0.98	0.97	0.97	1.01	1.01
C200-t2.7-R1.5-N50-A0.6-FR	0.17	15.61	14.55	0.93	0.92	0.90	1.02	1.04
C200-t2.7-R1.5-N50-A0.2-FR	0.34	16.67	16.13	0.97	0.96	0.96	1.01	1.01
C200-t2.7-R1.5-N50-A0.4-FR	0.34	16.67	15.13	0.91	0.91	0.89	1.00	1.02
C200-t2.7-R1.5-N50-A0.6-FR	0.34	16.67	13.75	0.82	0.85	0.82	0.97	1.01
Average							**1.00**	**1.02**
COV							**0.02**	**0.01**
Cold-formed ferritic stainless steel								
C200-t2.7-R1.5-N100-A0.2-FR	0.26	10.37	10.28	0.99	0.99	1.00	1.00	0.99
C200-t2.7-R1.5-N100-A0.4-FR	0.26	10.37	9.93	0.96	0.94	1.00	1.02	0.96
C200-t2.7-R1.5-N100-A0.6-FR	0.26	10.37	9.34	0.90	0.88	1.00	1.02	0.90
C200-t2.7-R1.5-N100-A0.2-FR	0.52	14.73	14.57	0.99	1.00	1.00	0.99	0.99
C200-t2.7-R1.5-N100-A0.4-FR	0.52	14.73	14.16	0.96	0.95	1.00	1.01	0.96
C200-t2.7-R1.5-N100-A0.6-FR	0.52	14.73	13.47	0.91	0.90	1.00	1.02	0.91
C200-t2.7-R1.5-N50-A0.2-FR	0.17	9.02	8.85	0.98	0.96	0.94	1.02	1.04
C200-t2.7-R1.5-N50-A0.4-FR	0.17	9.02	8.34	0.92	0.91	0.87	1.01	1.07
C200-t2.7-R1.5-N50-A0.6-FR	0.17	9.02	7.69	0.85	0.86	0.79	0.99	1.08
C200-t2.7-R1.5-N50-A0.2-FR	0.34	11.61	11.47	0.99	0.98	0.96	1.01	1.03
C200-t2.7-R1.5-N50-A0.4-FR	0.34	11.61	11.47	0.99	0.98	0.96	1.01	1.03
C200-t2.7-R1.5-N50-A0.6-FR	0.34	11.61	11.02	0.95	0.92	0.89	1.03	1.07
Average							**1.01**	**1.05**
COV							**0.01**	**0.02**

6.4. Proposed design equations for CFSS channel sections with edge-stiffened web holes

The FEA results for CFSS channel sections with edge-stiffened web holes under ITF and ETF loading conditions were used to propose design equations in the form of web crippling strength reduction factor ($R_{S,PROP}$). These equations as shown in Equations (36) and (37) are functions of *a/h*, *N/h* and *x/h*.

For ITF loading condition,

$$R_{S,PROP} = \alpha - \gamma\frac{\alpha}{h} + \lambda\frac{N}{h} + \delta\frac{q}{h} \qquad \leq 1.0 \qquad (36)$$

For ETF loading condition,

$$R_{S,PROP} = \alpha - \gamma\frac{\alpha}{h} + \lambda\frac{N}{h} + \delta\frac{q}{h} - \xi\frac{x}{h} \qquad \leq 1.0 \qquad (37)$$

where $\alpha, \gamma, \lambda, \delta, \xi$ are equation coefficients. The values for these coefficients are tabulated in Table 6.7 for each of the three stainless steel materials: austenitic, duplex, and ferritic, with both unfastened and fastened flanges.

Tables 17a-17b and 18a-18b affirm the high degree of prediction accuracy for the proposed equation. The reduction factors obtained from the proposed equations ($R_{S,PROP}$) closely align with those derived from the FEA results (R_S). Under ITF loading condition, the average ratios are 0.99 and 1.01 for channels with unfastened and fastened flanges, with *COV* at 0.02. For channels under ETF loading condition, the average ratio is 1.0 with *COV* at 0.03 for unfastened flanges and 0.02 for fastened flanges.

In contrast, the reduction factors from the proposed equation by Uzzaman et al. (R_{UZZ}) which is only applicable for channels with unfastened flanges, indicate an average ratio of 0.90 with *COV* at 0.04 for channels under ITF loading condition, and 0.91 with *COV* at 0.09 for channels under ETF loading

condition. It should be noted that *COV*s of the R_{FEA}/R_{UZZ} ratios for channels under ITF and ETF loading conditions are higher compared to the proposed equation presented in this thesis.

Table 6.7: Coefficient values for the proposed web crippling reduction factors for CFSS channel sections with edge-stiffened web holes

Loading condition	Support condition	Stainless Steel Material	α	γ	λ	δ	ξ
ITF	Unfastened flange	Austenitic	1.063	0.624	0.010	1.837	
		Duplex	1.080	0.555	-0.013	0.871	
		Ferritic	1.064	0.627	0.005	1.958	
	Fastened flange	Austenitic	1.087	0.424	-0.214	3.823	
		Duplex	1.069	0.582	-0.062	3.057	
		Ferritic	1.087	0.418	-0.211	3.743	
ETF	Unfastened flange	Austenitic	1.109	0.417	0.009	4.199	0.138
		Duplex	1.141	0.436	0.015	5.325	0.214
		Ferritic	1.108	0.420	0.026	4.195	0.145
	Fastened flange	Austenitic	0.978	0.201	0.087	1.751	-0.005
		Duplex	1.002	0.219	0.069	2.189	0.024
		Ferritic	0.976	0.199	0.086	1.740	-0.007

Table 6.8a: Comparison of web crippling strength reduction factor obtained from FEA results with proposed equation and with other calculation methods for CFSS channel sections with edge-stiffened web hole and unfastened flange under ITF loading condition

Specimen	N/h	q/h	P_{FEA} (kN)	$P_{FEA,SH}$ (kN)	R_S $[P_{FEA,SH}/ P_{FEA}]$	$R_{S,PROP}$	R_{UZZ}	$R_S/ R_{S,PROP}$	R_S/ R_{UZZ}
Cold-formed austenitic stainless steel									
C200-t2.7-R1.5-N100-A0.4-q3-FU	0.52	0.02	23.80	19.96	0.84	0.85	0.93	0.99	0.90
C200-t2.7-R1.5-N100-A0.6-q3-FU	0.52	0.02	23.80	16.93	0.71	0.72	0.85	0.98	0.84
C200-t2.7-R1.5-N100-A0.4-q5-FU	0.52	0.03	23.80	20.66	0.87	0.87	0.93	1.00	0.93
C200-t2.7-R1.5-N100-A0.6-q5-FU	0.52	0.03	23.80	17.64	0.74	0.74	0.85	1.00	0.87
C200-t2.7-R1.5-N100-A0.4-q7-FU	0.52	0.04	23.80	21.83	0.92	0.89	0.94	1.04	0.98
C200-t2.7-R1.5-N100-A0.6-q7-FU	0.52	0.04	23.80	18.76	0.79	0.76	0.86	1.03	0.92
C200-t2.7-R1.5-N50-A0.4-q3-FU	0.26	0.02	22.41	18.48	0.82	0.85	0.92	0.98	0.90
C200-t2.7-R1.5-N50-A0.6-q3-FU	0.26	0.02	22.41	15.34	0.68	0.72	0.84	0.95	0.81
C200-t2.7-R1.5-N50-A0.4-q5-FU	0.26	0.03	22.41	19.13	0.85	0.86	0.93	0.99	0.92
C200-t2.7-R1.5-N50-A0.6-q5-FU	0.26	0.03	22.41	15.96	0.71	0.74	0.85	0.96	0.84
C200-t2.7-R1.5-N50-A0.4-q7-FU	0.26	0.04	22.41	20.18	0.90	0.88	0.93	1.02	0.97
C200-t2.7-R1.5-N50-A0.6-q7-FU	0.26	0.04	22.41	17.03	0.76	0.76	0.85	1.00	0.89
Average								**0.98**	**0.89**
COV								**0.03**	**0.07**
Cold-formed duplex stainless steel									
C200-t2.7-R1.5-N100-A0.4-q3-FU	0.52	0.02	35.34	29.96	0.85	0.86	0.93	0.98	0.92
C200-t2.7-R1.5-N100-A0.6-q3-FU	0.52	0.02	35.34	25.25	0.71	0.75	0.85	0.95	0.84
C200-t2.7-R1.5-N100-A0.4-q5-FU	0.52	0.03	35.34	30.95	0.88	0.87	0.93	1.00	0.94
C200-t2.7-R1.5-N100-A0.6-q5-FU	0.52	0.03	35.34	26.35	0.75	0.76	0.85	0.98	0.87
C200-t2.7-R1.5-N100-A0.4-q7-FU	0.52	0.04	35.34	32.70	0.93	0.88	0.94	1.05	0.99

C200-t2.7-R1.5-N100-A0.6-q7-FU	0.52	0.04	35.34	27.86	0.79	0.77	0.86	1.02	0.92
C200-t2.7-R1.5-N50-A0.4-q3-FU	0.26	0.02	33.96	28.08	0.83	0.87	0.92	0.95	0.90
C200-t2.7-R1.5-N50-A0.6-q3-FU	0.26	0.02	33.96	22.98	0.68	0.76	0.84	0.89	0.80
C200-t2.7-R1.5-N50-A0.4-q5-FU	0.26	0.03	33.96	29.07	0.86	0.88	0.93	0.98	0.92
C200-t2.7-R1.5-N50-A0.6-q5-FU	0.26	0.03	33.96	24.05	0.71	0.77	0.85	0.92	0.83
C200-t2.7-R1.5-N50-A0.4-q7-FU	0.26	0.04	33.96	30.83	0.91	0.89	0.93	1.02	0.97
C200-t2.7-R1.5-N50-A0.6-q7-FU	0.26	0.04	33.96	25.48	0.75	0.78	0.85	0.97	0.88
Average								**0.96**	**0.88**
COV								**0.05**	**0.08**
Cold-formed ferritic stainless steel									
C200-t2.7-R1.5-N100-A0.4-q3-FU	0.52	0.02	24.19	20.29	0.84	0.85	0.93	0.99	0.91
C200-t2.7-R1.5-N100-A0.6-q3-FU	0.52	0.02	24.19	17.23	0.71	0.72	0.85	0.99	0.84
C200-t2.7-R1.5-N100-A0.4-q5-FU	0.52	0.03	24.19	21.00	0.87	0.87	0.93	1.00	0.93
C200-t2.7-R1.5-N100-A0.6-q5-FU	0.52	0.03	24.19	17.95	0.74	0.74	0.85	1.00	0.87
C200-t2.7-R1.5-N100-A0.4-q7-FU	0.52	0.04	24.19	22.20	0.92	0.89	0.94	1.03	0.98
C200-t2.7-R1.5-N100-A0.6-q7-FU	0.52	0.04	24.19	19.09	0.79	0.76	0.86	1.04	0.92
C200-t2.7-R1.5-N50-A0.4-q3-FU	0.26	0.02	22.65	18.77	0.83	0.85	0.92	0.98	0.90
C200-t2.7-R1.5-N50-A0.6-q3-FU	0.26	0.02	22.65	15.60	0.69	0.72	0.84	0.96	0.82
C200-t2.7-R1.5-N50-A0.4-q5-FU	0.26	0.03	22.65	19.43	0.86	0.87	0.93	0.99	0.93
C200-t2.7-R1.5-N50-A0.6-q5-FU	0.26	0.03	22.65	16.23	0.72	0.74	0.85	0.97	0.84
C200-t2.7-R1.5-N50-A0.4-q7-FU	0.26	0.04	22.65	20.49	0.90	0.89	0.93	1.02	0.97
C200-t2.7-R1.5-N50-A0.6-q7-FU	0.26	0.04	22.65	17.33	0.76	0.76	0.85	1.01	0.90
Average								**0.99**	**0.89**
COV								**0.03**	**0.07**

Table 6.8b: Comparison of web crippling strength reduction factor obtained from FEA results with proposed equation and with other calculation methods for CFSS channel sections with edge-stiffened web hole and fastened flange under ITF loading condition

Specimen	*N/h*	*q/h*	P_{FEA} *(kN)*	$P_{FEA,SH}$ *(kN)*	R_S $[P_{FEA,SH}/P_{FEA}]$	$R_{S,PROP}$	$R_S/R_{S,PROP}$
Cold-formed austenitic stainless steel							
C200-t2.7-R1.5-N100-A0.4-q3-FR	0.52	0.02	29.87	27.86	0.93	0.87	1.08
C200-t2.7-R1.5-N100-A0.6-q3-FR	0.52	0.02	29.87	23.72	0.79	0.78	1.02
C200-t2.7-R1.5-N100-A0.4-q5-FR	0.52	0.03	29.87	28.48	0.95	0.90	1.05
C200-t2.7-R1.5-N100-A0.6-q5-FR	0.52	0.03	29.87	24.44	0.82	0.82	1.00
C200-t2.7-R1.5-N100-A0.4-q7-FR	0.52	0.04	29.87	29.40	0.98	0.94	1.04
C200-t2.7-R1.5-N100-A0.6-q7-FR	0.52	0.04	29.87	25.85	0.87	0.86	1.01
C200-t2.7-R1.5-N50-A0.4-q3-FR	0.26	0.02	23.69	23.33	0.99	0.92	1.07
C200-t2.7-R1.5-N50-A0.6-q3-FR	0.26	0.02	23.69	21.27	0.90	0.84	1.07
C200-t2.7-R1.5-N50-A0.4-q5-FR	0.26	0.03	23.69	23.35	0.99	0.96	1.03
C200-t2.7-R1.5-N50-A0.6-q5-FR	0.26	0.03	23.69	21.79	0.92	0.88	1.05
C200-t2.7-R1.5-N50-A0.4-q7-FR	0.26	0.04	23.69	23.46	0.99	1.00	0.99
C200-t2.7-R1.5-N50-A0.6-q7-FR	0.26	0.04	23.69	22.49	0.95	0.92	1.04
Average							**1.04**
COV							**0.03**
Cold-formed duplex stainless steel							
C200-t2.7-R1.5-N100-A0.4-q3-FR	0.52	0.02	50.91	43.92	0.86	0.85	1.01
C200-t2.7-R1.5-N100-A0.6-q3-FR	0.52	0.02	50.91	36.98	0.73	0.74	0.99
C200-t2.7-R1.5-N100-A0.4-q5-FR	0.52	0.03	50.91	45.20	0.89	0.88	1.00
C200-t2.7-R1.5-N100-A0.6-q5-FR	0.52	0.03	50.91	38.45	0.76	0.77	0.98
C200-t2.7-R1.5-N100-A0.4-q7-FR	0.52	0.04	50.91	47.17	0.93	0.92	1.01

C200-t2.7-R1.5-N100-A0.6-q7-FR	0.52	0.04	50.91	41.57	0.82	0.80	1.02
C200-t2.7-R1.5-N50-A0.4-q3-FR	0.26	0.02	43.66	40.88	0.94	0.87	1.08
C200-t2.7-R1.5-N50-A0.6-q3-FR	0.26	0.02	43.66	33.60	0.77	0.75	1.02
C200-t2.7-R1.5-N50-A0.4-q5-FR	0.26	0.03	43.66	42.19	0.97	0.90	1.07
C200-t2.7-R1.5-N50-A0.6-q5-FR	0.26	0.03	43.66	34.77	0.80	0.78	1.02
C200-t2.7-R1.5-N50-A0.4-q7-FR	0.26	0.04	43.66	43.24	0.99	0.93	1.06
C200-t2.7-R1.5-N50-A0.6-q7-FR	0.26	0.04	43.66	36.77	0.84	0.82	1.03
Average							**1.04**
COV							**0.02**
Cold-formed ferritic stainless steel							
C200-t2.7-R1.5-N100-A0.4-q3-FR	0.52	0.02	30.14	28.23	0.94	0.87	1.08
C200-t2.7-R1.5-N100-A0.6-q3-FR	0.52	0.02	30.14	24.05	0.80	0.78	1.02
C200-t2.7-R1.5-N100-A0.4-q5-FR	0.52	0.03	30.14	28.84	0.96	0.91	1.05
C200-t2.7-R1.5-N100-A0.6-q5-FR	0.52	0.03	30.14	24.78	0.82	0.82	1.00
C200-t2.7-R1.5-N100-A0.4-q7-FR	0.52	0.04	30.14	29.75	0.99	0.95	1.04
C200-t2.7-R1.5-N100-A0.6-q7-FR	0.52	0.04	30.14	26.24	0.87	0.86	1.01
C200-t2.7-R1.5-N50-A0.4-q3-FR	0.26	0.02	23.96	23.61	0.99	0.92	1.07
C200-t2.7-R1.5-N50-A0.6-q3-FR	0.26	0.02	23.96	21.57	0.90	0.84	1.07
C200-t2.7-R1.5-N50-A0.4-q5-FR	0.26	0.03	23.96	23.64	0.99	0.96	1.03
C200-t2.7-R1.5-N50-A0.6-q5-FR	0.26	0.03	23.96	22.04	0.92	0.88	1.05
C200-t2.7-R1.5-N50-A0.4-q7-FR	0.26	0.04	23.96	23.72	0.99	1.00	0.99
C200-t2.7-R1.5-N50-A0.6-q7-FR	0.26	0.04	23.96	22.74	0.95	0.92	1.03
Average							**1.03**
COV							**0.03**

Table 6.9a: Comparison of web crippling strength reduction factor obtained from FEA results with proposed equation and with other calculation methods for CFSS channel sections with edge-stiffened web hole and unfastened flanges under ETF loading condition

Specimen	N/h	q/h	x/h	P_{FEA} (kN)	$P_{FEA,SH}$ (kN)	R_S $[P_{FEA,SH}/ P_{FEA}]$	$R_{S,PROP}$	R_{UZZ}	$R_S/ R_{S,PROP}$	R_S/ R_{UZZ}
Cold-formed austenitic stainless steel										
C200-t2.7-R1.5-N100-A0.4-q3-FU	0.52	0.016	0.712	11.30	10.20	0.90	0.91	1.00	0.99	0.90
C200-t2.7-R1.5-N100-A0.6-q3-FU	0.52	0.016	0.612	11.30	9.06	0.80	0.84	0.98	0.95	0.82
C200-t2.7-R1.5-N100-A0.4-q5-FU	0.52	0.026	0.712	11.30	10.82	0.96	0.96	1.00	1.00	0.96
C200-t2.7-R1.5-N100-A0.6-q5-FU	0.52	0.026	0.612	11.30	9.79	0.87	0.89	0.99	0.98	0.88
C200-t2.7-R1.5-N100-A0.4-q7-FU	0.52	0.036	0.712	11.30	11.43	1.01	1.00	1.00	1.01	1.01
C200-t2.7-R1.5-N100-A0.6-q7-FU	0.52	0.036	0.612	11.30	10.77	0.95	0.93	0.99	1.02	0.96
C200-t2.7-R1.5-N50-A0.4-q3-FU	0.26	0.016	0.842	8.76	7.85	0.90	0.89	1.00	1.00	0.90
C200-t2.7-R1.5-N50-A0.6-q3-FU	0.26	0.016	0.742	8.76	6.87	0.78	0.82	0.98	0.95	0.80
C200-t2.7-R1.5-N50-A0.4-q5-FU	0.26	0.026	0.842	8.76	8.34	0.95	0.94	1.00	1.01	0.95
C200-t2.7-R1.5-N50-A0.6-q5-FU	0.26	0.026	0.742	8.76	7.47	0.85	0.87	0.99	0.98	0.86
C200-t2.7-R1.5-N50-A0.4-q7-FU	0.26	0.036	0.842	8.76	8.78	1.00	0.98	1.00	1.02	1.00
C200-t2.7-R1.5-N50-A0.6-q7-FU	0.26	0.036	0.742	8.76	8.17	0.93	0.91	0.99	1.02	0.94
Average									**1.00**	**0.91**
COV									**0.03**	**0.09**
Cold-formed duplex stainless steel										
C200-t2.7-R1.5-N100-A0.4-q3-FU	0.52	0.016	0.712	16.09	14.28	0.89	0.90	1.00	0.98	0.89
C200-t2.7-R1.5-N100-A0.6-q3-FU	0.52	0.016	0.612	16.09	12.73	0.79	0.84	0.98	0.94	0.81
C200-t2.7-R1.5-N100-A0.4-q5-FU	0.52	0.026	0.712	16.09	15.29	0.95	0.96	1.00	0.99	0.95
C200-t2.7-R1.5-N100-A0.6-q5-FU	0.52	0.026	0.612	16.09	13.83	0.86	0.89	0.99	0.96	0.87

C200-t2.7-R1.5-N100-A0.4-q7-FU	0.52	0.036	0.712	16.09	16.50	1.03	1.00	1.00	1.03	1.03
C200-t2.7-R1.5-N100-A0.6-q7-FU	0.52	0.036	0.612	16.09	15.54	0.97	0.95	0.99	1.02	0.98
C200-t2.7-R1.5-N50-A0.4-q3-FU	0.26	0.016	0.842	12.47	10.86	0.87	0.87	1.00	1.00	0.87
C200-t2.7-R1.5-N50-A0.6-q3-FU	0.26	0.016	0.742	12.47	9.52	0.76	0.81	0.98	0.95	0.78
C200-t2.7-R1.5-N50-A0.4-q5-FU	0.26	0.026	0.842	12.47	11.71	0.94	0.93	1.00	1.01	0.94
C200-t2.7-R1.5-N50-A0.6-q5-FU	0.26	0.026	0.742	12.47	10.44	0.84	0.86	0.99	0.97	0.85
C200-t2.7-R1.5-N50-A0.4-q7-FU	0.26	0.036	0.842	12.47	12.64	1.01	0.98	1.00	1.03	1.01
C200-t2.7-R1.5-N50-A0.6-q7-FU	0.26	0.036	0.742	12.47	11.59	0.93	0.92	0.99	1.01	0.94
Average									**0.99**	**0.90**
COV									**0.04**	**0.10**
Cold-formed ferritic stainless steel										
C200-t2.7-R1.5-N100-A0.4-q3-FU	0.52	0.016	0.712	11.51	10.39	0.90	0.92	1.00	0.98	0.90
C200-t2.7-R1.5-N100-A0.6-q3-FU	0.52	0.016	0.612	11.51	9.23	0.80	0.85	0.98	0.95	0.82
C200-t2.7-R1.5-N100-A0.4-q5-FU	0.52	0.026	0.712	11.51	11.02	0.96	0.96	1.00	1.00	0.96
C200-t2.7-R1.5-N100-A0.6-q5-FU	0.52	0.026	0.612	11.51	9.97	0.87	0.89	0.99	0.97	0.88
C200-t2.7-R1.5-N100-A0.4-q7-FU	0.52	0.036	0.712	11.51	11.63	1.01	1.00	1.00	1.01	1.01
C200-t2.7-R1.5-N100-A0.6-q7-FU	0.52	0.036	0.612	11.51	10.96	0.95	0.93	0.99	1.02	0.96
C200-t2.7-R1.5-N50-A0.4-q3-FU	0.26	0.016	0.842	8.93	8.00	0.90	0.89	1.00	1.01	0.90
C200-t2.7-R1.5-N50-A0.6-q3-FU	0.26	0.016	0.742	8.93	7.00	0.78	0.82	0.98	0.96	0.80
C200-t2.7-R1.5-N50-A0.4-q5-FU	0.26	0.026	0.842	8.93	8.49	0.95	0.93	1.00	1.02	0.95
C200-t2.7-R1.5-N50-A0.6-q5-FU	0.26	0.026	0.742	8.93	7.61	0.85	0.86	0.99	0.99	0.86
C200-t2.7-R1.5-N50-A0.4-q7-FU	0.26	0.036	0.842	8.93	8.94	1.00	0.98	1.00	1.02	1.00
C200-t2.7-R1.5-N50-A0.6-q7-FU	0.26	0.036	0.742	8.93	8.32	0.93	0.91	0.99	1.03	0.94
Average									**1.00**	**0.91**
COV									**0.03**	**0.09**

Table 6.9b: Comparison of web crippling strength reduction factor obtained from FEA results with proposed equation and with other calculation methods for CFSS channel sections with edge-stiffened web hole and fastened flanges under ETF loading condition.

Specimen	*N/h*	*q/h*	*x/h*	P_{FEA} (kN)	$P_{FEA,SH}$ (kN)	R_S $[P_{FEA,SH}/ P_{FEA}]$	$R_{S,PROP}$	$R_S/ R_{S,PROP}$
Cold-formed austenitic stainless steel								
C200-t2.7-R1.5-N100-A0.4-q3-FR	0.52	0.016	0.712	18.22	17.79	0.98	0.97	1.00
C200-t2.7-R1.5-N100-A0.6-q3-FR	0.52	0.016	0.612	18.22	17.09	0.94	0.93	1.01
C200-t2.7-R1.5-N100-A0.4-q5-FR	0.52	0.026	0.712	18.22	18.04	0.99	0.99	1.00
C200-t2.7-R1.5-N100-A0.6-q5-FR	0.52	0.026	0.612	18.22	17.49	0.96	0.95	1.01
C200-t2.7-R1.5-N100-A0.4-q7-FR	0.52	0.036	0.712	18.22	18.20	1.00	1.00	1.00
C200-t2.7-R1.5-N100-A0.6-q7-FR	0.52	0.036	0.612	18.22	18.04	0.99	0.97	1.02
C200-t2.7-R1.5-N50-A0.4-q3-FR	0.26	0.016	0.842	12.88	12.56	0.98	0.95	1.02
C200-t2.7-R1.5-N50-A0.6-q3-FR	0.26	0.016	0.742	12.88	11.91	0.92	0.91	1.01
C200-t2.7-R1.5-N50-A0.4-q5-FR	0.26	0.026	0.842	12.88	12.63	0.98	0.97	1.01
C200-t2.7-R1.5-N50-A0.6-q5-FR	0.26	0.026	0.742	12.88	12.11	0.94	0.93	1.01
C200-t2.7-R1.5-N50-A0.4-q7-FR	0.26	0.036	0.842	12.88	12.69	0.99	0.99	1.00
C200-t2.7-R1.5-N50-A0.6-q7-FR	0.26	0.036	0.742	12.88	12.35	0.96	0.95	1.01
Average								**1.01**
COV								**0.01**
Cold-formed duplex stainless steel								
C200-t2.7-R1.5-N100-A0.4-q3-FR	0.52	0.016	0.712	28.63	27.71	0.97	0.97	1.00
C200-t2.7-R1.5-N100-A0.6-q3-FR	0.52	0.016	0.612	28.63	26.54	0.93	0.93	1.00
C200-t2.7-R1.5-N100-A0.4-q5-FR	0.52	0.026	0.712	28.63	28.36	0.99	0.99	1.00
C200-t2.7-R1.5-N100-A0.6-q5-FR	0.52	0.026	0.612	28.63	27.45	0.96	0.95	1.01

C200-t2.7-R1.5-N100-A0.4-q7-FR	0.52	0.036	0.712	28.63	28.79	1.01	1.00	1.01
C200-t2.7-R1.5-N100-A0.6-q7-FR	0.52	0.036	0.612	28.63	28.62	1.00	0.97	1.03
C200-t2.7-R1.5-N50-A0.4-q3-FR	0.26	0.016	0.842	20.37	19.44	0.95	0.95	1.01
C200-t2.7-R1.5-N50-A0.6-q3-FR	0.26	0.016	0.742	20.37	18.30	0.90	0.90	0.99
C200-t2.7-R1.5-N50-A0.4-q5-FR	0.26	0.026	0.842	20.37	19.79	0.97	0.97	1.00
C200-t2.7-R1.5-N50-A0.6-q5-FR	0.26	0.026	0.742	20.37	18.83	0.92	0.93	1.00
C200-t2.7-R1.5-N50-A0.4-q7-FR	0.26	0.036	0.842	20.37	20.04	0.98	0.99	0.99
C200-t2.7-R1.5-N50-A0.6-q7-FR	0.26	0.036	0.742	20.37	19.46	0.96	0.95	1.01
Average								**1.00**
COV								**0.01**
Cold-formed ferritic stainless steel								
C200-t2.7-R1.5-N100-A0.4-q3-FR	0.52	0.016	0.712	18.48	18.04	0.98	0.97	1.00
C200-t2.7-R1.5-N100-A0.6-q3-FR	0.52	0.016	0.612	18.48	17.32	0.94	0.93	1.00
C200-t2.7-R1.5-N100-A0.4-q5-FR	0.52	0.026	0.712	18.48	18.29	0.99	0.99	1.00
C200-t2.7-R1.5-N100-A0.6-q5-FR	0.52	0.026	0.612	18.48	17.73	0.96	0.95	1.01
C200-t2.7-R1.5-N100-A0.4-q7-FR	0.52	0.036	0.712	18.48	18.45	1.00	1.00	1.00
C200-t2.7-R1.5-N100-A0.6-q7-FR	0.52	0.036	0.612	18.48	18.28	0.99	0.97	1.02
C200-t2.7-R1.5-N50-A0.4-q3-FR	0.26	0.016	0.842	13.05	12.74	0.98	0.95	1.03
C200-t2.7-R1.5-N50-A0.6-q3-FR	0.26	0.016	0.742	13.05	12.09	0.93	0.91	1.02
C200-t2.7-R1.5-N50-A0.4-q5-FR	0.26	0.026	0.842	13.05	12.80	0.98	0.97	1.01
C200-t2.7-R1.5-N50-A0.6-q5-FR	0.26	0.026	0.742	13.05	12.28	0.94	0.93	1.01
C200-t2.7-R1.5-N50-A0.4-q7-FR	0.26	0.036	0.842	13.05	12.86	0.99	0.99	1.00
C200-t2.7-R1.5-N50-A0.6-q7-FR	0.26	0.036	0.742	13.05	12.53	0.96	0.95	1.01
Average								**1.01**
COV								**0.01**

Chapter 7: Reliability analysis

7.1 General

Reliability analysis was conducted to assess the reliability of the proposed design equations for CFSS channel sections with plain web and proposed design equations in the form of web crippling strength reduction factor for CFSS channel sections with unstiffened web holes ($R_{U,PROP}$) and with stiffened web holes ($R_{S,PROP}$). The reliability index (β) serves as a relative indicator of the design's safety and could be determined by using Eq. (38). AISI S100-16 [2] recommends a reliability index of 2.5 for cold-formed steel (CFS) structural members.

$$\varphi = 1.5(M_m F_m P_m) e^{-\beta \sqrt{V_M^2 + V_F^2 + C_P V_P^2 + V_Q^2}} \quad (38)$$

$$C_p = \left(1 + \frac{1}{n}\right)\left(\frac{m}{m-2}\right) \quad (39)$$

Where $M_m, F_m, and\ P_m$ are the mean values of the material factor (1.1), fabrication factor (1.0) and the tested-to-predicted load ratios, respectively. $V_M, V_F, V_{Q,}\ and\ V_P$ are the coefficient of variations (COVs) for material factor (0.1), fabrication factor (0.05), load effect (0.21) and tested-to-predicted load ratios, respectively. C_P is the correction factor determined by Eq. (39), and n and m are the number of specimens and degree of freedom ($m = n - 1$), respectively. A constant resistance factor (φ) equal to 0.85 was used in the reliability analysis.

7.2 Reliability analysis for the web crippling strength of CFSS channel sections without web holes

Reliability analysis for the proposed web crippling strength equation of CFSS channels section without web holes was conducted by comparing the values of the web crippling strength, P_{FEA}, obtained from the results of the parametric study with the values of the proposed web crippling strength, P_{PROP}, calculated using Eq. (33). Tables 7.1a and 7.1b summarizes the result of the reliability analysis. As can be seen from these tables, the reliability index, (β), is greater than the target index, with a minimum of 2.7 and 2.55 for ITF and ETF loading conditions, respectively, considering both fastened and unfastened flanges. This demonstrates that the proposed Eq. (33) is reliable to determine the web crippling strength of CFSS channels without a web hole.

Table 7.1a: Result of the reliability analysis for proposed web crippling strength equations of CFSS channels under ITF loading condition

(a) Unfastened sections

Ratio of equations	P_{FEA}/P_{PROP}		
	Austenitic stainless steel	Duplex stainless steel	Ferritic stainless steel
Data Number, n	154	154	152
Mean, P_m	1.00	0.99	0.99
Coefficient of variation, COV	0.04	0.03	0.04
Reliability index, β	2.75	2.70	2.73
Resistance factor, ϕ	0.85	0.85	0.85

(b) Fastened sections

Ratio of equations	P_{FEA}/P_{PROP}		
	Austenitic stainless steel	Duplex stainless steel	Ferritic stainless steel
Data Number, n	154	154	152
Mean, P_m	1.00	0.99	0.99
Coefficient of variation, COV	0.06	0.04	0.06
Reliability index, β	2.80	2.72	2.70
Resistance factor, ϕ	0.83	0.85	0.85

Table 7.1b: Result of the reliability analysis for proposed web crippling strength equations of CFSS channels under ETF loading condition

(a) Unfastened sections

Ratio of equations	P_{FEA}/P_{PROP}		
	Austenitic stainless steel	Duplex stainless steel	Ferritic stainless steel
Data Number, n	154	154	152
Mean, P_m	0.97	0.97	0.97
Coefficient of variation, COV	0.14	0.13	0.13
Reliability index, β	2.56	2.55	2.55
Resistance factor, ϕ	0.85	0.85	0.85

(b) Fastened sections

Ratio of equations	P_{FEA}/P_{PROP}		
	Austenitic stainless steel	Duplex stainless steel	Ferritic stainless steel
Data Number, n	154	154	152
Mean, P_m	0.99	0.99	1.00
Coefficient of variation, COV	0.04	0.06	0.04
Reliability index, β	2.72	2.66	2.73
Resistance factor, ϕ	0.85	0.85	0.85

7.3 Reliability analysis for the web crippling strength reduction factor of CFSS channel sections with unstiffened web holes

Reliability analysis for the proposed web crippling strength reduction factor for CFSS channels section with unstiffened web hole was conducted by comparing the values of the web crippling strength reduction factor, R_U, obtained from the results of the parametric study with the values of the proposed web crippling strength reduction factor, $R_{U,PROP}$, calculated using Eqs. (34) and (35). A summary of the reliability analysis is shown in Tables 7.2a and 7.2b. As observed from these tables, the reliability index, (β), is greater than the target index, with a minimum of 2.72 and 2.67 for ITF and ETF loading conditions, respectively. This indicates that the proposed Eqs. (34) and (35) are reliable in determining the web crippling strength reduction factor for CFSS channel sections with unstiffened web holes.

Table 7.2a: Result of the reliability analysis for proposed web crippling strength reduction factor of CFSS channels with unstiffened web hole under ITF loading conditions.

(a) Unfastened sections

Ratio of equations	$R_U/R_{U,PROP}$		
	Austenitic stainless steel	Duplex stainless steel	Ferritic stainless steel
Data Number, n	154	154	152
Mean, P_m	1.00	0.99	0.99
Coefficient of variation, COV	0.03	0.04	0.03
Reliability index, β	2.74	2.72	2.74
Resistance factor, ϕ	0.85	0.85	0.85

b) Fastened sections

Ratio of equations	$R_U/R_{U,PROP}$		
	Austenitic stainless steel	Duplex stainless steel	Ferritic stainless steel
Data Number, n	154	154	152
Mean, P_m	1.01	1.00	1.01
Coefficient of variation, COV	0.06	0.03	0.06
Reliability index, β	2.75	2.77	2.73
Resistance factor, ϕ	0.85	0.85	0.85

Table 7.2b: Result of the reliability analysis for proposed web crippling strength reduction factor of CFSS channels with unstiffened web hole under ETF loading condition

(a) Unfastened sections

Ratio of equations	$R_U/R_{U,PROP}$		
	Austenitic stainless steel	Duplex stainless steel	Ferritic stainless steel
Data Number, n	154	154	152
Mean, P_m	1.01	1.00	1.00
Coefficient of variation, COV	0.07	0.07	0.07
Reliability index, β	2.69	2.67	2.69
Resistance factor, ϕ	0.85	0.85	0.85

(b) Fastened sections

Ratio of equations	$R_U/R_{U,PROP}$		
	Austenitic stainless steel	Duplex stainless steel	Ferritic stainless steel
Data Number, n	154	154	152
Mean, P_m	1.00	1.00	1.00
Coefficient of variation, COV	0.02	0.01	0.02
Reliability index, β	2.80	2.79	2.80
Resistance factor, ϕ	0.85	0.85	0.85

7.4 Reliability analysis for the web crippling strength reduction factor of CFSS channel sections with edge-stiffened web holes

Reliability analysis for the proposed web crippling strength reduction factor for CFSS channels section with edge-stiffened web hole was conducted by comparing the values obtained from the results of the parametric study, R_S, with the calculated values from the proposed Eqs. (36) and (37), $R_{S,PROP}$. The result is summarized in Tables 7.3a and 7.3b. As observed from these tables, the reliability index, (β), is greater than the target index of 2.5. Considering both cases of channel sections with fastened and unfastened flanges, minimum β are 2.75 and 2.56 for ITF and ETF loading conditions, respectively. This is an indication that the proposed Eqs. (36) and (37) are reliable in determining the web crippling strength reduction factor for CFSS channel sections with edge-stiffened web holes.

Table 7.3a: Result of the reliability analysis for proposed web crippling strength reduction factor of CFSS channels with edge-stiffened web hole under ITF loading condition

(a) Unfastened sections

Ratio of equations	$R_S/R_{S,PROP}$		
	Austenitic stainless steel	Duplex stainless steel	Ferritic stainless steel
Data Number, n	154	154	152
Mean, P_m	1.00	1.00	1.00
Coefficient of variation, COV	0.03	0.04	0.03
Reliability index, β	2.76	2.75	2.77
Resistance factor, ϕ	0.85	0.85	0.85

(b) Fastened sections

Ratio of equations	$R_S/R_{S,PROP}$		
	Austenitic stainless steel	Duplex stainless steel	Ferritic stainless steel
Data Number, n	154	154	152
Mean, P_m	1.01	1.00	1.00
Coefficient of variation, COV	0.05	0.03	0.05
Reliability index, β	2.75	2.78	2.75
Resistance factor, ϕ	0.85	0.85	0.85

Table 7.3b: Result of the reliability analysis for proposed web crippling strength reduction factor of CFSS channels with edge-stiffened web hole under ETF loading condition

(a) Unfastened sections

Ratio of equations	$R_S/R_{S,PROP}$		
	Austenitic stainless steel	Duplex stainless steel	Ferritic stainless steel
Data Number, n	154	154	152
Mean, P_m	1.06	1.12	1.06
Coefficient of variation, COV	0.15	0.15	0.15
Reliability index, β	2.56	2.79	2.56
Resistance factor, ϕ	0.85	0.85	0.85

(b) Fastened sections

Ratio of equations	$R_S/R_{S,PROP}$		
	Austenitic stainless steel	Duplex stainless steel	Ferritic stainless steel
Data Number, n	154	154	152
Mean, P_m	1.00	1.00	1.00
Coefficient of variation, COV	0.02	0.02	0.02
Reliability index, β	2.79	2.80	2.79
Resistance factor, ϕ	0.85	0.85	0.85

Chapter 8: Conclusion

This thesis presents a comprehensive numerical study on the effects of edge-stiffened web holes on the web crippling strength of cold-formed stainless steel (CFSS) lipped channel sections under interior-two-flange (ITF) and end-two-flange (ETF) loading conditions. Three common stainless steel grades were used: EN 1.4509 (Ferritic), EN 1.4462 (Duplex) and EN 1.4301 (Austenitic). Finite element (FE) models were developed and validated against the experimental results reported by Yousefi et al. [36] and Chen et al. [7], which showed good agreement in terms of deformed shapes and failure load. With the validated FE model, a comprehensive parametric study comprising 3,744 finite element models was carried out to analyze the influence of various parameters on the web crippling strength of CFSS channel sections. The effects of flange condition (unfastened or fastened to the bearing plates), the ratio of inside bend radius to web thickness (*r/t*), the ratio of bearing length to web thickness (*N/t*), the ratio of web flat depth to thickness (*h/t*), ratio of hole diameter to web flat depth (*a/h*), ratio of hole distance to web flat depth (*x/h*), ratio of bearing length to web flat depth (*N/h*), and ratio of stiffener length to web flat depth (*q/h*) were investigated. Cases involving plain webs, unstiffened web holes and edge-stiffened web holes were included, with the web hole located at the centre of the bearing plates for ITF loading conditions and offset to the bearing plates for ETF loading conditions.

According to the result of the parametric study, the stainless steel material (austenitic, duplex or ferritic), loading condition (ITF or ETF), flange condition, hole size (*a/h* ratio), plate element (*N/h* ratio), hole position (*x/h* ratio), and edge-stiffener length (*q/h* ratio) have a large influence on the web crippling strength reduction factor of CFSS channel sections with unstiffened or edge-stiffened web holes. Design equations were developed and proposed in the form of web crippling strength for CFSS channel sections with plain web and web crippling strength reduction factors for CFSS channel sections with unstiffened and edge-stiffened web holes under ITF and ETF loading conditions based on non-linear regression analysis on the result of the study. Limitations of the proposed design equations are $\frac{h}{t} \leq 200, \frac{N}{t} \leq$

$70, \frac{r}{t} \leq 2.0, \frac{N}{h} \leq 0.5, \frac{a}{h} \leq 0.6, \frac{q}{t} < 3 \; and \; \theta = 90º$. The result calculated from the proposed equations was compared to the values obtained from the FE models in the parametric study, revealing an average ratio that closely approaches 1.0. Results of the FE models were also compared with current design standards and recent available design equations for CFSS and CFCS web crippling strength and web crippling strength reduction factors. This comparison shows that the predicted web crippling strengths from the current design standards (ASCE, AS/NZS, AISI, and Eurocode) are conservative for ITF and ETF loading conditions.

To evaluate the reliability of the proposed equations, a comprehensive reliability analysis was performed. It demonstrated that the proposed equations could accurately calculate the web crippling strength of CFSS channel sections with plain web and web crippling strength reduction factors for CFSS channel sections with unstiffened and edge-stiffened web holes under ITF and ETF loading conditions.

Proposed equations for CFSS channel sections with edge-stiffened web holes result to values close to 1.0. Therefore, it can be concluded that utilization of an edge-stiffened web hole yields nearly the same strength as an equivalent channel section with a plain web.

Chapter 9: Future Studies

In this study, the proposed design equations have certain limitations in terms of their applicability. Specifically, they are designed for channel sections made only of three common stainless steel grades under the typical ITF and ETF loading conditions. Furthermore, the equations for channels with unstiffened and edge-stiffened web holes are only applicable to channels with one circular web hole at its centre and channels with an edge-stiffener length-to-web thickness ratio (q/t) less than 3.0. In cases where the q/t ratio is equal to or greater than 3.0, the strength reduction factors are greater than 1.0, indicating web crippling strengths higher than those of channel sections with plain webs.

These limitations show the need for future studies in the following areas:

- Other grades of Only stCFSS channel sections should be investigated and web crippling strength coefficients should be proposed.
- For sections under interior-one-flange (IOF) and end-one-flange (EOF) loading conditions, it is necessary to develop web crippling strength design equations.
- For sections with more than one circular web hole (symmetrical or non-symmetrical holes) or sections with elongated web holes, web crippling strength equations are needed to be developed.
- For sections with edge-stiffener length to web thickness (q/t) ≥ 3, more tests and further research are required to develop web crippling strength equations.

References

[1] ABAQUS Analysis User's Manual-Version 6.14-2, ABAQUS Inc., USA, 2018.

[2] American Iron and Steel Institute (AISI). North America Specification for the Design of Cold-formed Steel Structural Members AISI S100-16;2016

[3] American Society of Civil Engineers (ASCE). Specification for the Design of Cold-formed Stainless Steel Structural Members. Reston, Va: SEI/ASCE 8-02; 2002.

[4] Australian/New Zealand Standard (AS/NZS), Cold-Formed Stainless Steel Structures, AS/NZS 4673:2001, Standards Australia, Sydney, Australia, 2001.

[5] Australian/New Zealand Standard (AS/NZS). Cold-Formed Steel Structures, AS/NZS 4600:2018. Standards Australia/ Standards New Zealand; 2018.

[6] Bock, M., Arrayago, I., Real, E., & Mirambell, E. (2013). Study of web crippling in ferritic stainless steel cold formed sections. Thin-Walled Structures, 69, 29-44.

[7] Chen, B., Roy, K., Fang, Z., Uzzaman, A., Chi, Y., & Lim, J. B. (2021). Web crippling capacity of fastened cold-formed steel channels with edge-stiffened web holes, un-stiffened web holes and plain webs under two-flange loading. Thin-Walled Structures, 163, 107666.

[8] Eurocode 3: Design of steel structures – Part 1.4 (EN 1993-1-4). General rules – Supplementary rules for stainless steels. Brussel: European Committee for Standardization (CEN); 2006.

[9] Eurocode 3: Design of steel structures-Part 1-3 (EN 1993-1-3). General rules – Supplementary rules for cold-formed members and sheeting. Brussel: European Committee for Standardization (CEN); 2006.

[10] Fang, Z., Roy, K., Chi, Y., Chen, B., & Lim, J. B. (2021, December). Finite element analysis and proposed design rules for cold-formed stainless steel channels with web holes under end-one-flange loading. In Structures (Vol. 34, pp. 2876-2899). Elsevier.

[11] Fang, Z., Roy, K., Ma, Q., Uzzaman, A., & Lim, J. B. (2021, October). Application of deep learning method in web crippling strength prediction of cold-formed stainless steel channel sections under end-two-flange loading. In Structures (Vol. 33, pp. 2903-2942). Elsevier.

[12] Fang, Z., Roy, K., Padiyara, S., Chen, B., Raftery, G. M., & Lim, J. B. (2023, January). Web crippling design of cold-formed stainless steel channels under interior-two-flange loading condition using deep belief network. In Structures (Vol. 47, pp. 1967-1990). Elsevier.

[13] Fang, Z., Roy, K., Uzzaman, A., & Lim, J. B. (2022). Numerical simulation and proposed design rules of cold-formed stainless steel channels with web holes under interior-one-flange loading. Engineering Structures, 252, 113566.

[14] Gunalan, S., & Mahendran, M. (2015). Web crippling tests of cold-formed steel channels under two flange load cases. Journal of Constructional Steel Research, 110, 1-15.

[15] Hsiao L, Yu W, Galambos, T. V. (1988). Load and resistance factor design of cold-formed steel: Calibration of the AISI design provisions. Ninth Progress Report, Civil Engineering Study 88-2, University of Missouri-Rolla, Missouri, U.S.A.

[16] IBM Corp. (2022). IBM SPSS Statistics for Windows (Version 29.0). IBM Corp.

[17] Korvink, S. A., Van den Berg, G. J., & Van der Merwe, P. (1995). Web crippling of stainless steel cold-formed beams. Journal of Constructional Steel Research, 34(2-3), 225-248.

[18 Korvink, S. A., Van den Berg (1994). Web crippling of stainless steel cold-formed beams. Proc., 12th Int. Specialty Conf. On Cold-Formed Steel Structures, University of Missouri-Rolla, St. Louis, pp. 551–569.

[19] Lian, Y., Uzzaman, A., Lim, J. B., Abdelal, G., Nash, D., & Young, B. (2016). Effect of web holes on web crippling strength of cold-formed steel channel sections under end-one-flange loading condition–Part I: Tests and finite element analysis. Thin-Walled Structures, 107, 443-452.

[20] Lian, Y., Uzzaman, A., Lim, J. B., Abdelal, G., Nash, D., & Young, B. (2016). Effect of web holes on web crippling strength of cold-formed steel channel sections under end-one-flange loading condition-Part II: Parametric study and proposed design equations. Thin-Walled Structures, 107, 489-501.

[21] Lian, Y., Uzzaman, A., Lim, J. B., Abdelal, G., Nash, D., & Young, B. (2017). Web crippling behaviour of cold-formed steel channel sections with web holes subjected to interior-one-flange loading condition-Part I: experimental and numerical investigation. Thin-Walled Structures, 111:103–12.

[22] Lian, Y., Uzzaman, A., Lim, J. B., Abdelal, G., Nash, D., & Young, B. (2017). Web crippling behaviour of cold-formed steel channel sections with web holes subjected to interior-one-flange loading condition–Part II: parametric study and proposed design equations. Thin-Walled Structures, 114, 92-106.

[23] Nguyen, V. V., Hancock, G. J., & Pham, C. H. (2017). Analyses of thin-walled sections under localised loading for general end boundary conditions–Part 1: Pre-buckling. Thin-Walled Structures, 119, 956-972.

[24] Nguyen, V. V., Hancock, G. J., & Pham, C. H. (2017). Analyses of thin-walled sections under localised loading for general end boundary conditions–Part 2: Buckling. Thin-Walled Structures, 119, 973-987.

[25] Nguyen, V. V., Hancock, G. J., & Pham, C. H. (2017). New developments in the direct strength method (DSM) for the design of cold-formed steel sections under localised loading. Steel Construction, 10(3), 227-233.

[26] Nguyen, V. V., Hancock, G. J., & Pham, C. H. (2020). Consistent and simplified direct strength method for design of cold-formed steel structural members under localized loading. Journal of Structural Engineering, 146(6), 04020090.

[27] Uzzaman, A., Lim, J. B., Nash, D., & Roy, K. (2020). Cold-formed steel channel sections under end-two-flange loading condition: Design for edge-stiffened holes, unstiffened holes and plain webs. Thin-Walled Structures, 147, 106532.

[28] Uzzaman, A., Lim, J. B., Nash, D., & Roy, K. (2020). Cold-formed steel channel sections under end-two-flange loading condition: Design for edge-stiffened holes, unstiffened holes and plain webs. Thin-Walled Structures, 147, 106532.

[29] Uzzaman, A., Lim, J. B., Nash, D., & Roy, K. (2020). Web crippling behaviour of cold-formed steel channel sections with edge-stiffened and unstiffened circular holes under interior-two-flange loading condition. Thin-Walled Structures, 154, 106813.

[30] Uzzaman, A., Lim, J. B., Nash, D., & Roy, K. (2020). Web crippling behaviour of cold-formed steel channel sections with edge-stiffened and unstiffened circular holes under interior-two-flange loading condition. Thin-Walled Structures, 154, 106813.

[31] Uzzaman, A., Lim, J. B., Nash, D., & Young, B. (2017). Effects of edge-stiffened circular holes on the web crippling strength of cold-formed steel channel sections under one-flange loading conditions. Engineering Structures, 139, 96-107.

[32] Uzzaman, A., Lim, J. B., Nash, D., Rhodes, J., & Young, B. (2012). Cold-formed steel sections with web openings subjected to web crippling under two-flange loading conditions—part I: Tests and finite element analysis. Thin-Walled Structures, 56, 38-48.

[33] Uzzaman, A., Lim, J. B., Nash, D., Rhodes, J., & Young, B. (2012). Cold-formed steel sections with web openings subjected to web crippling under two-flange loading conditions—Part II: Parametric study and proposed design equations. Thin-Walled Structures, 56, 79-87.

[34] Yousefi, A. M., Lim, J. B., & Charles Clifton, G. (2018). Web crippling behavior of unlipped cold-formed ferritic stainless steel channels subject to one-flange loadings. Journal of structural engineering, 144(8), 04018105.

[35] Yousefi, A. M., Lim, J. B., & Charles Clifton, G. (2018). Web crippling behavior of unlipped cold-formed ferritic stainless steel channels subject to one-flange loadings. Journal of structural engineering, 144(8), 04018105.

[36] Yousefi, A. M., Lim, J. B., & Clifton, G. C. (2017).. Cold-formed ferritic stainless steel unlipped channels with web openings subjected to web crippling under interior-two-flange loading condition – Part I: Tests and finite element model validation. Thin-Walled Structures, 116, 333–41

[37] Yousefi, A. M., Lim, J. B., & Clifton, G. C. (2017). Cold-formed ferritic stainless steel unlipped channels with web openings subjected to web crippling under interior-two-flange loading condition–Part II: Parametric study and design equations. Thin-Walled Structures, 116, 342-356.

[38] Yousefi, A. M., Lim, J. B., & Clifton, G. C. (2019). Web crippling strength of perforated cold-formed ferritic stainless steel unlipped channels with restrained flanges under one-flange loadings. Thin-Walled Structures, 137, 94-105.

[39] Yousefi, A. M., Lim, J. B., Uzzaman, A., Lian, Y., Clifton, G. C., & Young, B. (2016). Web crippling strength of cold-formed stainless steel lipped channel-sections with web openings subjected to interior-one-flange loading condition. Steel and Composite Structures, 21(3), 629-659.

[40] Zhou, F., & Young, B. (2006). Cold-formed stainless steel sections subjected to web crippling. Journal of Structural Engineering, 132(1), 134-144.

[41] Baddoo, N. (2009). Designing structural stainless steel members to Eurocode 3. New steel construction, 17(4).